Universidade de São Paulo

Instituto de Astronomia, Geofísica e Ciências Atmosféricas

Departamento de Astronomia

Raphael Augusto Pereira de Oliveira

Assembly history of the Magellanic Bridge and Small Magellanic Cloud Wing from star clusters

Histórico de formação da Ponte de Magalhães e Asa da Pequena Nuvem de Magalhães a partir de aglomerados de estrelas

São Paulo

2023

Raphael Augusto Pereira de Oliveira

Assembly history of the Magellanic Bridge and Small Magellanic Cloud Wing from star clusters

Histórico de formação da Ponte de Magalhães e Asa da Pequena Nuvem de Magalhães a partir de aglomerados de estrelas

Thesis presented to the Departamento de Astronomia, Instituto de Astronomia, Geofísica e Ciências Atmosféricas, Universidade de São Paulo, as a partial requirement to obtain the degree of PhD in Science.

Area: Astronomy
Advisor: Prof. Dr. Beatriz L. S. Barbuy
Co-advisor: Prof. Dr. Francisco F. S. Maia

Versão Corrigida. O original encontra-se disponível na Unidade.

São Paulo

2023

Acknowledgements

adventures together and the care and infinite love that make our days easier to handle. I also thank my longtime friends (especially Ítalo, Murylo and Lincoln), which I also consider as family, I hope we continue together for many more decades.

"Science is not perfect. It can be misused. It is only a tool. But it is by far the best tool we have, self-correcting, ongoing, applicable to everything. [...] We must understand the Cosmos as it is and not confuse how it is with how we wish it to be. The obvious is sometimes false; the unexpected is sometimes true."

Carl Sagan, *Cosmos*, 1980

"We are just an advanced breed of monkeys on a minor planet of a very average star. But we can understand the Universe. That makes us something very special."

Stephen Hawking, *Der Spiegel*, 1988

Resumo

Os aglomerados estelares localizados no Sistema de Magalhães são muito importantes na determinação do histórico de formação estelar e evolução química e dinâmica da Pequena e Grande Nuvens de Magalhães (SMC e LMC). A Ponte de Magalhães é a estrutura formada por forças de maré e pressão de arraste durante uma colisão recente entre a LMC e SMC, o par de galáxias-satélite mais próximo da Via Láctea. A análise da idade e assinatura química de sua população estelar é crucial para distinguir o modelo mais adequado acerca da origem e evolução do sistema Nuvens-Via Láctea. Há duas vertentes principais: *(i)* as Nuvens de Magalhães eram satélites independentes e se ligaram recentemente, há ~ 2 bilhões de anos; *(ii)* o Sistema de Magalhães é antigo e está em sua primeira passagem próximo à Via Láctea nos últimos ~ 2 bilhões de anos. Neste contexto, a importância dos aglomerados da Ponte de Magalhães tem sido negligenciada na literatura. O cenário de sua formação durante uma colisão há $200-300$ milhões de anos, tal como proposto pelos modelos, implicaria assinaturas cinemáticas e gradientes de idade e metalicidade ao longo de sua extensão, os quais ainda precisam ser comprovados observacionalmente. Para explorar essa questão, esse trabalho combinou dados fotométricos profundos dos *surveys* VISCACHA e SMASH, obtendo homogeneamente idade, metalicidade, distância, parâmetros estruturais e massa de 33 aglomerados da Asa/Ponte, com ferramentas estatísticas robustas e modernas tais como cadeias de Markov via Monte Carlo e aprendizado de máquina. Dentre os 33 aglomerados, foram identificados dois grupos: 13 aglomerados bem estudados mais velhos do que a Ponte, com idades entre 0.5 e 4.7 bilhões de anos e [Fe/H] < -0.6; e 15 aglomerados mais jovens que 200 milhões de anos e com [Fe/H] > -0.5, provavelmente formados na própria Ponte. Os resultados principais incluem: *(i)* as idades e metalicidades foram determinadas pela primeira vez para 9 e 18 aglomerados, respectivamente; *(ii)* fo-

ram detectadas duas quedas de metalicidade na relação idade-metalicidade da Ponte, com idades similares às da formação da Ponte e da Corrente de Magalhães; *(iii)* uma massa estelar de $3 - 5 \times 10^5 \, M_\odot$ foi estimada para a Ponte, mais de uma magnitude acima de estimativas anteriores; *(iv)* os aglomerados formados na Ponte são jovens e ricos em metais, com $[\text{Fe/H}] \sim -0.4$. O estudo também envolveu a análise de aglomerados em outras regiões da SMC e uso de dados de espectroscopia para refinar os resultados.

Abstract

The stellar clusters located in the Magellanic System are very important in the determination of the star formation history and chemodynamical evolution of the Small and Large Magellanic Clouds (SMC and LMC). The Magellanic Bridge is the structure formed by tidal forces and ram pressure during a recent collision between the LMC and SMC, the pair of satellite galaxies closest to the Milky Way. The analysis of the ages and chemical signatures of its stellar population is crucial to distinguish which is the most adequate model to explain the origin and evolution of the Magellanic Clouds-Milky Way system. There are currently two competing scenarios: *(i)* the Magellanic Clouds were independent satellites and got bound recently, at $\sim 2\,\mathrm{Gyr}$ ago; *(ii)* the Magellanic System is old and on its first passage across the Milky Way in the last $\sim 2\,\mathrm{Gyr}$. In this context, the importance of the Bridge stellar clusters has been neglected in the literature. Its formation scenario during a collision some $200-300$ million years ago, as proposed by the models, would imply kinematic signatures, as well as age and metallicity gradients along its extension, which still need to be observationally confirmed. To elucidate this question, this work combined deep photometric data of the VISCACHA and SMASH surveys, homogeneously deriving age, metallicity, distance, structural parameters and mass of 33 Wing/Bridge clusters, by means of robust and modern tools such as Markov chain Monte Carlo and machine learning. Two groups were identified among the 33 clusters: 13 well-studied clusters older than the Bridge, with ages between 0.5 and 4.7 billion years and [Fe/H] < -0.6; and 15 clusters younger than 200 million years and with [Fe/H] > -0.5, probably formed in the Bridge itself. The main results include: *(i)* the ages and metallicities were derived for the first time for 9 and 18 clusters, respectively; *(ii)* two metallicity dips were detected in the Bridge age-metallicity relation, with ages similar to the formation of the Magellanic Bridge

and Stream; *(iii)* a stellar mass of $3 - 5 \times 10^5 M_\odot$ was estimated for the Bridge, more than one order of magnitude higher than previous estimates; *(iv)* the Bridge clusters are young and metal-rich, with [Fe/H] ~ -0.4. The study also involved the analysis of clusters in other SMC regions and the use of spectroscopic data to refine the results.

List of Figures

List of Tables

Notation

In the present thesis, the period is used as decimal separator, following the English notation of the International System of Units (SI). All acronyms and astrophysical quantities (with the respective units in the SI standards, unless otherwise stated) applied in this work, and frequently adopted in the literature, are listed below.

Acronyms and abbreviations

- AMR – Age-Metallicity relation
- CMD – Color-Magnitude Diagram
- DECam – Dark Energy Camera at the Blanco 4-m Telescope (CTIO)
- FoV – Field of View of the telescope
- GMM – Gaussian Mixture Model
- HB – Horizontal Branch
- *HST* – Hubble Space Telescope
- IMF – Initial Mass Function
- LMC and SMC – Large and Small Magellanic Clouds
- MB – Magellanic Bridge
- MCs – Magellanic Clouds
- MCMC – Markov Chain Monte Carlo
- MS, MSTO – Main Sequence, Main-Sequence Turnoff
- RA; Dec. – Right Ascension; Declination (equatorial coordinates)
- RDP – Radial number Density Profile

- RGB; SGB – Red Giant and SubGiant Branches

- SAM; SOI – SOAR Adaptive optics Module; SOAR Optical Imager

- SMASH – Survey of the Magellanic Stellar History (DECam)

- SOAR – Southern Astrophysical Research Telescope (4.1 m)

- SIRIUS – Statistical Inference of physical paRameters of sIngle and mUltiple populations in Stellar clusters

- VISCACHA – VIsible Soar photometry of star Clusters in tApii and Coxi HuguA

- VMC – VISTA near-infrared *YJKs* survey of the Magellanic Clouds system

Astrophysical quantities and units

- Ages: presented in Myr (10^6 yr) or Gyr (10^9 yr)

- $d_\odot$: heliocentric distance in kpc (1 pc = 3.26 light-years = 3.086×10^{16} m)

- $(m - M)_0$: absolute distance modulus, where $d_\odot[\text{kpc}] = 10^{[(m - M_0) - 10]/5}$

- $(m - M)_\lambda$: apparent distance modulus in the λ filter, where $(m - M)_\lambda = (m - M)_0 + A_\lambda$

- $E(B - V)$: foreground reddening or color excess, caused by interstellar extinction

- r_t and r_c: tidal and core radii in arcseconds (arcsec), defined in the King radial profile

- $\rho(r)$: number density of stars at a radius r, in arcsec^2

- m_λ: apparent magnitude in the λ filter

- M_V: absolute visual magnitude

- $M_\odot$: solar mass, which corresponds to 1.988×10^{30} kg

Contents

Chapter 1

Introduction

1.1 The Milky Way neighborhood and Magellanic System

Seen from the Earth, our Milky Way (MW) galaxy looks like a bright, hazy and diffuse band across the entire celestial sphere, a notable feature that gave rise to its name. The Galaxy appears as a band because its central and disk-shaped structures are viewed from within the Orion Arm, the spiral arm where the Solar System is located (at a distance to the Galactic center of 8.2 ± 0.1 kpc from Bland-Hawthorn and Gerhard 2016 or 8.18 ± 0.03 kpc from GRAVITY Collaboration et al. 2019). The real shape of the MW probably resembles a barred spiral galaxy, with a diameter of $50 - 60$ kpc (López-Corredoira et al., 2018). More specifically, it was classified as "SB(rs)bc II" or "SAB(rs)b II" (de Vaucouleurs and Pence, 1978; Bland-Hawthorn and Gerhard, 2016), meaning that it has a central barred structure ("SAB" means a less developed bar), with spiral arms emerging from a weak ring of stars and gas around the nucleus in an intermediate stage "bc" between early- and late-type, and luminosity class II. Given the high mass of the Bulge, it is not excluded that the MW could be an Sb type galaxy (Barbuy et al., 2018).

Like a typical spiral galaxy, the MW has three main structural components: a central, compact bulge with a bar, containing a number of globular clusters (GCs); a disk in the Galactic plane containing the spiral arms, divided into a younger thin disk and an older thick disk (scale heights of 350 pc and 1 kpc, respectively); and the halo, a spheroidal structure containing an old, metal-poor stellar population and GCs. The latter structure is usually subdivided into: stellar Halo, which actually contains stars and GCs; a gaseous Galactic corona (Savage, 1995); and a dark matter Halo extending far beyond the aforementioned components, up to a radius of 292 ± 61 kpc (Deason et al., 2020).

Besides the billions of stars with their own planetary systems (isolated or grouped in star clusters), the interstellar clouds of gas and dust, and a central supermassive black hole, the MW contains around 59 smaller satellite galaxies. These galaxies are gravitationally bound to the MW, lying within the central $300 - 400\,\mathrm{kpc}$ (i.e. mostly within the edge of the dark matter halo), and are a strong evidence of the hierarchical formation in galaxies similar to the MW. They are mainly dwarf spheroidal or dwarf elliptical galaxies, such as the Sculptor dwarf galaxy (the first to be discovered, in 1937, at a galactocentric distance of $90\,\mathrm{kpc}$; e.g. Karachentsev et al. 2004), the Sagittarius dwarf galaxy (one of the largest and the second satellite galaxy closest to the MW, at $\sim 20\,\mathrm{kpc}$; Karachentsev et al. 2004) and Canis Major, the closest one at $\sim 13\,\mathrm{kpc}$ from the MW center and a matter of controversy regarding whether it is indeed a dwarf spheroidal or an overdensity of the MW disk (Momany et al., 2004). Along with the Andromeda's (M31) own system of satellite galaxies (at $\sim 800\,\mathrm{kpc}$ to the MW) and the Triangulum Galaxy (M33, most probably a satellite of M31 or possibly an independent system with its own satellites; Martínez-Delgado et al., 2022), they comprise most of the Local Group galaxies. Exceptions include NGC 6822, IC 1613, Wolf-Lundmark-Melotte galaxy and Pegasus dwarf irregular galaxy, which are often called "field galaxies" for not being associated with either the MW or Andromeda (van den Bergh, 2007). As a consequence of the morphological segregation, these galaxies are mostly dwarf irregulars, typically filled with more gas and star formation (Einasto et al., 1974).

In the cosmological context, dwarf galaxies are the protagonists of one of the problems faced by ΛCDM simulations in reproducing the observed distribution of matter in the Universe: the missing satellites problem (Klypin et al., 1999; Moore et al., 1999). For the MW, there is a difference of one order of magnitude between the counts of simulated dark matter subhaloes and observed dwarf galaxies. Recent deep, wide-field surveys (e.g. SDSS, DES, Pan-STARRS, *Gaia*; Willman et al., 2005; Bechtol et al., 2015; Laevens et al., 2015; Torrealba et al., 2019) have revealed several ultra-faint dwarf galaxies and stellar streams (remnants of disrupting satellites, such as the Sagittarius stream) in the Galactic halo. It is widely accepted that the MW was assembled over billions of years through hierarchical accretion, starting by an early collapse to form the bulge and followed by the formation of the thick disk and inner halo (Bland-Hawthorn and Gerhard, 2016).

The brightest MW satellite galaxies, and the only ones visible to the naked eye, are the Large and Small Magellanic Clouds (LMC and SMC), which are also among the largest

satellites. Due to their notable brightness in the southern skies, they have been observed since prehistory. The first records of their observation are from petroglyphs found in Chile and Arabian books; but also indigenous cultures from Australia, southern Africa and South America had their own names for the Clouds. In the Tupi-Guarani language, the MW has been long referred to as *Tapi'i rapé* ("path of the tapir", due to a close constellation of a tapir), whereas the LMC and SMC are called *Tapi'i* and *Coxi Hugua* respectively, which means the water fountains of the tapir and musk hog. As detailed in Dennefeld (2020), the first mention of the MCs by Europeans was made in 1520 by the crew of the Portuguese explorer Fernão de Magalhães, during his circumnavigation of the world between 1519 and 1522. However, the MCs were long called with the Latin terms *Nubecula Major* and *Minor*, before the current names of Large and Small Magellanic Clouds became common in the middle of the eighteenth century.

The MCs, the pair of satellite galaxies closest to the MW, constitute a unique laboratory to study gravitational interactions between them and with the MW. They have well-defined distances with $\sim 1\%$ uncertainties: the LMC is at a distance of 49.59 ± 0.54 kpc (Pietrzyński et al., 2019) and SMC is at 62.44 ± 0.81 kpc (Graczyk et al., 2020). Although both galaxies are classified as irregular dwarf galaxies, the LMC shares common features with spiral galaxies: it presents a flat disk morphology, with a single spiral arm and a warped stellar bar. In contrast, the SMC presents a cigar-shaped, triaxial structure, with a line-of-sight depth of up to 14 kpc in the inner regions (Subramanian and Subramaniam, 2012) and ~ 23 kpc in the eastern part (Nidever et al., 2013). Using CaII triplet (CaT) lines in the spectra of field red giants, Cole et al. (2005) derived an average $[Fe/H] = -0.37 \pm 0.15$ for the LMC, and Parisi et al. (2016) derived -0.9 ± 0.2 for SMC.

The MCs are physically close (~ 20 kpc) and gravitationally associated to each other, and there are hypotheses that they could be part of a larger system. Based on the evidence that some bright MW satellites seem to trace the orbit of the MCs, Lynden-Bell (1976) suggested that the Ursa Minor and Draco dwarf galaxies were associated to the MCs gaseous trail, being probably debris of a Greater Magellanic Galaxy. Based on more recent evidence of ΛCDM models and the discovery of associations of dwarf galaxies close to the Local Group, D'Onghia and Lake (2008) proposed that the MCs were the largest members of a group of dwarf galaxies that has been accreted into the MW halo, the Magellanic Group. In such scenario, seven of the eleven brightest MW dwarfs would have been part of
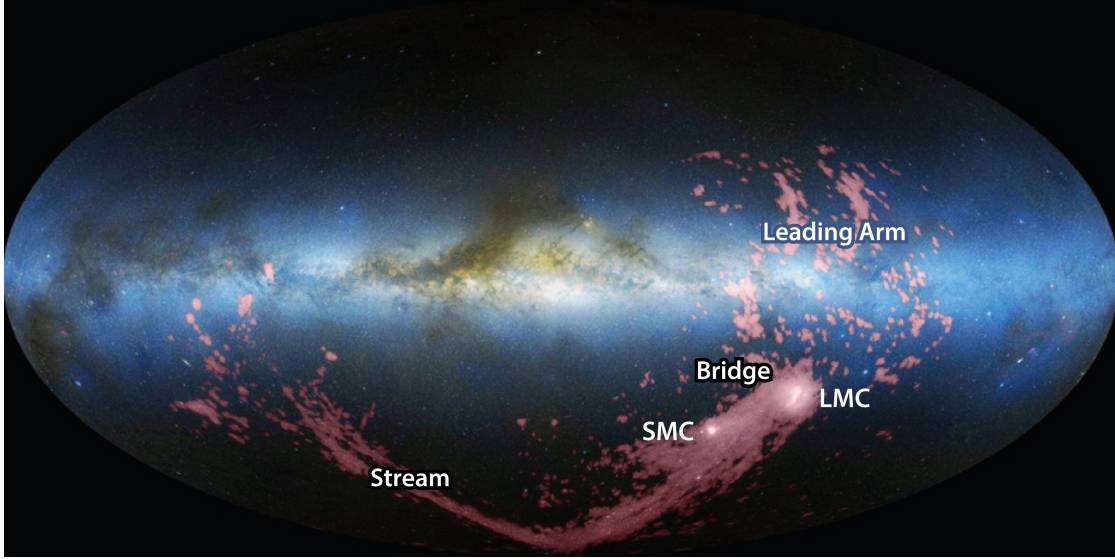
Figure 1.1: Hammer-Aitoff projection with an all-sky panorama of the Milky Way in optical wavelengths (Mellinger, 2009), centred in the bulge, and HI observations of the Magellanic Clouds overlaid (Nidever et al., 2010). The tidal HI structures spans over 200° on the sky, namely the Bridge, Stream and Leading Arm (the last two fragmented in small cloudlets). Extracted from D'Onghia and Fox (2016).

it, including Ursa Minor and Draco. The discovery of many ultra-faint MW satellites aligned with either LMC or SMC orbits strengthens the latter scenario, and future kinematic studies and detection of more ultra-faint dwarfs are crucial to validate it.

Given the intense interaction between the MCs and the MW, we have the opportunity to observe closely a variety of phenomena associated to galaxy evolution, including tidal stripping (mutual gravitational interactions that pull gas and stars out of their potential wells; e.g. Besla et al., 2010), ram pressure stripping (dragging mostly gas as the MCs pass through the extended gaseous MW halo; e.g. Mastropietro et al., 2005), dynamical friction and merger-induced star formation (Navarrete et al., 2023). These mechanisms also take place in farther galaxies and even larger scales, e.g. in the intracluster medium and jellyfish galaxies present within galaxy clusters. In the present case, they are evident in the current morphology, gaseous content and stellar populations of the Magellanic System, and reflect its intense past interaction history, as described in the following sections.

The so-called Magellanic System consists not only of these two satellite galaxies, but also of structures formed due to perturbations from the gravitational interaction between them and the MW: two purely gaseous HI structures, one of them extending towards the System orbit (Leading Arm) and the other in the opposite direction (Magellanic Stream);

and a third structure connecting the MCs, the Magellanic Bridge. These structures stretch over 200° on the sky mainly into negative Galactic latitudes, as presented in Figure 1.1, which combines a panoramic view of our Galaxy (Mellinger, 2009) with 21-cm observations from a radio telescope (Nidever et al., 2010).

Simulations and observations have shown that the majority of galaxies in the Universe have either been or are still part of an interacting system, and the MCs are no exception. The gaseous structures of the Magellanic System were the first signs of tidal interactions of the MW with the MCs, where the first of the three structures to be discovered was the Bridge, from 21-cm observations. In a first moment, Kerr et al. (1954) noted that the HI distribution in the MCs was more extended than their stars, and then Hindman et al. (1963) detected the bridge of neutral hydrogen connecting the MCs. Some years later, after a previous detection of high-velocity clouds near the south Galactic pole, Mathewson et al. (1974) traced them back to the MCs and named them as Magellanic Stream. They also detected a counterpart on the other side of the MCs (the Leading Arm, at $b > 0°$), but the nature of its connection with the MCs was only confirmed decades later, after kinematic and metallicity studies (Putman et al., 1998; Lu et al., 1998).

The Stream and the Leading Arm are the most prominent high-velocity clouds of the southern Galactic hemisphere, meaning that their kinematics are not compatible with the rotation models of the MW disk (e.g. Wakker and van Woerden, 1997). In this sense, the Stream is evidence of a massive ($\sim 10^9 M_\odot$) and ongoing gas accretion into the MW halo (Putman et al., 1998; Bland-Hawthorn and Gerhard, 2016). Until very recently, the Leading Arm was thought to contain only gas, but two works have revealed the presence of stars probably formed in situ: Casetti-Dinescu et al. (2014) discovered 19 young field stars ($1 - 250\,\mathrm{Myr}$) at a mean distance of $\sim 21\,\mathrm{kpc}$, and Price-Whelan et al. (2019) discovered the young star cluster Price-Whelan 1, deriving $117\,\mathrm{Myr}$, $\mathrm{[Fe/H]} = -1.14$, a low-mass of $1200\,M_\odot$ and $28.7\,\mathrm{kpc}$ (closer to the MW than predicted by models).

The gaseous structures of the Magellanic System have a total gas mass of $2 \times 10^9 M_\odot$, of which 1/4 is neutral, atomic gas ($4.9 \times 10^8 M_\odot$) and 3/4 is ionized gas (Barger et al., 2013; Fox et al., 2014). Separately, the Stream accounts for $2.7 \times 10^8 M_\odot$, the Bridge for $1.8 \times 10^8 M_\odot$ and the Leading Arm for $3 \times 10^7 M_\odot$ (Brüns et al., 2005) of the HI mass budget. The combined mass of $M_\mathrm{HI} \sim 5 \times 10^8 M_\odot$ is comparable with the HI mass of each galaxy at the current time ($4.4 \times 10^8 M_\odot$ for the LMC; $4.0 \times 10^8 M_\odot$ for the SMC). Since

the MCs do not contain a significant mass of ionized gas, the total gas mass of the three gaseous structures is almost twice that of both galaxies together, implying that the LMC and SMC should have been richer in gas than they are today.

Regarding the stellar mass, the Bridge is the only one of the gaseous structures that hosts a considerable stellar component. This component was first discovered by Irwin et al. (1985), with an estimated age of $\sim 100\,\text{Myr}$. Assuming a Kroupa initial mass function and a stellar population of $10\,\text{Gyr}$, Harris (2007) computed a stellar mass of $1.5 \times 10^4 M_\odot$. This mass seems underestimated when looking at the large number of star clusters in the Wing/Bridge region (see Section 1.4), therefore we also obtain a new estimate in this work, based on individual cluster masses. As described in D'Onghia and Fox (2016), the Bridge has always been treated as a different object from the other two structures, because it is not purely gaseous, but hosts a stellar population, and it is likely to have been formed at a different time.

1.2   Origin of the Magellanic System

As the pair of interacting galaxies closest to the MW, the Magellanic Clouds are the best laboratories to study the dynamical evolution of galaxies and the results of star formation through time. Several N-body dynamical and hydrodynamical simulations have been improving our understanding of the System origin and evolution, as well as of their gaseous structures. As discussed in D'Onghia and Fox (2016), besides the existence of the gaseous features and their distribution over $200°$ on the sky, these models have to explain and reproduce the observational features arising from the gaseous and stellar components. The main features are related to the Stream, which presents a structure with two filaments (each one with a metallicity close to either the LMC or SMC ones), has most of the gas in ionized form ($\sim 10^9 M_\odot$; Fox et al., 2014), and contains almost no stars.

The location of the gaseous Leading Arm ahead the System orbit and across the Galactic plane indicates that it has a dominating tidal origin. On the other hand, the Stream was probably formed from tidal and ram-pressure stripping in the interaction of the MCs with the Galactic corona. It has a complex shape of interwoven filaments, first observed by Cohen (1982). Further kinematic and chemical studies, along with HI observations and simulations (e.g. Hammer et al., 2015), traced back each filament to the LMC or SMC
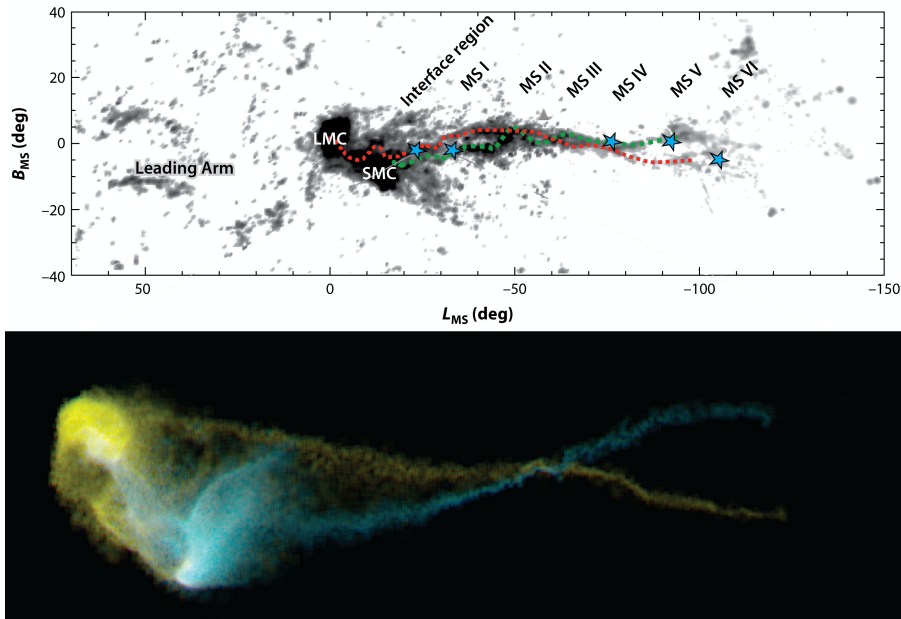
Figure 1.2: Comparison between the observed HI data from GASS (McClure-Griffiths et al., 2009, upper panel) and the result of a simulation of the Magellanic Clouds and the Stream (Hammer et al., 2015, lower panel), with a collision $100 - 300\,\mathrm{Myr}$ ago. Metallicity measurements throughout the Stream (blue stars) has confirmed the existence of two gaseous filaments (dotted lines) that can be traced back to the SMC and LMC, as predicted by the model. Extracted from D'Onghia and Fox (2016).

(Nidever et al., 2008), as shown in Figure 1.2.

In the last half century, several studies have tried to explain the origin of the Stream, each with a series of observational evidence available at the time. They can be summarised in two types of scenarios: the tidal models, where all the material is pulled from the MCs due to gravitational interactions (e.g. Fujimoto and Sofue, 1976); and drag models, where the gas was stripped by ram pressure as the MCs passed through the Galactic corona or disk (e.g. Moore and Davis, 1994). However, new kinematic data gave rise to two main models attempting to describe the formation of the LMC-SMC pair, both showing that the Stream originated from a mutual interaction in their bound orbit around the MW (Diaz and Bekki, 2011) or before they were accreted by the MW (Besla et al., 2012).

In the first model (Diaz and Bekki, 2011), commonly referred to as the bound scenario, the MCs were formed as independent MW satellites, and gradually approached until the LMC captured the SMC around $2\,\mathrm{Gyr}$ ago. Since then, the LMC-SMC pair would be in a bound orbit dominated by the gravitational forces from the MW, and have completed two close encounters (at $1.2\,\mathrm{Gyr}$ and $0.25\,\mathrm{Gyr}$ ago). Although this model can reproduce the two filaments and the Stream composition, the tidal effects would also remove a stellar
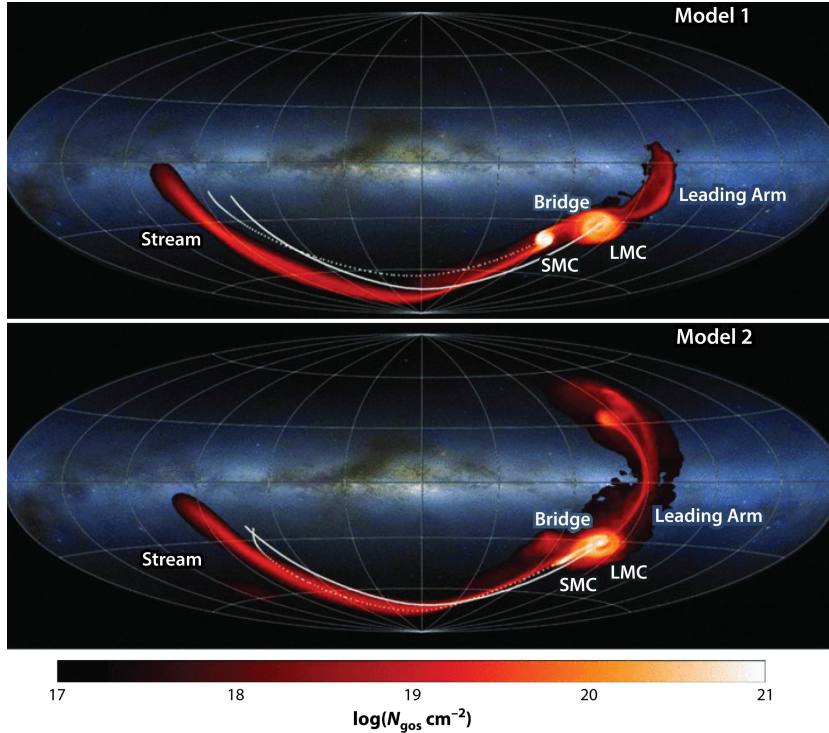
Figure 1.3: Projection of the streams of gas predicted by the models from Besla et al. (2012), where the solid and dotted white lines show the orbital trajectory of the LMC and SMC. The models consider that the SMC has crossed the $R_{200} = 117$ kpc of the LMC at ~ 7 Gyr ago, and that the entire System crossed the $R_{200} = 220$ kpc of the MW at 1 Gyr ago. In Model 1 (upper panel), the SMC has completed two passages about the LMC; and in Model 2 (lower panel), it has completed three. Extracted from D'Onghia and Fox (2016).

component from the SMC, not yet observed in the Stream.

According to the second model (bound scenario; Besla et al., 2007, 2012), the MCs constitute an old interacting system that has just completed its first perigalactic passage, and has entered the tidal radius of the MW in the last ~ 2 Gyr. It also predicts a recent frontal encounter between the Clouds, changing drastically the SMC structure by removing large quantities of material and originating the Stream (Figure 1.3[1]). This scenario demonstrates that the morphology and internal kinematics of the System can be explained by the interactions between the MCs alone and does not require any interaction with the MW potential, which is consistent with the low metallicity of the Stream. Therefore, it agrees with the observed features of the Stream (formed before the System was accreted by the MW) and Leading Arm, but predicts HI and HII densities 10 and 100 times lower than observed, respectively. It also fails in predicting the chemical composition of the Stream, as it neglects the gaseous component stripped from the LMC.

---

[1] R_{200} is the radius where the average density is 200 times the critical density of the Universe (ρ_c).

Both the classical and new scenarios are able to reproduce the large-scale gas structure (Stream, Leading Arm, gaseous Bridge and old RR Lyrae Bridge), as detailed in Dias et al. (2021). Recent measurements of high-precision proper motions (PMs) of the Clouds from multi-epoch Hubble Space Telescope (*HST*) data showed that the Clouds are moving too fast to be orbiting the MW. Kallivayalil et al. (2006, 2013) concluded that the System is completing its first passage around the MW or is on a very eccentric orbit, which refutes the predictions from Diaz and Bekki (2011). The second scenario, from Besla et al. (2012), is in agreement with the *HST* PMs, which suggest at least one recent encounter between the MCs in the last 500 Myr. As discussed in D'Onghia and Fox (2016) and Patel et al. (2020), the main challenge is to determine whether the LMC is on a parabolic or bound orbit around the MW, which depends more on the model inputs (MW mass distribution, total mass and virial radius) than in improving the precision of PM measurements.

Finally, the model from Besla et al. (2012) reproduces the formation of the Bridge from a front collision of the SMC with the LMC center, at around $200 - 300$ Myr ago, inducing star formation episodes and possibly leaving a chemical signature as a metallicity gradient. There is no observational evidence to support or refute this scenario so far.

1.3   The Magellanic Bridge (inter-Cloud region)

The MCs are separated by a distance of ~ 20 kpc, which corresponds to the approximate extension of the Magellanic Bridge, with a ~ 10 kpc depth (Jacyszyn-Dobrzeniecka et al., 2016). As discussed in Section 1.1, the Bridge is known to contain both neutral and ionized gas (HI and HII), and an important stellar population, which suggests that it was formed in a particular scenario. With a HI mass of $1.8 \times 10^8 M_\odot$, the Bridge contains a significant fraction of the gas mass of the System, and its components can be associated to the main body of both MCs (McGee and Newton, 1986). The SMC region that connects to the Bridge is the SMC Wing, an elongated structure that was first detected by Shapley (1940). Distorted structures are also observed in the LMC, such as a ring-like feature in its periphery (e.g. Santos et al., 2020). The Bridge presents a higher concentration of stars in the western part, where it connects with the SMC Wing, and another halfway between the MCs (OGLE island; Skowron et al., 2014).

A closer look of the gaseous Bridge is given in Figure 1.4, extracted from Barger et al.
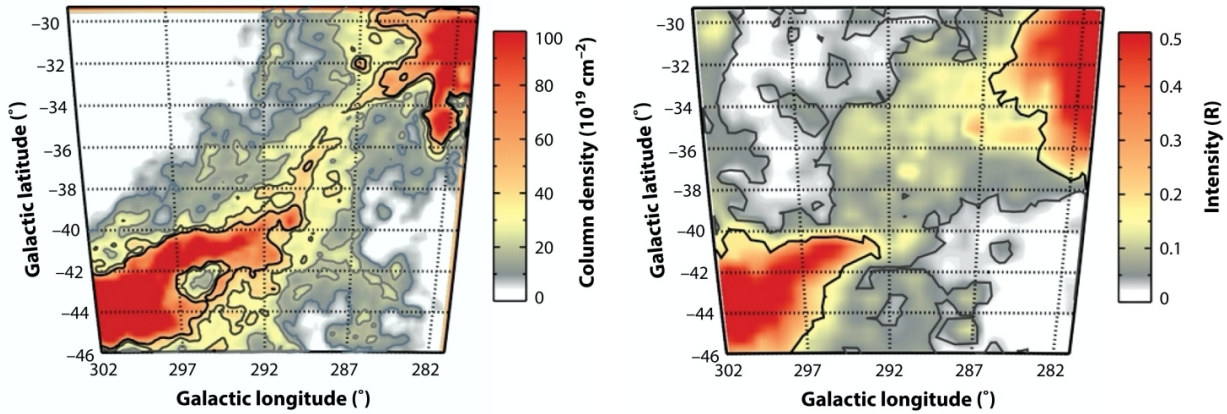
Figure 1.4: The Magellanic Bridge shown in HI and Hα maps, from the Galactic All Sky Survey (GASS) and Wisconsin H-Alpha Mapper (WHAM). The SMC is located on the lower left, and the LMC on the upper right. It is interesting to note that the Bridge is contained in a common envelope of HI and Hα with the Clouds, and its border with the SMC contains more gas, similarly to the stellar distribution. Extracted from Barger et al. (2013).

(2013). In this study it is estimated a HII mass of $(0.7-1.7) \times 10^8 M_\odot$ over the Bridge region with $M_{\rm HI} = 3.3 \times 10^8 M_\odot$ (twice the mass from Brüns et al., 2005), showing that the MCs and the Bridge share a common HI envelope. They show that the ionising radiation from the MW and extragalactic background is not enough to reproduce the observed Hα flux, indicating that the MCs had a close encounter and are still interacting. The interactions in such a gas-rich System can trigger star formation, changing its dynamical and chemical evolution. Metallicity measurements of the gas from absorption lines found $[{\rm M/H}] = -1.0$ and -1.3 for two massive stars at different sight lines (Lehner et al., 2008), and -0.8 using a background quasar (Misawa et al., 2009). Despite being a small sample, these values are closer to the SMC metallicity ($[{\rm Fe/H}] \sim -0.8$) than to the LMC ($[{\rm M/H}] \sim -0.3$; Rolleston et al., 2002), suggesting that the Bridge may have formed from SMC material.

Unlike the gaseous component, the stellar mass of the Bridge ($1.5 \times 10^4 M_\odot$) is thousands of times lower than the one of the LMC ($3 \times 10^9 M_\odot$; van der Marel et al., 2002) and of the SMC ($3 \times 10^8 M_\odot$; Stanimirović et al., 2004). After the first detections of a blue, young stellar population in the Bridge by Westerlund and Glaspey (1971) and Irwin et al. (1985, 1990), posterior studies have shown the existence of a large number of stellar associations distributed from the LMC halo to the SMC Wing (e.g. Demers et al., 1991; Grondin et al., 1992; Demers and Battinelli, 1998), with ages between 10 and 100 Myr.

Recent N-body simulations predicted that gas and stars were pulled out from the SMC through tidal interactions (Harris, 2007) and possibly dragged from the LMC to the Bridge

(Besla et al., 2012), during the most recent encounter of the MCs about $100 - 300\,\mathrm{Myr}$ ago (Gardiner and Noguchi, 1996; Zivick et al., 2018). By comparing the kinematics of the LMC disk from *Gaia* PMs and N-body simulations, Choi et al. (2022) concluded that this encounter was direct (i.e. impact parameter smaller than the radius of the LMC stellar disk), with an impact parameter between 5 and $10\,\mathrm{kpc}$ depending on the assumed impact timing. The value of $100 - 300\,\mathrm{Myr}$ is quite consistent with independent constraints from orbital modelling of the System (Zivick et al., 2018) and with the ages of the young stellar population found in the Bridge, which have probably formed in situ, reinforcing that it is a star forming region.

According to the models, such a scenario for the Bridge formation would have two implications: *(i)* the presence of an older stellar population, which would have been stripped from either MCs; *(ii)* a metallicity gradient along the Bridge increasing toward the LMC due to the minor contribution of the LMC gas (D'Onghia and Fox, 2016). Concerning the first point, several works have failed in finding the older population (e.g. Harris, 2007), leading to an incorrect conclusion that the material stripped from the Clouds was very nearly a pure gas. However, more recent studies have found it (Bagheri et al., 2013; Noël et al., 2013; Skowron et al., 2014), including intermediate-age $(1 - 3\,\mathrm{Gyr})$ and old $(> 3\,\mathrm{Gyr})$ star clusters (Bica et al., 2015; Perren et al., 2015). Using *Gaia* data of RR Lyrae stars, Belokurov et al. (2017) detected a second branch of the Bridge composed of an old stellar population, usually called as Southern Bridge.

Several studies combining PMs from *HST*, *Gaia* and from the VISTA Magellanic Clouds survey (VMC; Cioni et al., 2011) have analysed the kinematics of the LMC (Schmidt et al., 2022), SMC (Zivick et al., 2018) and Bridge (Zivick et al., 2019; Schmidt et al., 2020). Schmidt et al. (2020) obtained mean PMs of $1.80 \pm 0.25\,\mathrm{mas\,yr^{-1}}$ in right ascension and $-0.72 \pm 0.13\,\mathrm{mas\,yr^{-1}}$ in declination in the Bridge, confirming a flow motion from the SMC to the LMC and suggesting that the Bridge is stretching, with its borders close to the SMC and LMC moving apart.

The MCs are extremely rich in extended objects (such as stellar clusters, associations, emission nebulae, supernova remnants, and tidal dwarf galaxies; Bica et al., 2008, 2020), and the same applies to the stellar component of the Bridge. As it is expected that the distribution of star clusters follow streams of gas formed by tidal forces, the Bridge clusters may provide valuable information about the spatial distribution and chemical enrichment

of the Bridge stellar content, thus helping constrain its origin and possible recent MC encounters.

1.4   Star clusters in the Magellanic Clouds and Bridge

Unlike the Magellanic Stream, the Bridge contains a substantial stellar population with mass of $1.5 \times 10^4 M_\odot$ (Harris, 2007), mostly present in extended objects such as star clusters and associations. By measuring the ages (star formation history), chemical abundances, and kinematics of these stars, it is possible to obtain constraints on the dynamical evolution that formed the Bridge, and to study star formation from tidal debris in such a close System. Star clusters and associations host stars of similar age, chemical composition and distance, preserve their initial mass function (distribution of birth masses of its stars), and are commonly called "relics", "fossils" or "chemical clocks". The study of these objects is essential for understanding the galactic age-metallicity relation (AMR, e.g. Cignoni et al., 2013), age distribution (e.g. Glatt et al., 2010), dynamics (e.g. Subramanian et al., 2017), structure (e.g. Maia et al., 2014) and cluster distribution, as they are important tracers of the star formation history and chemodynamical evolution of the MCs.

The study of SMC clusters started with the catalogues by Kron (1956) and Lindsay (1958). Several works have complemented them with newly identified objects (Westerlund and Glaspey, 1971; Hodge and Wright, 1974) and reorganised them, with several contributions by Prof. Eduardo Bica: Bica and Schmitt (1995), Bica and Dutra (2000) and Bica et al. (2020) for the SMC and Bridge; Bica et al. (1999) for the LMC; and Bica et al. (2008) for the entire Magellanic System. In the general catalogues including the LMC, Bica et al. (2008) compiled 9305 extended objects in the Magellanic System, of which 144 are located in the Bridge. Recently, Bica et al. (2020) obtained 2741 entries solely for the SMC and Bridge (a factor of 2 more than Bica et al., 2008), of which 449 are located in the region defined as the Bridge and SMC Wing.

In a pioneer work, Bica et al. (2015) analysed 14 stellar clusters of the Bridge, deriving young ages of $\sim 10^8$ years (or 100 Myr) and discussing that they probably formed in situ. However, the authors claimed that the possibility of an older stellar population cannot be excluded, since the star formation may be mixed with old stars. Bagheri et al. (2013), for example, found ages from 400 Myr to 5 Gyr for red giant stars in the Bridge, arguing that
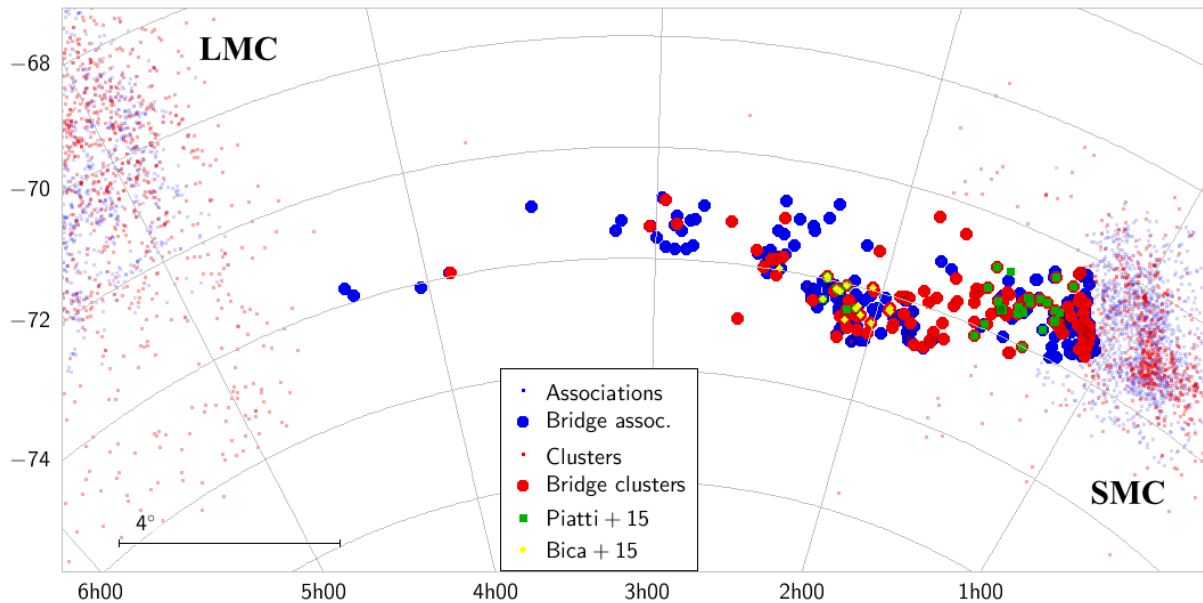
Figure 1.5: Orthographic sky projection showing the equatorial coordinates of the clusters and associations in the entire System, as catalogued by Bica et al. (2008, 2020). The 129 clusters and 320 associations (and transition objects) located in the Bridge are marked with larger circles. The targets studied in previous works are marked in green (Piatti et al., 2015) and yellow Bica et al. (2015).

most of them have been brought to the Bridge by tidal effects. Piatti et al. (2015) found four star clusters with ages from 1.0 to 6.3 Gyr (out of a total of 36), proving that there is indeed a mixture of populations in the Bridge.

Therefore, the study of the star formation history of the Bridge stellar population is quite complex, and requires deeper investigation since there are very few studies on this problem. In this thesis research, we obtained new observations of 33 Wing/Bridge clusters (Section 2), covering from the SMC to the middle of the Bridge (RA $< 3^h$), in order to study their star formation history and the metallicity gradients to be compared with those expected by the models. Photometric data from the SMASH and VMC surveys were also used as complement for a few clusters. According to Bica et al. (2020), the Wing/Bridge contains 129 clusters and 320 associations, so that our present sample corresponds to one fourth of the total. Figure 1.5 shows the entire Bica et al. (2008) catalogue, highlighting the Wing/Bridge objects, as well as the ones studied by Piatti et al. (2015) and Bica et al. (2015); a similar plot with the present sample is shown in Section 2.1.

Figure 1.6, extracted from Bica et al. (2020), shows the spatial distribution of all objects with available ages and metallicities in the literature. It is clear that the SMC have many more age determinations than the Bridge; in general, the central parts are filled with more
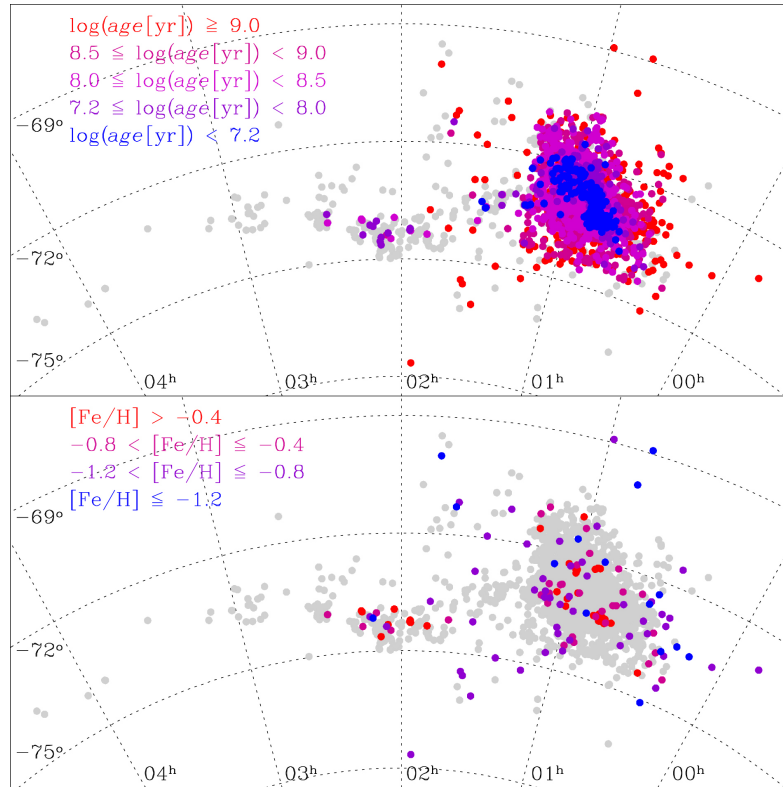
Figure 1.6: Spatial distribution in equatorial coordinates of the ages and metallicities available in the literature for the objects and associations in the SMC and Bridge. The objects in gray have no age or metallicity available. The Bridge has very few clusters with assigned age or metallicity values, mostly young clusters around RA $\sim 2^{\rm h}$. For the SMC, it is clear that younger and more metal-rich objects ([Fe/H] ~ -0.5) populate the central regions, whereas the older ones are located in the outskirts. Extracted from Bica et al. (2020).

young, metal-rich clusters than the outskirts (mostly > 300 Myr). Looking specifically at the Wing/Bridge, ages are available for 143 objects (46 clusters) mostly from Grondin et al. (1992), Parisi et al. (2014), Piatti et al. (2015) and Bica et al. (2015), whereas metallicities are available for 30 objects from Bica et al. (2015), Perren et al. (2017) and Parisi et al. (2009, 2015, the only ones from spectroscopy). The incidence of more young, metal-rich ([Fe/H] ~ -0.5) clusters near the SMC center deviates from the mean SMC metallicity ([Fe/H] $= -0.9 \pm 0.2$; Parisi et al., 2016), but is consistent with the star formation history of the SMC central region derived by Rubele et al. (2018) with VMC data.

The metallicity gradients (mainly obtained by photometric means) in the LMC and SMC are relatively well known (e.g. Cioni, 2009; Parisi et al., 2016; Choudhury et al., 2016, 2018). However, the lack of data and analysis in the Magellanic Bridge stellar populations leaves it with almost no information on gradients. Figure 1.7, also from Bica et al. (2020), shows the distribution of the age and metallicity of SMC and Bridge clusters
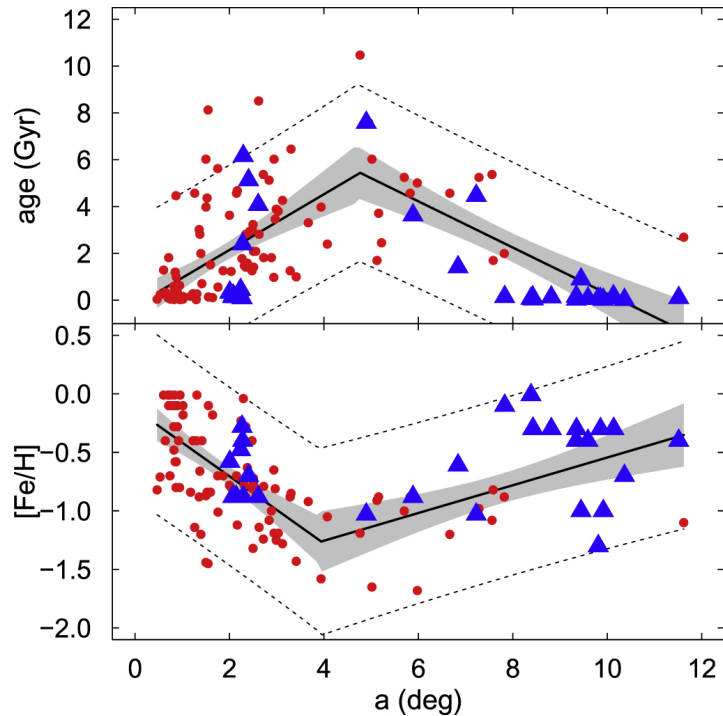
Figure 1.7: Age and metallicity of SMC and Bridge clusters as a function of the deprojected distance to the SMC center, computed from concentric ellipses (Piatti et al., 2005). Most of the clusters follow a gradient of increasing age and decreasing metallicity up to $a = 4 - 5°$, and an inversion after that. Extracted from Bica et al. (2020), updated in Section 6.

(red and blue symbols, respectively), as a function of the deprojected distance to the SMC center. The exact value of a(deg) is obtained from concentric ellipses with $b/a = 1/2$ and inclination of $45°$, as proposed by Piatti et al. (2005). In the figure, a linear regression with a breakpoint was fitted, showing an inversion of the gradients around $4 - 5°$: the ages increase up to 5 Gyr at this point and then inverts, whereas the metallicity decreases until $[\text{Fe/H}] = -1.2$ and then inverts. Figures 1.6 and 1.7, as well as a detailed age-metallicity relation, are updated in this work (see Section 6).

There are few precise age and metallicity estimates for the Bridge stellar systems, since they are predominantly investigated via photometry, being subject to low-quality photometry, incompleteness, and insensitiveness of the adopted photometric bands or methods. Moreover, the heterogeneity of the photometric (depth, seeing, adopted bands) and spectroscopic data (spectral resolution, spectral range, integration time), and of the adopted methods (isochrone fitting, distance calibration and metallicity) hamper a global analysis of the Bridge. In this sense, we carry out a comprehensive study in order to unveil the nature of the Bridge, by adopting a uniform methodology, applied to homogeneous photometric and spectroscopic data, and covering objects over all the Bridge extension.

1.5   Goals and structure of this thesis

As discussed in Harris (2007), no detailed analysis of the star formation history of the Bridge stellar populations have been performed so far. In this doctoral thesis, we carried out a homogeneous analysis of the age and metallicity of the objects in the SMC Wing and until halfway the Bridge (RA < 3^h). This allowed us to detect gradients and chemical signatures predicted by the dynamical (Diaz and Bekki, 2011; Besla et al., 2012) and chemical evolution models (e.g. Tsujimoto and Bekki, 2009), then contributing to a better understanding of the formation and evolution scenarios of the Magellanic System (D'Onghia and Fox, 2016), as well as providing important constraints for future dynamical and chemical models. The results obtained for clusters in other SMC regions (Northern Bridge, Counter-Bridge and West Halo) are also present, as well as some results obtained from a CaT analysis in GMOS spectra.

This thesis is structured as follows. In Chapter 2, we present the adopted databases: VISCACHA, SMASH and a tentative with VMC. In Chapter 3, the implemented methods and tools are presented in three parts: derivation of structural parameters from radial density profiles, statistical decontamination, and derivation of the fundamental parameters from statistical isochrone fitting. Chapter 4 presents the results obtained for the 33 Wing/Bridge clusters with VISCACHA data: for the structural (Oliveira et al., in prep.) and fundamental parameters (Oliveira et al., submitted to MNRAS), as well as some initial results with SMASH data (Oliveira et al., in prep.), evaluating them in terms of the gradients, spatial distribution and age-metallicity relation, as compared to the literature. In Chapter 5, the results obtained with a parallel works with clusters in other SMC regions (complemented with GMOS spectra in Dias et al. 2021, 2022; and Bica et al. 2022) and with RR Lyrae in bulge GCs (with OGLE and *Gaia* data; Oliveira et al., 2022) are shown. Finally, in Chapter 6, the conclusions and perspectives are drawn, including a follow-up both with photometry and spectroscopy.

Chapter 2

Data: photometry of Wing/Bridge star clusters

The present analysis of Wing/Bridge star clusters, started in 2019, was initially based solely on photometric data obtained within the VISCACHA collaboration. At that time, the first paper (Maia et al., 2019) and internal data release had just been published, with data for 88 clusters observed until 2016B. The study of the Bridge is one of the goals of the VISCACHA survey, which obtains deep, high-quality photometry of clusters located in the outskirts of the MCs, usually neglected in the literature in terms of age and metallicity. In the semesters 2019B-2021B, new observations of Wing/Bridge clusters with the SOuthern Astrophysical Research (SOAR) telescope were carried out with some limitations, due to bad weather and telescope closures due to COVID-19 pandemic.

In order to increase the sample, we also explored the photometric data from the Survey of the MAgellanic Stellar History (SMASH; Nidever et al., 2017) and VISTA YJK_S survey of the Magellanic Clouds system (VMC; Cioni et al., 2011). Together, they cover the entire Bridge extension with some limitations regarding spatial resolution and photometric depth. Figure 2.1 compares VISCACHA and SMASH data for the same cluster, showing colour-magnitude diagrams (CMDs) of the stars within decreasing radii around the cluster centre. The limiting magnitudes are similar, but the last CMDs present the niche of VISCACHA data: $V \sim 24\,\mathrm{mag}$ depth and stellar full width at half maximum (FWHM) $\sim 0.6\,\mathrm{arcsec}$ due to adaptive optics, allowing to study compact, old clusters down to $8\,\mathrm{Gyr}$ with faint sequences. For the MCs, it is only surpassed by HST ($V \lesssim 25\,\mathrm{mag}$, FWHM $\sim 0.1\,\mathrm{arcsec}$, available for the very central parts of ~ 100 clusters; Milone et al. 2023) and the future LSST survey ($r < 27.5\,\mathrm{mag}$, FWHM $\sim 0.7\,\mathrm{arcsec}$; Ivezić et al., 2019).

The VMC survey shares similar goals about the determination of the spatially-resolved star-formation history and the study of the 3D structure of the System, with near-infrared
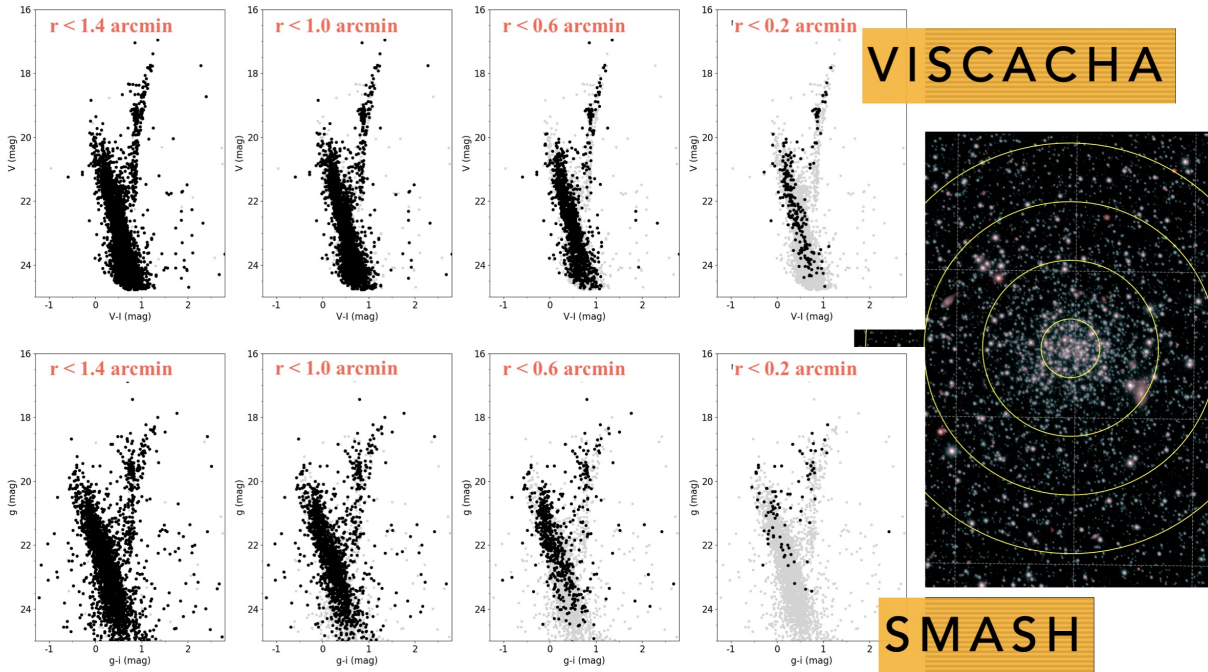
Figure 2.1: Comparison between VISCACHA (V vs. $V - I$, upper panels and composite BVI image) and SMASH (g vs. $g - r$, lower panels) photometry. The panels limit the stars inside a decreasing radius between $r < 1.4$ and 0.2 arcmin around the centre. The CMDs show similar magnitude limits, but the ones from VISCACHA are clearly more complete in the central regions, a consequence of using the adaptive optics system of the SOAR telescope (SAM). Extracted from Dias (2019).

photometry. It produced several important contributions, including some about star clusters and Bridge (e.g. Piatti et al., 2014, 2015; Schmidt et al., 2020), but the data are not deep enough for our purposes of obtaining a precise isochrone fitting for MCs clusters. Figure 2.2 compares the VMC data for the Bridge cluster L114 to the deep VISCACHA photometry obtained in 2016B. In this case, the VMC CMD is complete until $J < 20.5$ mag, a magnitude where the main sequence (MS) is still too vertical for a cluster in this age range of $30 - 40$ Myr, not providing enough constraints for the isochrone fitting. In the case of old clusters with MSTO around $V \sim 22 - 23$ mag, the situation is even worse. However, VMC data still can be useful in our case as a constraint for the reddening of the bright stars, as well as a first assessment of the photometry for young clusters to plan a follow-up for deeper observations.

Previous works have collected heterogeneous photometric data of large cluster samples to derive age and other fundamental parameters (e.g. Pietrzynski and Udalski, 2000; Palma et al., 2016; Perren et al., 2017), producing data with different qualities, photometric bands and analysis techniques, that precludes a hard constraint on the star formation history of the System. Recent photometric surveys observed mainly the inner regions of the MCs
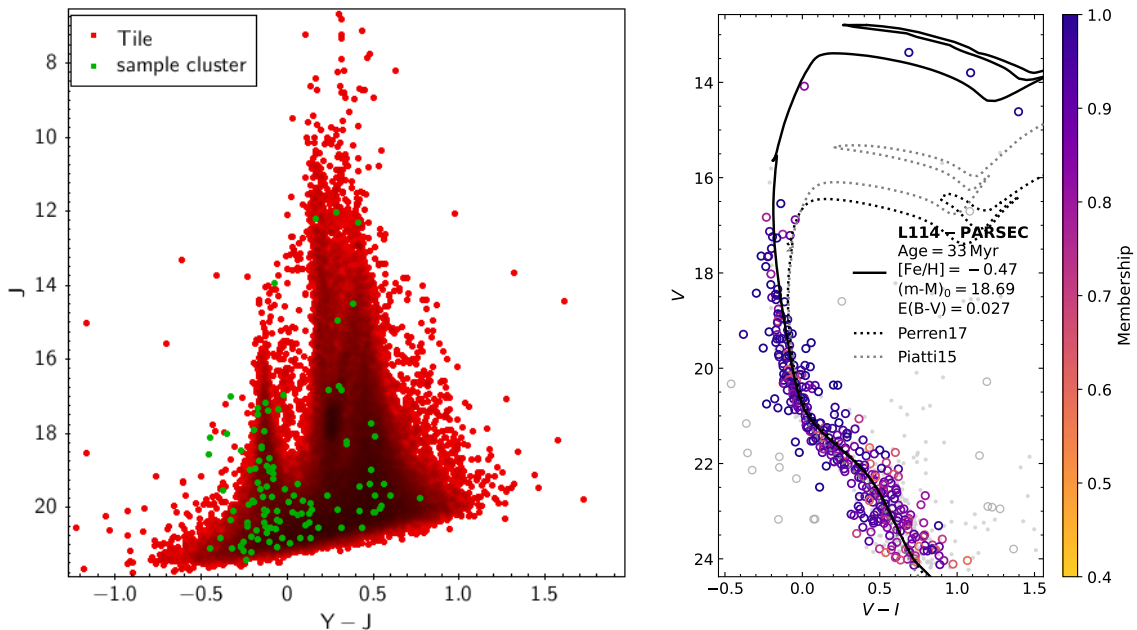
Figure 2.2: Comparison between the CMDs J vs. $Y-J$ (VMC) and V vs. $V-I$ (VISCACHA) for the young cluster L114. The evolutionary stages are clearly defined in the VISCACHA CMD, whereas the other CMD shows the same four giants above $J = 14\,\mathrm{mag}$ and a well-defined MS until $J = 19\,\mathrm{mag}$, but too much scatter below that due to incompleteness.

with increasingly better instruments (MCPS, Zaritsky et al. 2002; OGLE-IV, Udalski et al. 2015; STEP, Ripepi et al. 2014; DES, Abbott et al. 2018; *Gaia*, Gaia Collaboration et al. 2016; Skymapper, Wolf et al. 2018), but did not intend to obtain such deep, high-resolution imaging of the outermost clusters of the MCs. A detailed summary of these surveys is given in Maia et al. (2019, their table 1), and a summary of the VISCACHA, SMASH and VMC surveys are given in Table 2.1. Sections 2.1 and 2.2 provide further details about the two surveys adopted in this work, VISCACHA and SMASH, respectively.

Table 2.1 - Observational details of the VISCACHA (Maia et al., 2019), SMASH (Nidever et al., 2017) and VMC (Cioni et al., 2011) surveys. VISCACHA covers hundreds of clusters in the MCs outskirts, whereas the other two cover almost entirely the MCs, Bridge and other parts of the System. This table is based on table 1 from Maia et al. (2019).

Survey	Telescope	Field of view	Filters	Limiting mag.	Seeing
VISCACHA	SAMI @ SOAR 4.1 m	$3 \times 3\,\mathrm{arcmin}^2$	$B,\ V,\ I$	$V < 24\,\mathrm{mag}$	0.6 arcsec
SMASH	DECam @ Blanco 4 m	$r = 1.2°$	$ugriz$	$g < 24.8\,\mathrm{mag}$	$\sim 1.0\,\mathrm{arcsec}$
VMC	VIRCAM @ VISTA 4.1 m	$1.2° \times 1.2°$	JHK_S	$J < 21\,\mathrm{mag}$	$\sim 1.0\,\mathrm{arcsec}$
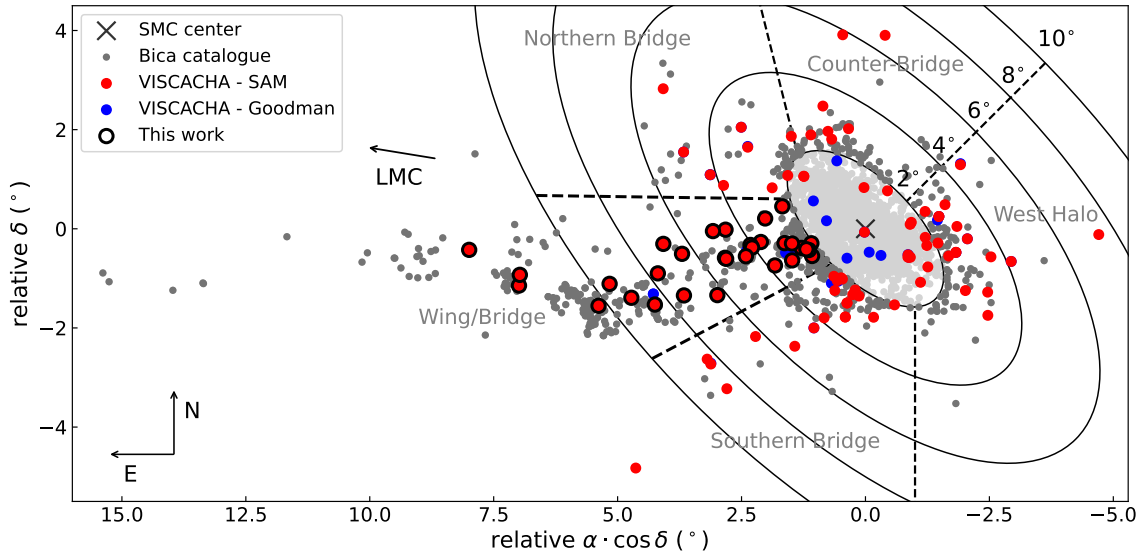
Figure 2.3: Projected distribution of the 2665 stellar clusters and associations from Bica et al. (2020, grey dots), with coordinates relative to the SMC centre ($0^h 52^m 45^s$, $-72°49'43''$; Crowl et al., 2001). The objects observed in VISCACHA with the SAM and Goodman instruments are marked in red and blue respectively, and the present sample of 33 Wing/Bridge clusters is marked with a black border. The arrow points to the direction of the LMC centre.

2.1   The VISCACHA survey

The VISCACHA survey[1] (PI B. Dias; Maia et al., 2019) is an ongoing project based on deep photometric observations of stellar clusters present at the periphery of the Magellanic Clouds and Bridge, usually not covered by large surveys. The acronym VISCACHA stands for "VIsible Soar photometry of star Clusters in tApii and Coxi HuguA", whereas viscacha is also the name of the little rodents, of the family of the chinchillas, that are native in the South America (mostly in the Atacama desert), where the SOAR telescope is based and where VISCACHA team has most of its members.

The observations use the adaptive optics module (SAM) at the SOAR 4.1 m telescope, in order to obtain a good spatial resolution even close to the central regions of faint, compact clusters. In order to achieve a deep photometry ($V \sim 24$ mag), long exposures of 20 and 30 minutes (after co-addition) are obtained in the V and I filters respectively, combined with short exposures to sample the bright stars. These aspects allow us to generate high-quality CMDs particularly for the old, compact clusters located in dense fields (with a field of view of 3.1×3.1 arcmin^2), usually not possible with wide-field surveys. The team

---

[1] `http://www.astro.iag.usp.br/~viscacha/`

has observed ~ 220 clusters since 2015, of which 33 are located in the Wing/Bridge region. Figure 2.3 shows the projected distribution of all the observed clusters in VISCACHA (including with Goodman in blue, as backup instrument), the present sample (black borders) and the Bica et al. (2020) catalogue. The ellipses are concentric around the SMC centre, and have $b/a = 1/2$ and inclination of $45°$, as proposed by Piatti et al. (2005), with the SMC outer regions subdivided according to Dias et al. (2021).

Maia et al. (2019) described a variety of problems that can be addressed with the VISCACHA data, such as the position dependence of the structural parameters of the clusters (Santos et al., 2020), the age/metallicity gradients and AMR, star formation history, 3D structure of the System from the distances. All these problems are explored in the present work. Maia et al. (2019) detail the instrumentation, data reduction, completeness, as well as the results of structural and fundamental parameters for nine benchmark clusters. The data were pre-processed using the IRAF CCDRED package, with cosmic ray removal with the CRUTIL package; astrometric calibrations was performed MSCCMATCH task using the *Gaia* EDR3 catalogue (Gaia Collaboration et al., 2021); point-spread function (PSF) photometry was carried out with a modified version of the `StarFinder` code (Diolaiti et al., 2000). Fields from Stetson (2000) and MCPS (Zaritsky et al., 2002) were used for photometric calibration. These steps were performed mainly by Prof. Francisco Maia.

The adaptive optics (AO) instrumentation reduces the effects of atmospheric turbulence by deforming the mirror to compensate the distortions in an incoming wavefront. In the case of the SAM@SOAR ground-layer system, the AO is obtained with an ultraviolet laser beam, an artificial guide star used as a wavefront reference (Tokovinin et al., 2016). Under ideal conditions, the instrument gives a PSF with FWHM of ~ 0.5 and $0.4\,$arcsec in the V and I filters respectively[2], which is close to the mean atmosphere-free seeing at Cerro Pachón. The spatial resolution obtained by VISCACHA is better than the aforementioned surveys, which allows to deblend the stellar sources even in very crowded regions. Figure 2.4 presents a comparison between the I-filter images of the cluster HW20 obtained with SAM and the SOAR Optical Imager (SOI, without AO) under comparable conditions, with a resulting stellar FWHM of 0.44 and $1.19\,$arcsec respectively (Maia et al., 2019).

Compared to other surveys covering the MCs, the VISCACHA data reach more than $2\,$mag deeper (e.g. 2MASS, MCPS, VMC), obtaining a signal-to-noise ratio of $S/N \approx 10$

---

[2] `http://www.ctio.noao.edu/soar/content/about-sam`
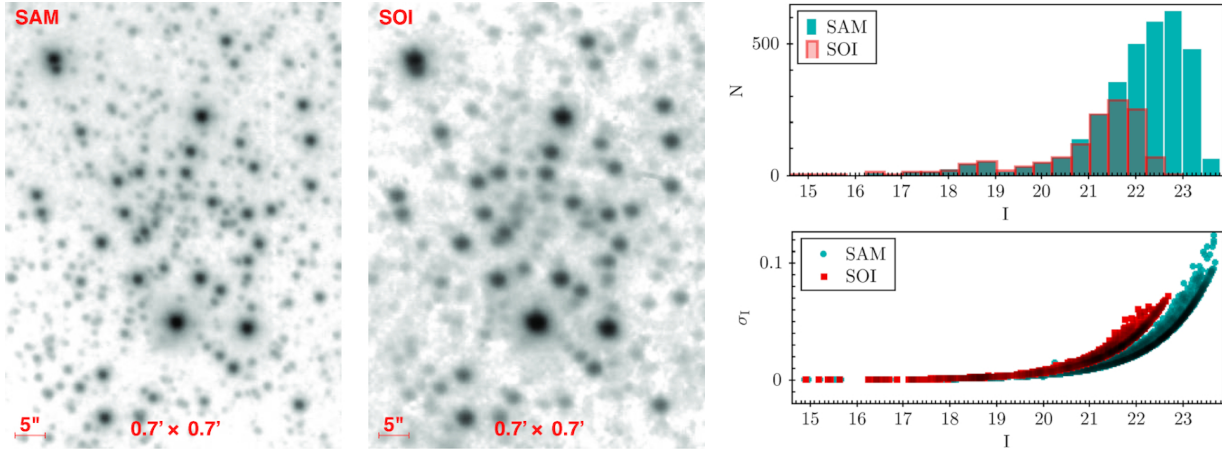
Figure 2.4: (Left:) VISCACHA observations for HW20 in the I filter, obtained with SAM (adaptive optics) and SOI. The resulting stellar FWHM are 0.44 arcsec and 1.19 arcsec, respectively. *(Right:)* Comparison of the photometric depth obtained with SAM and SOI for the same cluster, with the number of sources and photometric errors as a function of the I magnitude, under the same conditions. Extracted from Maia et al. (2019).

at $V \sim 24$ mag, very similar with those achieved by SMASH (5σ point source detection, i.e. $S/N = 5$ at $g \sim 24.8$; Nidever et al., 2017). These features usually reach well beyond the MSTO at $V = 21-22$ mag (or $22-23$ mag for the older clusters), with an angular resolution good enough to resolve crowded fields, allowing us to analyse not only the massive, young to intermediate-age clusters, but also unexplored low-mass and old clusters.

A total of 33 Wing/Bridge clusters were observed through the 2016B-2021B semesters, with two duplets located in the same SAMI field (HW81+HW82, L92+L93). Figure 2.5 shows the colour composite images obtained with the V and I filters for eight sample clusters. Table 2.2 presents the log of VISCACHA observations for the sample clusters, containing the observation date, airmass, seeing and the measured image quality (< 1 arcsec in most cases). All the sample clusters have RA $< 3^{\mathrm{h}}$, whereas the Wing/Bridge extends from $1^h 20^m$ to $\sim 4^h 30^m$ (Harris, 2007; Dias et al., 2021) beyond RA $= 3^{\mathrm{h}}$ there are essentially no clusters but sparse associations (see Figure 1.5), for which the AO is not very useful. Six associations were observed with the Goodman@SOAR imager (larger field of view of 7.2 arcmin diameter, data quality similar to SOI) so far, mostly located close to the SMC (blue symbols in Figure 2.3), namely NGC456, NGC460, ASS67, WG5, ASS65 and ASS66. They will be analysed in a future work, after we get more observations of objects closer to the LMC. Five LMC clusters close to the Bridge connection with the southwestern LMC were observed with SAMI and will be analysed in a future work.
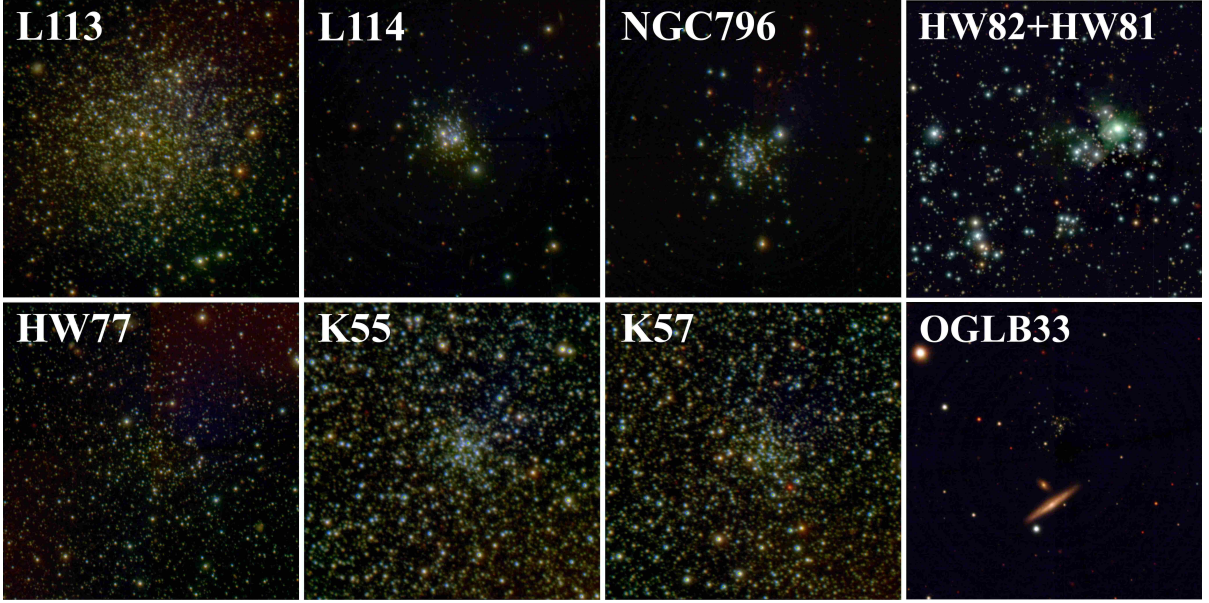
Figure 2.5: Composite *BVI* images of eight (out of 33) Wing/Bridge clusters obtained with VISCACHA data. The images have a field a view of $3 \times 3\,\mathrm{arcmin}^2$, with North up and East to the left. The pair of clusters contains a very young, farther cluster on the right (HW81, $4\pm1\,\mathrm{Myr}$, $[\mathrm{Fe/H}] = -0.11\pm0.18$; see Table 4.2) and a young cluster on the lower left (HW82, $50 \pm 13\,\mathrm{Myr}$, $[\mathrm{Fe/H}] = -0.41 \pm 0.15$). OGLB33 is a very compact, old cluster, and contains a galaxy close to the line-of-sight (2MFGC 2124, $z \sim 0.057$; Jones et al., 2009).

Table 2.2 - Log of VISCACHA observations of Wing/Bridge clusters, separated by semester (2016-2021B). The coordinates are from Bica et al. (2020) or the average of the SAMI field for the two pairs. The seeing and FWHM are given for the *V* and *I* bands, obtained combining short and long exposures (3×400s and 3×600s, respectively).

Cluster	RA	Dec.	Date	Airmass	Seeing*	FWHM
	(h:m:s)	(°:′:″)			(arcsec)	(arcsec)
K55	01:07:32.5	−73:07:14	2016-09-28	1.47	0.8, 0.9	1.0, 0.8
K57	01:08:14.0	−73:15:27	2016-09-28	1.55	0.7, 0.8	0.8, 0.7
HW71se	01:15:32.2	−72:22:44	2016-11-03	1.35	1.4, 1.3	1.3, 0.9
HW77†	01:20:11.0	−72:37:19	2016-11-05	1.36	0.9, 0.9	0.5, 0.3
BS187†	01:31:01.8	−72:51:01	2016-11-03	1.38	1.3, −	1.4, 1.1
BS198	01:47:57.9	−73:07:47	2016-09-24	1.49	1.1, 1.3	1.1, 0.7
L113	01:49:30.3	−73:43:40	2016-11-05	1.47	0.9, 1.0	0.6, 0.4
L114	01:50:19.3	−74:21:21	2016-11-05	1.43	0.8, 0.9	0.5, 0.4
NGC 796	01:56:44.6	−74:13:10	2016-11-05	1.77	−, −	0.6, 0.4
L92+L93	01:12:38.9	−73:28:11	2017-10-22	1.45	1.0, 1.0	1.0, 0.9
L109†	01:33:14.3	−74:09:58	2017-10-22	1.60	0.8, 0.8	0.9, 0.6

Continued on next page...

Tabela 2.2 - continued

Cluster	RA	Dec.	Date	Airmass	Seeing*	FWHM
HW86	01:42:23.3	-74:10:28	2017-10-22	1.49	1.0, 0.9	0.9, 0.7
HW55†	01:07:20.0	−73:22:39	2018-10-05	1.55	0.8, 0.7	1.1, 1.0
OGLB 33	02:41:03.6	−73:15:12	2018-12-12	1.39	0.8, 0.8	0.9, 0.6
HW63†	01:10:12.3	−73:12:32	2019-10-05	1.53	−, −	0.9, 1.0
L91	01:12:51.6	−73:07:07	2019-10-05	1.37	−, −	0.7, 0.6
B147	01:14:50.5	−73:06:49	2019-10-05	1.45	−, −	0.8, 0.7
WG1	01:42:52.7	−73:20:09	2019-10-05	1.52	−, −	0.8, 0.7
WG13	02:02:40.9	−73:56:23	2019-12-22	1.46	0.8, 0.7	0.9, 0.7
BS245	02:27:27.6	−73:58:27	2020-11-11	1.43	0.8, −	0.8, 0.5
HW75	01:17:29.9	−73:34:15	2020-11-11	1.41	0.6, 0.5	0.6, 0.4
HW78	01:21:20.7	−73:05:40	2020-11-13	1.39	−, −	1.3, 1.1
HW81+HW82	01:24:17.0	−73:09:18	2020-11-11	1.37	−, −	0.7, 0.5
L101	01:23:44.2	−73:12:29	2020-11-13	1.37	1.1, −	1.5, 1.2
L104	01:25:26.1	−73:23:17	2020-11-12	1.40	−, 0.4	0.7, 0.4
L107	01:31:06.7	−73:24:45	2020-11-12	1.38	0.8, 0.6	0.6, 0.5
L110	01:34:26.0	−72:52:28	2020-11-11	1.37	−, 0.7	0.6, 0.4
HW59†	01:08:53.5	−73:14:51	2021-11-07	1.44	−, −	0.6, 0.6
ICA45	02:27:13.3	−73:45:27	2021-11-09	1.39	0.6, −	0.7, 0.5
B165	01:30:50.5	−73:26:03	2021-11-11	1.44	0.8, 0.9	1.2, 0.9
BS226	02:05:41.9	−74:22:53	2021-11-11	1.43	0.9, −	0.9, 0.9

† Clusters in common with the GMOS sample from Dias et al. (in prep.)

∗ Those marked with - could not be retrieved from the site seeing monitor

2.2 Survey of the MAgellanic Stellar History (SMASH)

The Survey of the MAgellanic Stellar History (SMASH; PI D. Nidever; Nidever et al., 2017) is a survey that covered uniformly 2400 deg^2 of the Magellanic System, with the *ugriz* photometric system of the Dark Energy Camera (DECam). The camera is mounted at the prime focus of the Blanco 4 m Telescope at the Cerro Tololo Inter-American Observatory (CTIO), and covers a circular region of 2.2 deg wide with a mosaic of 62 CCDs.

The first data release (DR1) was presented in Nidever et al. (2017) and contains ∼ 100 million objects distributed in 61 fields. The SMASH DR2 was released in September 2019 (Nidever et al., 2021), with 4 billion measurements for 360 million objects (averages over several exposures), distributed in 197 fields. Some of them are shown in Figure 2.6, covering
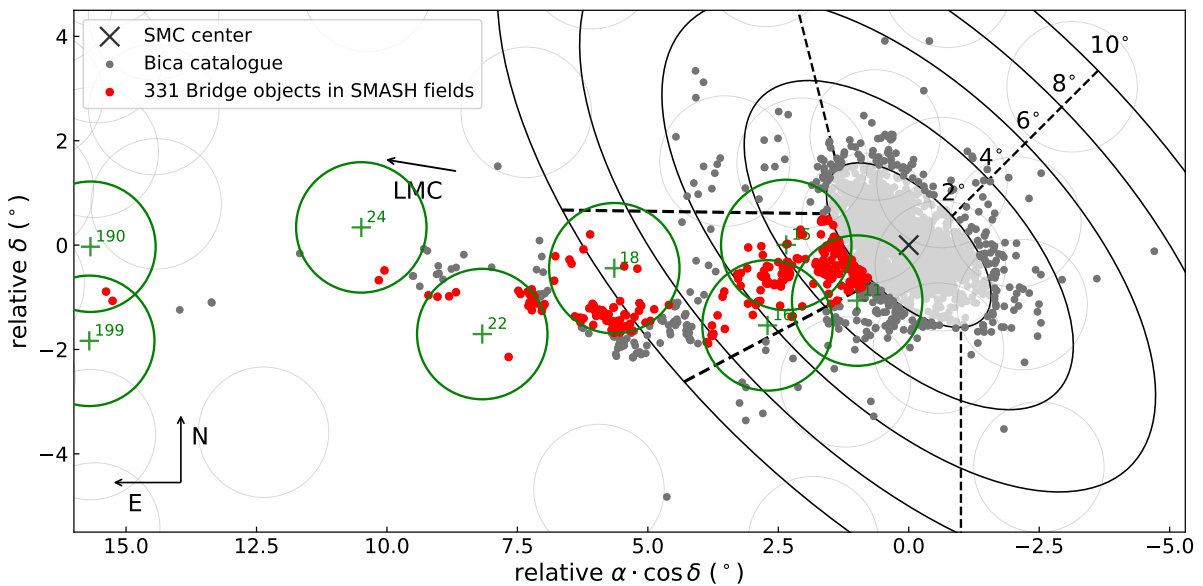
Figure 2.6: Same projection as Figure 2.3, showing that SMASH DR2 fields (Nidever et al., 2021) cover the entire SMC main body and portions of the outer regions, including the Bridge. The ~ 300 Wing/Bridge objects inside the fields of interest are marked in red.

entirely the LMC and SMC, and distributed homogeneously in the other components of the System (Bridge in green, Stream and Leading Arm).

Not by chance, the study of the Stream and the other gaseous components is one of the SMASH central goals, which is to identify extended, low-surface brightness stellar populations associated with galactic halos and tidal debris. It was meant as a complement to the Dark Energy Survey, which covers the northern periphery of the MCs, including the Stream (e.g. Koposov et al., 2015). Other goals involve the derivation of the star formation history over a large age range and in regions with large radii, and the identification of new clusters. Dias (2019) showed that, despite covering less objects, VISCACHA can constrain the ages of clusters slightly older than with SMASH, due to the use of AO.

We obtained the SMASH DR2 data from the NOAO Data Lab[3], already reduced and calibrated for the SDSS *ugriz* filters (Fukugita et al., 1996). We implemented an ADQL[4]-based code to recover automatically complete catalogues of an entire field and then isolate the cluster region. The gaps between the detectors hinders the star counts and the photometry itself, both important for the fitting of King profiles and isochrones. In order to account for these gaps, we applied the quality flags from Martínez-Delgado et al. (2019)

---

[3] `https://datalab.noao.edu/smash/smash.php`

[4] Astronomical Data Query Language, used to retrieve tables from large databases.
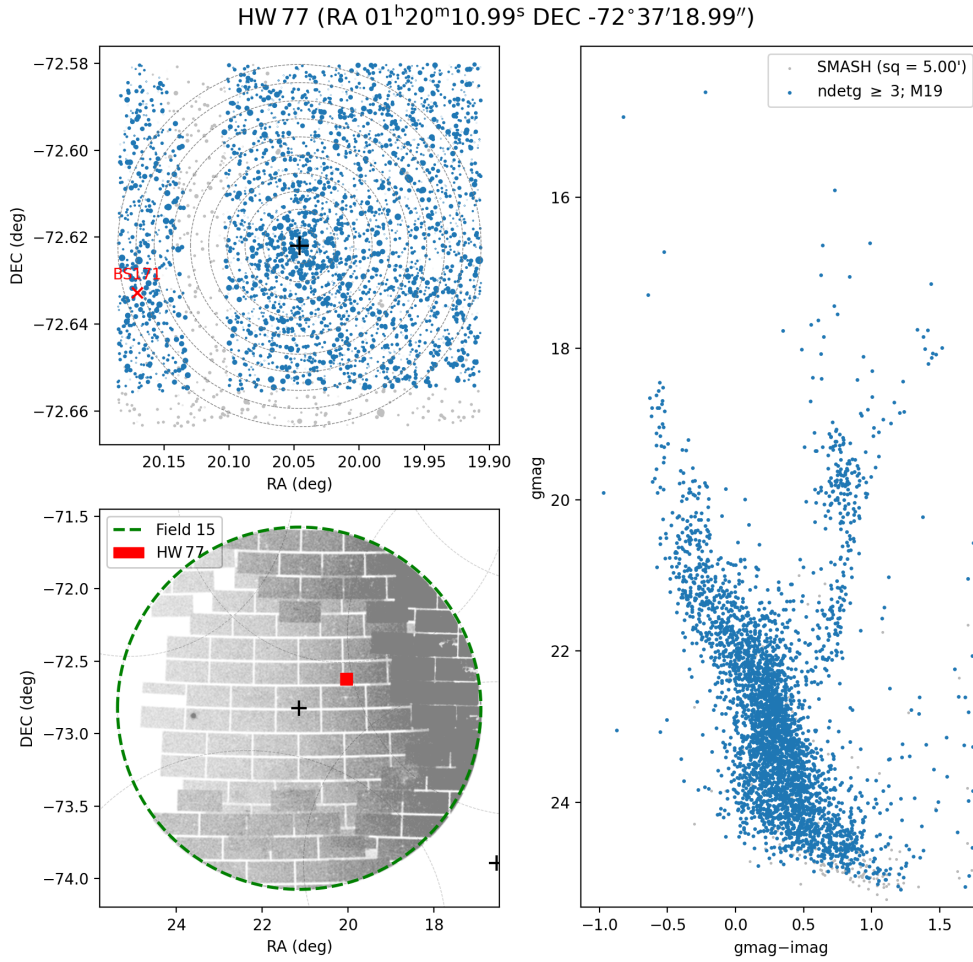
Figure 2.7: SMASH data for the Wing/Bridge cluster HW77, close to vertical and horizontal gaps (identified with $ndetg \geq 3$ and flags from Martínez-Delgado et al., 2019). *(Left:)* Equatorial coordinates of the sources retrieved in a field of $5 \times 5 \, \text{arcmin}^2$ (upper panel) and of the entire Field 15 (lower panel). *(Right:)* g vs. $g-i$ CMD with the stars outside the gap shown in blue, clearly contaminated with a lot of field stars.

and detected the stripes in RA and Dec. corresponding to the gaps by using the number of detections in the g filter ($ndetg < 3$). Figure 2.7 shows this procedure for the Wing/Bridge cluster HW77 inside the SMASH field 15, located close to a vertical and a horizontal gap. The fraction of cluster stars inside the gaps are then taken into account in all steps of the analysis (see Chapter 3), and the coordinate ranges that correspond to a vertical and/or horizontal gap are recorded in the catalogue header. The SMASH fields cover more than 300 of the 449 Bridge objects, but less than 1/3 of them have good quality data and are more than 1 arcmin distant from the detector gaps. Fifteen of them are in common with the VISCACHA sample and a selection of them is being studied (Oliveira et al., in preparation; see Section 4.3).
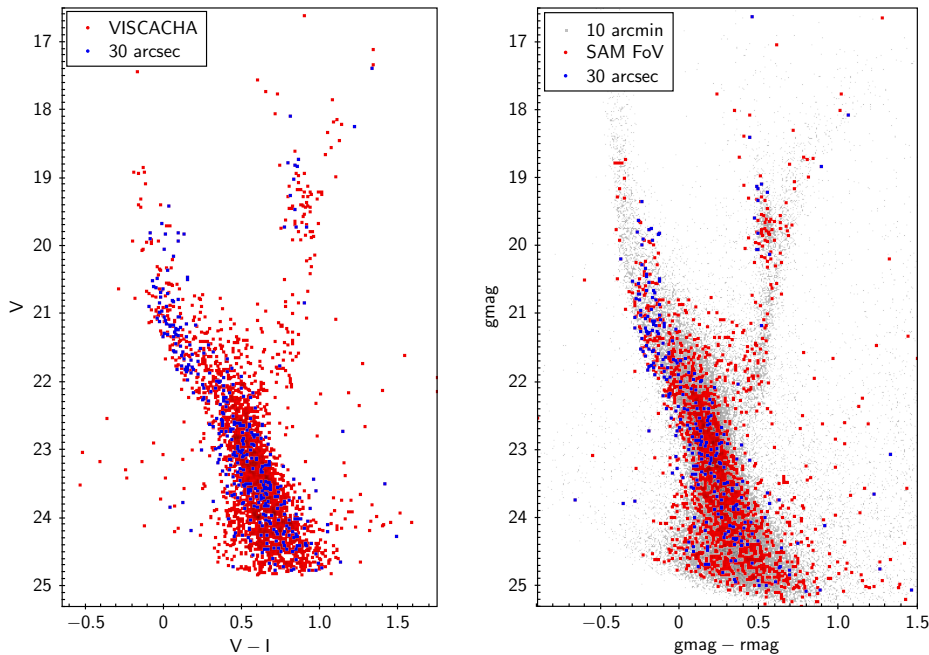
Figure 2.8: Comparison between the CMDs of Wing/Bridge cluster HW77, as observed by VISCACHA (left panel) and SMASH (right panel). The VISCACHA data were obtained in a night with perfect conditions for the use of AO. The limiting magnitude are comparable in both CMDs (V and $g \sim 24.5$). The red points correspond to the SAM FoV of 3×3 arcmin, and the blue ones are the central 30 arcsec (mostly member stars). The isochrone fits in both CMDs are shown in Figures 4.10 and 4.11.

Figure 2.8 gives a comparison between the *BVI* photometry from VISCACHA and *ugriz* from SMASH for the Wing cluster HW77 (1.4 Gyr; Piatti et al., 2015). The VISCACHA data for this cluster were obtained in a night with ideal weather conditions for the use of AO; consequently, a FWHM of 0.5 and 0.3 arcsec were obtained in the V and I filters, and a limiting magnitude larger than $V \sim 24$ mag was achieved. Nidever et al. (2017) state that the 5σ point source depths for the SMASH photometry are 23.9, 24.8, 24.5, 24.2 and 23.5 mag for the *ugriz* filters, respectively, with a median seeing of 0.7 arcsec. Therefore, in terms of limiting magnitudes, the VISCACHA data obtained in ideal conditions is comparable to SMASH. The comparative results obtained for HW77 with the two photometric systems are presented in Section 4.3, providing very similar results.

Nidever et al. (2021) explain that the strategy of the SMASH survey is continued as part of the DECam Local Volume Exploration survey (DELVE; Drlica-Wagner et al., 2022). DELVE gathers archival data from several DECam surveys (e.g. SMASH, DES) with new observations and reprocess the photometry, obtaining more homogeneous data

with a depth comparable to SMASH. Their available footprints[5] suggests that the entire Magellanic System is covered, including the Bridge. From a quick comparison of the DELVE photometry for HW77 and other clusters and association in the Bridge, we conclude that it covers a larger fraction of the Bridge, with missing data for some objects and low-quality data around bright stars. After carefully checking DELVE data for the entire Bridge extension, we proposed to observe 36 clusters and associations (not covered by VIS-CACHA, SMASH and DELVE) with the Goodman@SOAR imager, in order to complete the sample and get a more homogeneous derivation of ages and metallicities.

---

[5] `https://delve-survey.github.io/#progress`

Chapter 3

Methodology: analysis of the photometric data

In order to ensure a robust and homogeneous analysis, we have implemented methods with machine learning and Bayesian inference for parameters derivation, the latter applying the Markov chain Monte Carlo sampling (MCMC, with the `emcee` code; Foreman-Mackey et al., 2013). Our analysis includes three steps to be applied to all clusters and associations on the Bridge with available data: a new code for fitting King models (King, 1962) to radial density (and brightness) profiles to obtain structural parameters (Section 3.1); adaptations to a code for statistical decontamination of field stars present in the photometry, involving machine learning methods (Section 3.2); and adaptations to the `SIRIUS` code for statistical isochrone fitting in the decontaminated CMDs (Section 3.3).

Some of the tools were developed and applied during my Master studies (Oliveira, 2019; Souza et al., 2020; Oliveira et al., 2020) or in previous projects (Maia et al., 2010), and are being improved in this work, in collaboration with other members of the group. Other works in which some of these tools are also applied are described in Chapter 5.

3.1   Structural parameters from the radial distribution of stars

The King profile (King, 1962) is an empirical model that reproduces the radial density profile (RDP) of stars in a star cluster, i.e. how stars are distributed in a cluster around its centre. It is based on four structural parameters: tidal radius (r_t, the most important to this work), i.e. the cluster truncation radius or the radius at which the surface density reaches zero after subtracting the background density; core radius r_c, a scale factor defined as the distance at which the projected stellar density (or the apparent surface brightness) drops by half of its central value; central surface density (ρ_0) and density of background

stars (ρ_{bg}). Other structural parameters such as the half-light, half-mass and Jacobi radii are frequently adopted in the literature (e.g. Bonatto and Bica, 2008; Santos et al., 2020; Gatto et al., 2021) but are outside of the scope of this thesis.

The King analytical profile to model the RDP was derived empirically by King (1962) for globular clusters and is given by the expression:

$$\rho(r) = \rho_0 \left[\frac{1}{\sqrt{1 + (r/r_c)^2}} - \frac{1}{\sqrt{1 + (r_t/r_c)^2}} \right]^2 + \rho_{\text{bg}} , \qquad (3.1)$$

where $\rho(r)$ is the predicted stellar density at a radius r measured from the cluster centre. We can easily check that the density $\rho(r)$ drops to the background density level for $r = r_t$, and that it drops to $\sim 1/3$ of the central value for $r = r_c$. By integrating $\rho(r)$ with respect to $2\pi r dr$, it is possible to obtain the number of stars enclosed in a specific radius to the center (equation 18 of King, 1962) or alternatively the fraction of r_t at which a percentage of the cluster stars is enclosed (see Section 3.2).

By assuming that all stars follow the same mass-luminosity relation, according to King (1962, which naturally assumes that all stars have the same mass and that the cluster is spherically symmetric), it is also possible to derive an expression for the surface brightness profile (SBP), i.e. how the luminosity per unit area decreases with the radius, in units of mag/arcsec^2. Following Santos et al. (2020), the surface brightness at a radius r, in terms of the central surface brightness (μ_0), r_c and r_t, is given by:

$$\mu(r) = \mu_0 + 5 \log \left[1 - \frac{1}{\sqrt{1 + (r_t/r_c)^2}} \right] - 5 \log \left[\frac{1}{\sqrt{1 + (r/r_c)^2}} - \frac{1}{\sqrt{1 + (r_t/r_c)^2}} \right] . \quad (3.2)$$

Studies of young LMC clusters by Elson, Fall e Freeman (1987, EFF) have shown that they do not appear to be tidally truncated and present very large haloes, possibly caused by the cluster expansion due to mass loss or relaxation. In this case, their EFF models, defined as $\mu(r) = \mu_0(1 + r^2/a^2)^{-\gamma/2}$ where a is related to the r_c and γ is the power law slope at larger radii, may provide better results. Dynamical models (e.g. King, 1966; Gieles and Zocchi, 2015) would be even more suitable, but to reach a good precision they require the velocity distribution of the cluster outer regions. According to King (1966), his empirical model from 1962 is very close to the dynamical one for clusters with $c = \log(r_t/r_c) \lesssim 1.5$, which is compatible with the present sample (the largest is 1.07 for HW55; see Table 4.1).
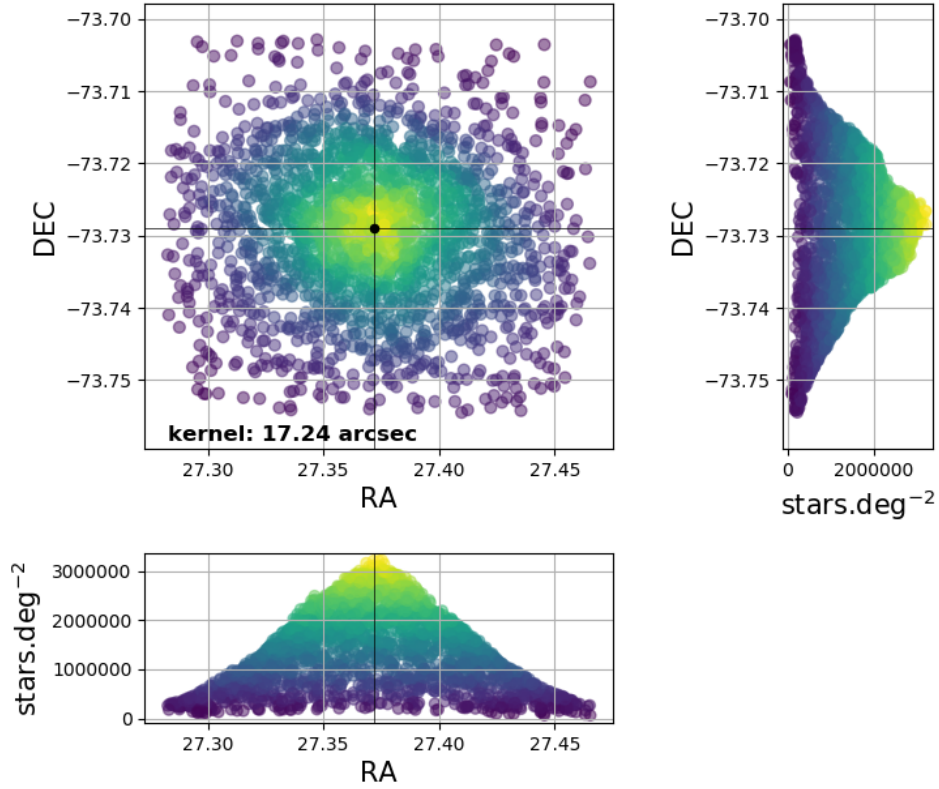
Figure 3.1: Layout of the method implemented to generate the radial density profile (lower right panel). The upper left panel presents the equatorial coordinates of all N stars detected in the photometry of L113, each star with a local calculation of the density in a circle containing $\sqrt{N}$ stars. The other two panels present the 1D projections in each coordinate.

At this first moment, we decided to apply only the King models to RDPs and leave the SBPs for a future work, as well as the EFF and dynamical models.

We developed a `Python` code from scratch to produce a reliable RDP from the coordinates of the observed photometry, followed by a statistical fitting of King empirical models to obtain the structural parameters. It is a crucial first step in the analysis of the photometric data of star clusters, since the tidal radius and background density are considered in the statistical decontamination of field stars (detailed in Section 3.2).

The traditional approach to obtain an RDP consists on performing stellar counts in concentric rings around the cluster centre, resulting in a density vs. radius plot with only a few points. In order to get a more robust statistics even for clusters and associations with few stars, we opted for an alternative approach: evaluate the density around each of the N stars retrieved in the photometry, using a circle (in the RA-Dec. plane) with an adaptive radius R_i that contain $\sqrt{N}$ stars, through $\rho_i = \sqrt{N}/(\pi \cdot R_i^2)$. This allows us to avoid one the major problems faced by the traditional, fixed-sized annular bins, so that regions with

high stellar density will be probed by smaller circles (improving the resolution towards the centre), while sparser ones will be probed by larger circles (improving the statistics towards outer regions). In this way, every star contributes with a local stellar density estimation, as shown in Figure 3.1 for the Bridge cluster L113 with VISCACHA data.

The stellar crowding and completeness, specially near the cluster centre, are very important and can accounted for by adding artificial stars to the field (e.g. Maia et al., 2019) or a similar method. However, since at this point we are primarily interested in the cluster tidal radius (to give a measure of its size and be applied in the decontamination), we leave the correction for completeness to a future work (Oliveira et al., in preparation). As discussed in Santos et al. (2020), differently from the core radius, the tidal radius and cluster centre derived from RDPs are largely unaffected by incompleteness.

In order to fit the King models on the RDP data, the determination of the best set of structural parameters is based on a likelihood function together with the MCMC method (Foreman-Mackey et al., 2013). This sampling method spreads a number of independent, random walkers in a 6-dimensional parameter space, namely: $\alpha_{\rm cen}$, $\delta_{\rm cen}$, ρ_0, r_c, r_t and $\rho_{\rm bg}$. The central coordinates of the cluster are also considered as a free parameter, since the radius of all stars to the centre is recalculated in each iteration.

The random walkers perform a given number of steps in the parameter space, looking for the convergence in a solution that will maximise the likelihood. The likelihood corresponds to the probability that a given King model represents the distribution of stellar densities as a function of the radius in the RDP. In our case, the likelihood L_i is given by a chi-square (χ^2) comparing the density around star i to that predicted by the model j (with tentative parameters σ_0, r_c, r_t and $\rho_{\rm bg}$) at the radius which the star is located:

$$L_i = \exp(-\chi_i^2) \propto \exp\left[-\frac{(\rho_{i,data} - \rho_{j,model})^2}{2\sigma_{i,data}^2}\right] \, , \tag{3.3}$$

where $\rho_{i,data}$ is the density around the star i, $\rho_{j,model}$ is the density predicted by the tentative King model at the radius r, and $\sigma_{i,data}$ is the statistical Poissonian error of each density estimation, i.e. $\sigma_{i,data} = \sqrt{N}/(\pi \cdot R_i^2)$. The final likelihood of a tentative model is given by the natural logarithm of the product with the contribution of all N stars:

$$\mathcal{L} = \ln\prod_{i=1}^{N} L_i = \sum_{i=1}^{N} \ln(L_i) \propto \sum_{i=1}^{N}\left[-\frac{(\rho_{i,data} - \rho_{j,model})^2}{2\sigma_{i,data}^2}\right] \, . \tag{3.4}$$
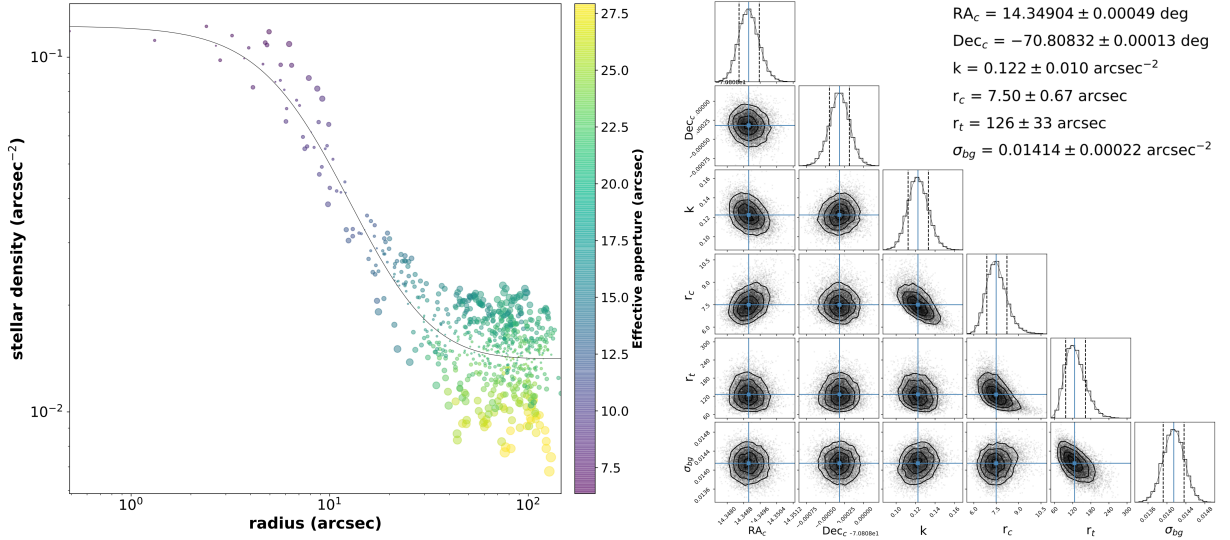
Figure 3.2: (Left:) Radial density profile of HW33 with the best fit King model, colour-coded by the aperture size necessary to include $\sqrt{N}$ stars. *(Right:)* Corner plots with the posterior probability distributions obtained from MCMC. The diagonal panels show the posterior for the six free parameters, and the remaining ones show the correlations between each two parameters. A skewed gaussian is fitted to each histogram to account for distributions with tails, and the corresponding solution and 1σ is given in the upper right. The dashed lines correspond to the 16 and 84th percentiles.

For each combination of six tentative parameters, the function $\mathcal{L}$ returns a value which the higher it is, the more plausible that this combination of parameters is the best solution for the cluster. The sampling of the 6D-parameter space is performed by the `emcee` package ("The MCMC Hammer"[1]; Foreman-Mackey et al., 2013) and shown graphically in the so-called corner plot (`corner.py`[2]; Foreman-Mackey, 2016). This plot illustrates 1D and 2D projections of the posterior probability distributions of the solution, showing the confidence intervals and correlations between the parameters.

Figure 3.2 shows an example of our results for HW33, which are also shown in Chapter 4. As given in the diagonal panels of the corner plot, the method provides a posterior probability distribution in the form of a histogram, marking the median and the 16th/84th percentiles in each parameter. Since there are some cases where the posterior presents non-symmetric features (e.g. a tail), we fit a skewed gaussian to the posterior distributions to achieve a more consistent peak and symmetric 1σ uncertainties. Figure 3.3 shows the evolution of each walker's state in the simulated MCMC chain (called tracer plot) for HW33.

---

[1] `https://emcee.readthedocs.io/en/v2.2.1/`

[2] `https://corner.readthedocs.io/en/latest/`
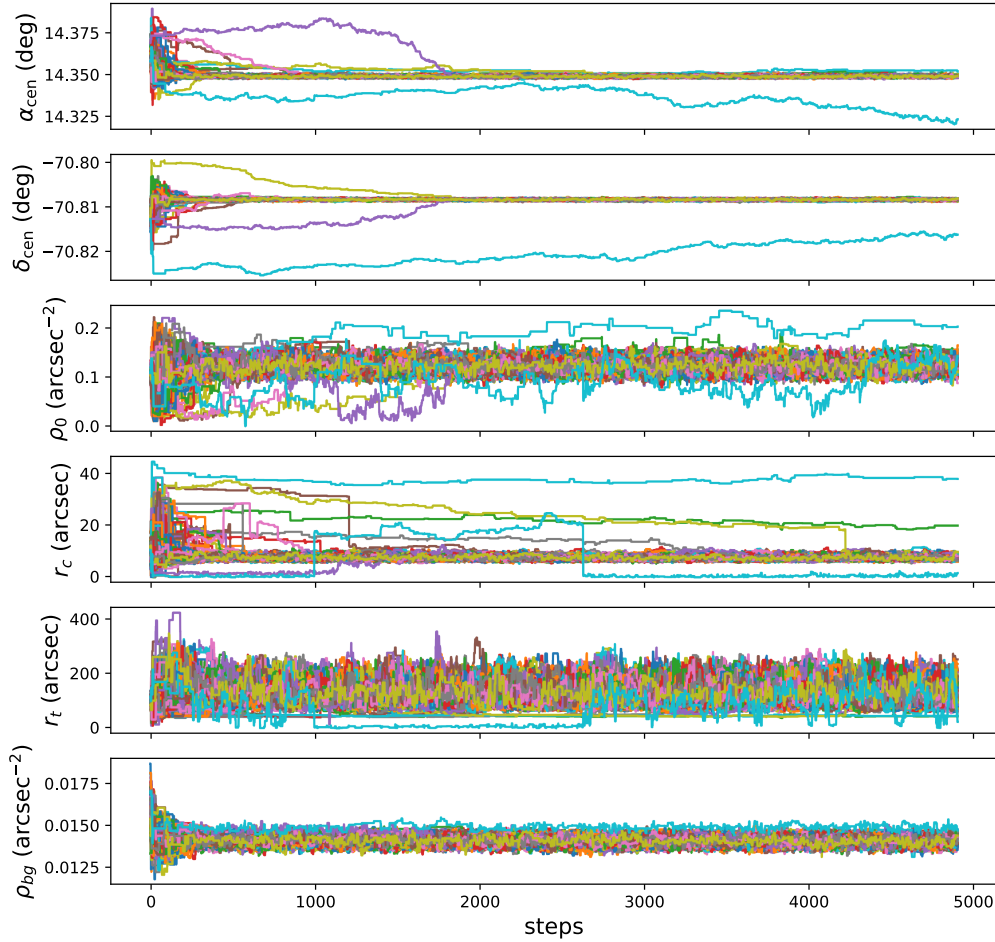
Figure 3.3: Tracer plots showing the evolution of the convergence of walkers in the simulated chains for HW33 (same as Figure 3.2). Each panel shows the convergence for each parameter, whereas each line corresponds to an independent walker. In this case, the convergence of the walkers (related to the autocorrelation time) is reached with 4900 steps.

The chains are executed until the current autocorrelation time[3] is shorter than the 1% of the current chain length (i.e. the current number of steps) and its variation since the last iteration is smaller than 1%, leading to convergence. Since each parameter has its own autocorrelation time, they can converge at different chain lengths; overall, the tidal radius was the slowest parameter to converge in our chains. In the case of HW33, the walkers were very scattered in the tidal radius (leading to larger uncertainties), but convergence is reached for all parameters after 4900 steps, according to convergence tests.

It is interesting to note that this method can be applied to other astronomical objects with structure predicted by models, such as ultra-faint dwarf galaxies (Richstein et al.,

---

[3] The autocorrelation time in MCMC methods is an estimate of the number of number of steps required for the walkers to lose memory and become decoupled of their current state.

2022). When applied to SBPs, the method can also be used to derive integrated cluster masses from integrated magnitudes and simple stellar populations' models and, if applicable, to extrapolate the mass for a cluster for which the full extent has not been observed. The results of this method are shown in Section 4.1, as applied for the 33 Wing/Bridge clusters with VISCACHA data, along with a comparison with the literature (Hill and Zaritsky, 2006; Santos et al., 2020).

3.2 Statistical decontamination: cleaning the data

There are several physical processes that hinder the photometry and characterisation of stellar clusters and associations, such as the contamination by field (non-member) stars in the line of sight, the stellar crowding in more compact clusters, the interstellar reddening (not as high in the Bridge as toward the MCs; e.g. Skowron et al., 2021) and increasingly fainter stars due to the large distances. The stellar crowding and large distances problems are mitigated in the VISCACHA photometry, by using the adaptive optics to increase the spatial resolution (not present in SMASH data), and by obtaining very deep photometry compared to other surveys (see Section 2).

However, concerning the presence of field stars, we need to implement a membership analysis, in order to obtain a final CMD containing only the higher-membership-probability stars. It can be achieved by two methods, depending on the available data: astrometric, using proper motions, parallaxes and radial velocities (more precise, e.g. Bellini et al., 2009; Oliveira et al., 2022), or photometric, directly from the positions and magnitudes. *Gaia* proper motions are available until $G \sim 20 - 21 \, \mathrm{mag}$ with an uncertainty $> 1.2 \, \mathrm{mas \, yr^{-1}}$ (Lindegren et al., 2018), therefore in the case of MCs clusters ($V_{\mathrm{MSTO}} \sim 22 \, \mathrm{mag}$) we use the measured positions and magnitudes. Based on some aspects of Bonatto and Bica (2007), Maia et al. (2010) developed a method that also takes into account the spatial distribution of stars. Since it has been successfully used in the VISCACHA data, we adopted it in this work and I started to work with Prof. Francisco in improving some features.

This method is based on the definition of a nearby region (at $r > r_t$) as a field sample (i.e. containing only field stars), and how its photometry compares with that of the cluster region ($r < r_t$, containing member and field stars) in the CMDs. Evaluating the expression for the number of stars as a function of the radius (King, 1962) for several combinations
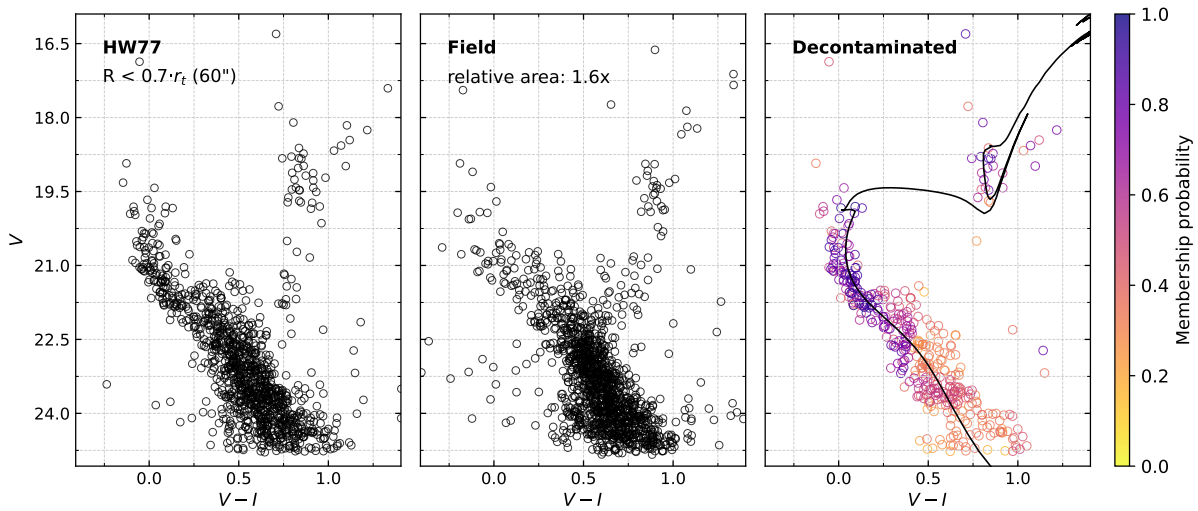
Figure 3.4: V vs. *V − I* CMDs for the SMC Wing/Bridge cluster HW77 with VISCACHA data, showing the inputs and the output of the statistical decontamination method. *(Left:)* Initial CMD with the stars inside 60 arcsec (i.e. 70% of the derived tidal radius). *(Middle:)* Initial CMD with all the stars outside the tidal radius, with a relative area 1.6 greater than that of the first CMD. *(Right:)* Final decontaminated CMD, colour-coded by the membership probability and with a PARSEC isochrone of ∼ 1 Gyr overlaid.

of r_c and r_t, it becomes clear that the vast majority $(> 99\%)$ of cluster stars are within a radius of $\sim 0.7 \cdot r_t$ independent of the concentration parameter c (see figure 1 from Bonatto and Bica, 2008). Therefore, in the decontamination method, it is not necessary to extend the cluster region up to $r < r_t$, but it is enough to limit in $0.7 \cdot r_t$, avoiding to include too many field stars in the initial cluster sample.

The statistical comparison between the initial samples for cluster and field is carried out in a 2D CMD with axes $(V, V − I)$ for VISCACHA, and 3D $(g, g − r, r − i)$ for SMASH data. The comparison is made star-by-star, based on the photometric similarity of the star with the nearby field, and on its distance from the centre; then assigning a membership probability value depending on the overdensity around the star position in the cluster and field CMDs, using several grid configurations. A detailed description is given in Maia et al. (2010). My main contributions to the method were in inserting more constraints, such as the density around each star (see Section 3.1) as an additional constraint when comparing the cluster with the field sample, and porting the entire code to `Python`.

Figure 3.4 illustrates the decontamination method for the Wing/Bridge cluster HW77 with VISCACHA photometry: the initial CMDs contain the defined cluster and field regions $(r < 0.7 \, r_t$ and $r > r_t)$ and the last one contain the stars that remained as probable
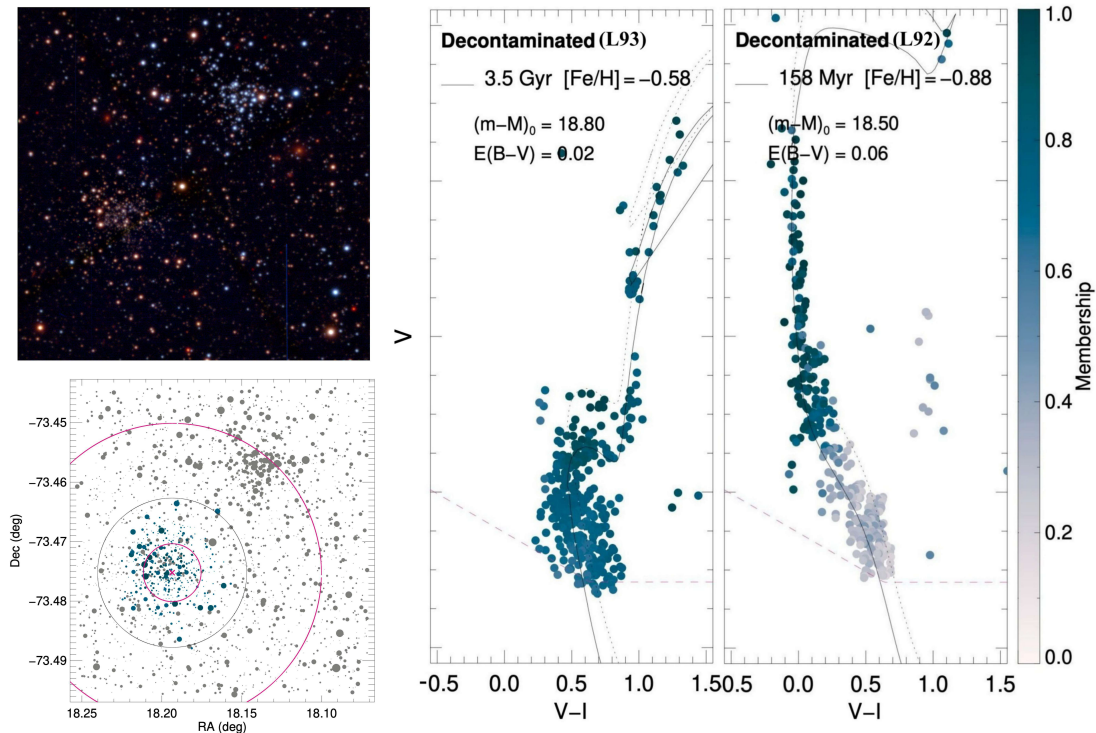
Figure 3.5: Decontamination process for the pair L92+L93, inside the same SAMI field of $3 \times 3\,\text{arcmin}^2$ (upper left). The lower left panel shows the core and tidal radii of L93 as pink circles, and the assumed radius for the cluster sample ($0.5\,r_t = 47''$) in black. The two CMDs show the decontaminated photometry for the clusters, with a visual isochrone fit. The dotted lines correspond to the best-fit isochrone displaced vertically to account for binaries, whereas the dashed lines mark the completeness limit as obtained from a number count histogram.

members after all the CMD comparisons and cuts in the final statistics. For this particular cluster, it is not clear from the initial CMD whether it is an old cluster with the MSTO around 22.5 mag or is much younger with the MSTO around $V \sim 20$ mag, but the decontamination make it clear that HW77 is more probably an intermediate-age cluster of 1 Gyr. Figure 3.5 shows another interesting case, where the SAMI field of view ($3 \times 3\,\text{arcmin}^2$) contain two clusters: L93 in the left, more compact, with red stars and probably older; L92 in upper right, with blue, more sparse stars and probably younger. The decontamination successfully separated the most probable members of each cluster, allowing to derive precise ages of 3.0 ± 0.3 Gyr and 117 ± 28 Myr for them (see Section 4.2). As the membership is available for each star, it is used as a weight in the isochrone fitting method (Section 3.3), giving more weight for the stars assigned with higher membership values.

We are also implementing a complementary method of statistical decontamination including machine learning tools (e.g. decision trees or random forest). Gao (2018) adopted a random forest method to characterize the open cluster M67, based on proper motions

from *Gaia* DR2. In the case of the MCs, the proper motions are available only for giant and supergiant stars, but it is still seems feasible to adequately train a machine learning method with the VISCACHA and SMASH photometry, in order to exclude field stars and recover a membership probability.

3.3 Fundamental parameters from color-magnitude diagrams

The Hertzsptrung-Russell diagram (HRD) was developed independently by the chemist Ejnar Hertzsprung and the astronomer Henry Norris Russell in the early 1900s, and plots the luminosity of the stars versus their effective temperature (or spectral type, somewhat related to the initial mass). In its observational counterpart, the diagram is called colour-magnitude diagram (CMD), and plots the absolute magnitude versus the stellar color, e.g. M_V vs. $B-V$. The evolutionary path of an individual star in the HRD is defined primarily by its initial mass and chemical composition, passing through the different evolutionary stages during its life, as traced by the stellar evolutionary tracks.

On the other hand, for a group of coeval stars such as stellar clusters and associations, these diagrams are a record of the current state of the object. In order to determine the fundamental parameters of a stellar population in the CMD, a set of isochrones (from the Greek: *isos* means "equal" and *chronos* means "time") of different stellar evolution models (e.g. PARSEC, DSED, BaSTI; Bressan et al., 2012; Dotter et al., 2008; Pietrinferni et al., 2004) is available, since they reproduce the observed distribution in color and magnitude, in a sequence of simulated masses. At the time of the cluster formation, the distribution of birth masses of the stars is given by the initial mass function (IMF, e.g. Salpeter, 1955; Kroupa, 2001), after that each individual mass evolves to the present-day mass function. According to the PARSEC models, the main sequence (MS) of young systems contain massive stars (up to $7.5 M_\odot$ for 30 Myr and $2.2 M_\odot$ for 0.5 Gyr), whereas for old Galactic globular clusters the MS is dominated by low-mass stars, between 0.1 and $0.8 M_\odot$ (Oliveira, 2019), since the most massive stars experienced a faster evolution.

Isochrones with different ages and metallicities (as shown in Figure 3.6, from Bressan et al., 2012) are tested with varying apparent distance moduli and reddening values. The distance modulus and reddening move the isochrones from the absolute to the apparent plane, to a quantity that depends on the extinction coefficient of the adopted filters. The
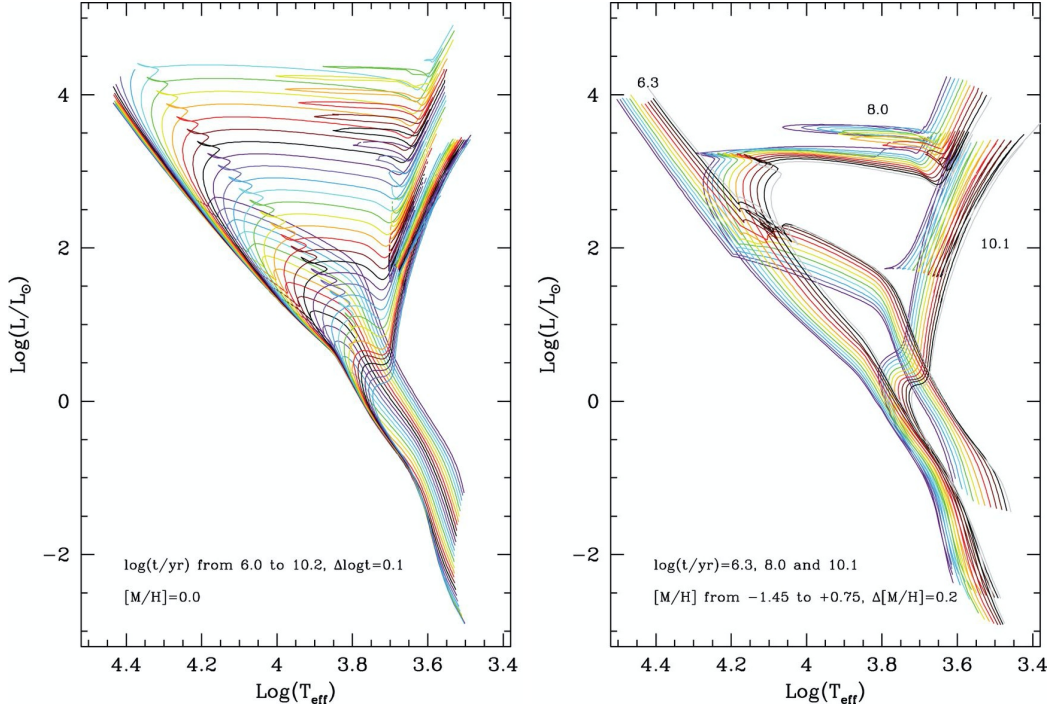
Figure 3.6: Examples with PARSEC isochrones in the HR diagram, with a variation of ages (1 Myr to 15.8 Gyr, left panel) and metallicities (ages of 2 Myr, 100 Myr and 12.6 Gyr, right panel). In this case, the adopted metallicity [M/H] is equal to [Fe/H], since [α/Fe] = 0. Larger values of age and metallicity correspond to isochrones towards the redder regions of the diagram. Extracted from Bressan et al. (2012).

VISCACHA CMDs are V vs. $V - I$ ($UBVRI$ system; Bessell, 1990), whereas the SMASH ones are g vs. $g - i$ (SDSS-$ugriz$ system; Fukugita et al., 1996). In the case of the SMASH multiband data, this specific CMD was selected because Nidever et al. (2017) describe some issues in the correction for nonlinear effects in the calibration of the DECam passbands to the SDSS system, which are more significant in the u and r bands. For a generic CMD λ_1 vs. $\lambda_2 - \lambda_3$, the isochrone is shifted down by an apparent distance modulus $(m - M)_{\lambda_1}$ value, which is transformed to absolute distance modulus and heliocentric distance by:

$$(m - M)_0 = (m - M)_{\lambda_1} - \frac{A_{\lambda_1}}{A_V} \cdot R_V \cdot E(B - V) \tag{3.5}$$

$$d_\odot[\text{kpc}] = 10^{[(m-M)_0 - 10]/5} , \tag{3.6}$$

where A_{λ_1}/A_V is the extinction coefficient[4] for the λ_1 filter and $R_V = A_V/E(B - V) \sim 3.1$ is the total-to-selective extinction ratio (Cardelli et al., 1989). The horizontal shift to the

---

[4] Provided in the PARSEC database (`http://stev.oapd.inaf.it/cgi-bin/cmd`): $A'_V/A_V = 1.00096$, $A_I/A_V = 0.59893$, $A_g/A_V = 1.22651$ and $A_i/A_V = 0.68311$

right is given by the reddening $E(\lambda_2 - \lambda_3)$, which relates to $E(B - V)$ through:

$$E(\lambda_2 - \lambda_3) = R_V \cdot E(B - V) \cdot \left[\frac{A_{\lambda_2}}{A_V} - \frac{A_{\lambda_3}}{A_V} \right] \ . \tag{3.7}$$

The isochrone fitting consists in the determination of the best combination of parameters (age, metallicity, distance modulus and reddening) that defines an isochrone as resembling the distribution of the cluster stars in the CMD. A traditional approach for the isochrone fitting is the visual inspection of the isochrones against the CMD, or automated processes with a limited parameter space to be explored. There are some good open-source tools for isochrone fitting with a variety of stellar evolutionary models, such as `BASE-9` (von Hippel et al., 2014) and `ASteCA` (Perren et al., 2015). Since the isochrone fitting process is very degenerate (i.e. different sets of parameters produce similar outputs), a robust and self-consistent approach is required to provide a reliable solution.

Since 2017, our group has been developing a code with a Bayesian approach, adaptable to different photometric systems and sets of isochrone models, but with an unique feature of also determining ages of the multiple stellar populations in old globular clusters. It was named `SIRIUS` (an acronym for "Statistical Inference of physical paRameters of sIngle and mUltiple populations in Stellar clusters"), and was adopted in several works of the group (Kerber et al., 2019; Ortolani et al., 2019; Oliveira et al., 2020; Souza et al., 2020; Dias et al., 2021, 2022; Bica et al., 2022).

As already discussed, the parameter space is 4-dimensional: age (in a log scale), metallicity [Fe/H], distance modulus $(m - M)_0$ and reddening $E(B - V)$. Since the CMD is a 2D diagram with independent axes, in contrast with the King models in RDPs (Section 3.1, where $\rho(r)$ is a function of the radius), a different likelihood function L_i is adopted here, combining a chi-square in magnitude and color:

$$L_i \propto \exp \left[-\frac{(mag_j - mag_i)^2}{2\sigma_{mag}^2} \right] \cdot \exp \left[-\frac{(col_j - col_i)^2}{2\sigma_{col}^2} \right] \ , \tag{3.8}$$

where the indices i and j correspond to each star and isochrone point, respectively, and σ_{mag} and σ_{col} are the photometric errors. The total likelihood $\mathcal{L}$ is obtained summing the contribution of each star i (out of a total of N stars) comparing its color and magnitude to those of the j-th isochrone point (which contains M points) closer to this star. To obtain the closest isochrone point to the star, the maximum function is adopted to maximise the likelihood, as given below:
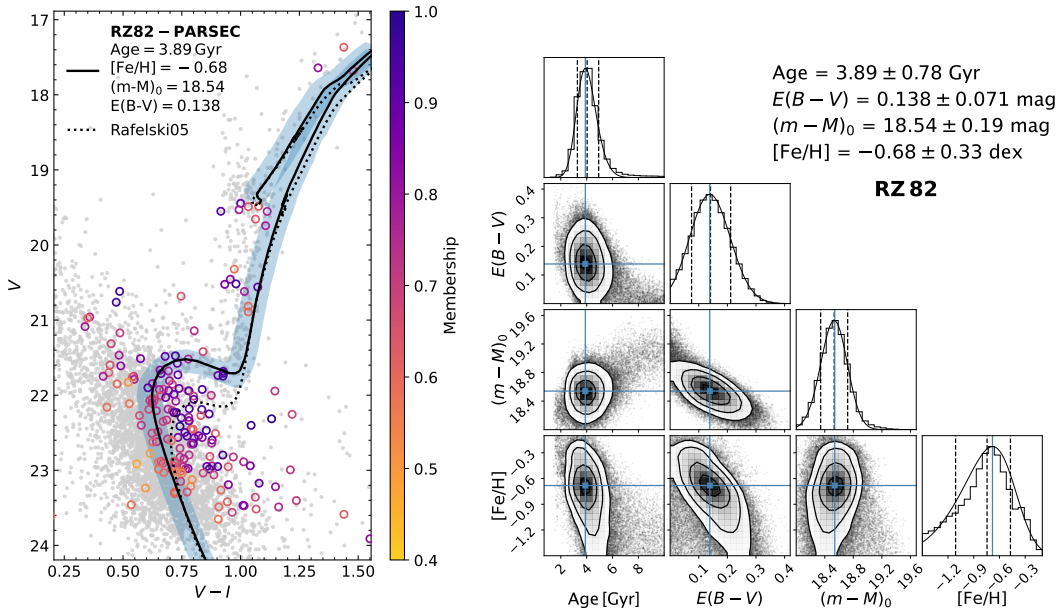
Figure 3.7: Results obtained with the `SIRIUS` code for the cluster RZ 82, with VISCACHA data (Bica et al., 2022). *(Left:)* Best-fitting PARSEC isochrone in the observed CMD, with a shaded region representing the solutions within 1σ. *(Right:)* Corner plot with the posterior distributions in the free parameters (age, metallicity, distance modulus and reddening).

$$\mathcal{L} \propto \sum_{i=1}^{N} \max \left[-\sum_{j=1}^{M} \frac{(mag_j - mag_i)^2}{2\sigma_{mag}^2} + \frac{(col_j - col_i)^2}{2\sigma_{col}^2} \right] . \tag{3.9}$$

According to these equations, for each set of parameters, a value of $\mathcal{L}$ is given by the summation of two Gaussian distributions (or two χ^2 functions), comparing all the stars to the isochrone points. As in Section 3.1, for each set of parameters, the answer is a number that indicates how plausible that this set is the solution. Here, the MCMC method is also applied to sample the parameter space, converging to the best solution and providing the confidence intervals and correlations between the parameters.

Figure 3.7 shows an example of the isochrone fitting obtained for the SMC cluster RZ82, with VISCACHA data from Bica et al. (2022, of which I am co-author). The V vs. $V - I$ CMD shows the member stars colour-coded by membership and the best-fitting PARSEC isochrone of $\sim 4\,\text{Gyr}$ and $[\text{Fe/H}] = -0.68$, along with a shaded region with the possible solutions within 1σ considering all the simulated MCMC chains. The corner plot shows the posterior distributions in the free parameters. The results for the Wing/Bridge clusters are shown in Section 4.2.

Within the goals of the present analysis, I have been adapting the `SIRIUS` code to work with PARSEC isochrones covering a larger age range (1 Myr to 10 Gyr; Bressan et al., 2012)

than those adopted for Galactic GCs ($> 10\,$Gyr; Oliveira et al., 2020), and incorporating improvements for better fitting young and intermediate-age clusters, such as modifications in the likelihood function (e.g. membership probability and number of neighbour stars on the CMD), pre-selection of stars and priors based on the MSTO and red clump position to better constrain the posterior. The number of neighbour stars is obtained within a box of $0.2\,$mag in magnitude and 10% of the color range, in order to give a smaller weight for regions that contain more stars[5] (e.g. main sequence stars) and a larger weight in the other sequences. The membership probability (p_{memb}), number of neighbour stars (n_*) and set of priors ($P(\phi)$) are added to Equation 3.9, which becomes:

$$\mathcal{L} \propto \sum_{i=1}^{N} \left[-\chi^2_{\mathrm{mag,i}} - \chi^2_{\mathrm{col,i}} + \ln(p_{memb,i}) - \ln(n_*) \right] + P(\phi) \,. \tag{3.10}$$

These adaptations turned into a branch of the SIRIUS code, more focused on dealing with CMDs from VISCACHA and SMASH (Chapter 2), low-mass clusters and associations (with fewer stars) and some tests with synthetic CMDs, as well as dealing with the statistical decontamination of field stars (Section 3.2). With the derived fundamental parameters, after correcting the photometry for completeness, it is possible to obtain the cluster mass function from the isochrone mass-luminosity relation (Maia et al., 2014; Bica et al., 2022), which can give hints about the IMF, mass loss due to dynamical effects and cluster dissolution. In the present work, a completeness correction was not applied yet, so we follow an alternative approach using calibrations of the clusters ages, metallicities and integrated magnitudes (e.g. Maia et al., 2014), which are not severely hampered by incompleteness, to obtain the clusters masses (see Section 3.3.1).

3.3.1 Mass estimation from the integrated magnitudes

Figure 3.8 presents a mass estimation for RZ82, by using the completeness-corrected luminosity function (constructed from the absolute magnitude in the V filter) and applying the isochrone mass-luminosity relation to obtain the corresponding mass function (Bica et al., 2022). A power law was fitted to the logarithmic plot of $\xi(m)$, in units of stars$\cdot\mathrm{M}_\odot^{-1}$, as a function of $m(M_\odot)$ to obtain $\alpha = 1.73 \pm 0.46$ in the expression $\xi(m) \propto m^{-\alpha}$, which

---

[5] A more precise approach to take this weight into account would be to access the initial mass function along the isochrone points and compute the relative number of stars in each CMD sequence. This method will be implemented in future version of the SIRIUS code.
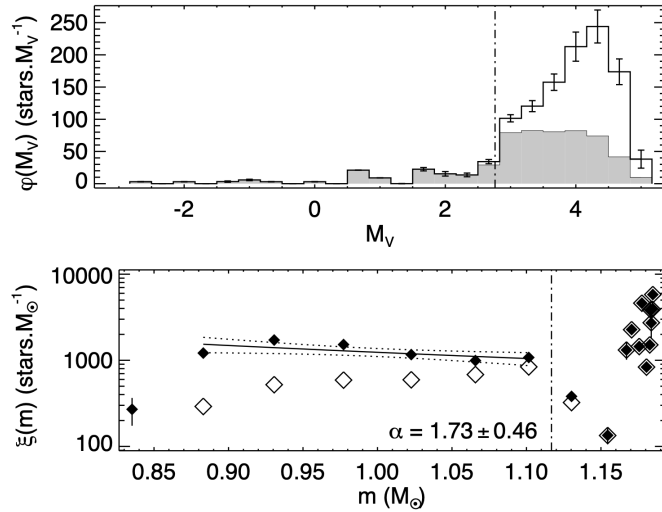
Figure 3.8: Initial and completeness corrected luminosity function (filled and empty bins, upper panel) and corresponding mass functions (open and filled diamonds, respectively in the bottom panel) for RZ82 cluster, the same of Figure 3.7. The vertical dotted line corresponds to the MSTO. A power-law fit was obtained for the stars brighter than the MSTO to derive a total mass of $2\,800\,M_\odot$ (Bica et al., 2022).

can be compared to the classical slopes of Salpeter (1955, $\alpha = 2.35$ for $0.4 < m < 10\,M_\odot$) and Kroupa (2001, $\alpha = 1.35$ for $0.08 < m < 0.5\,M_\odot$, $\alpha = 2.35$ for $m > 0.5\,M_\odot$).

When no completeness corrections are available, the mass can be estimated by adding up the star flux of all member stars, to obtain an integrated apparent V magnitude (V_{int}) using calibrations with age and metallicity from the literature (e.g. Maia et al., 2014). First, the dereddened flux is obtained for each star with $f_{V,i} = 10^{-0.4(V-A_V)}$, where A_V contains the $E(B-V)$ derived in the isochrone fitting. The integrated magnitude V_{int} is then determined with $V_{int} = -2.5\log_{10}(\sum_i f_{V,i})$ and the absolute integrated magnitude is given by $M_{V,int} = V_{int} - (m-M)_0$. Finally, the mass and its uncertainty was calculated following the calibration with age and metallicity (fixed at $Z = 0.004$) of simple stellar population models given by Maia et al. (2014, their equation 4 and table 2). Mass uncertainty comes from propagation of errors[6] in M_V, age, extinction and distance. The determination of cluster masses allowed us to estimate the stellar mass of the Magellanic Bridge and compare it to the value from Harris (2007, $1.5 \times 10^4\,M_\odot$), to be presented in Section 4.2.

---

[6] The error propagation gives $\sigma_{V-A_V} = \sqrt{\sigma_V^2 + 3.1^2 \cdot \sigma_{E(B-V)}^2}$; $\sigma_{f_{V,i}} = \sigma_{V-A_V} \cdot 0.92103 \cdot f_{V,i}$ for the dereddened flux of each star i; $\sigma_{Vint} = \sigma_{\sum f_V} \cdot 1.0857/\sum f_V$ for the integrated apparent magnitude V_{int} of the cluster; and $\sigma_{M_v,int} = \sqrt{\sigma_{Vint}^2 + \sigma_{(m-M)_0}^2}$ for the integrated absolute magnitude $M_{V,int}$.

Chapter 4

Results: Wing/Bridge clusters

In this Chapter, I present the results obtained for the 33 Wing/Bridge clusters with VISCACHA data, showing the results from the structural analysis (Section 4.1; Oliveira et al., in prep.) and from the statistical isochrone fitting (Section 4.2; Oliveira et al., submitted to MNRAS), followed by a discussion of the implications of these results in the Bridge formation scenario. Section 4.3 presents the first results of a follow-up with SMASH data for some clusters (Oliveira et al., in prep.). Section 4.4 presents a comparison of the present results with the literature.

As discussed in Chapter 1, the different formation models available for the Magellanic System would imply kinematic signatures, as well as age and metallicity gradients along the Bridge extension. Particularly for its stellar population, it is believed that during the close encounter of the Clouds that probably originated the Bridge ($\sim 200 - 300\,\mathrm{Myr}$ ago; Zivick et al., 2018; Choi et al., 2022), an older population (mostly closer to the SMC Wing) would have been disrupted and displaced to the Bridge, whereas a younger population would have formed in situ. In this sense, the main goals of this work are to unveil the nature of the Bridge by adopting a uniform methodology for a significant fraction of its 129 clusters and 330 associations (Bica et al., 2020), checking whether the observed star formation history and gradients match those expected by the models (Besla et al., 2012).

4.1   Structural parameters: 33 clusters from VISCACHA

Santos et al. (2020, Paper II) have recently analysed 83 clusters located at the periphery of the MCs with VISCACHA data (the entire internal data release 1, presented in Maia et al., 2019), and derived different structural parameters (mainly r_t and r_c) which depends

on the position and deprojected distance to the LMC center (and not deprojected in the case of SMC clusters). As observed in Paper II, it is expected that the Wing/Bridge objects (as well as those in other regions under less intense tidal forces) will present more sparse structures, corresponding to a smaller concentration parameter ($c = \log_{10}(r_t/r_c)$).

Table 4.1 gives the derived structural parameters with the respective uncertainties for all the 33 Wing/Bridge clusters with VISCACHA data. The new centres present a very small variation in the tenths of arcseconds, compared to the ones from Bica et al. (2020). The fit did not converge in all the parameters for HW59 and B147, and in none of them for L101; in these cases, the decontamination was carried out within a visual radius (instead of r_t) to limit the cluster sample. In the case of B147, the derived central density is so low compared to the background that the its centre barely stands out in the plots, resulting in large uncertainties in determining the new centre. As in Paper II, we obtained a tidal radius larger than the SAMI field of view ($r_t \gtrsim 100\,\mathrm{arcsec}$) for 11 clusters, probably biased toward smaller values.

Table 4.1 - Results obtained of new center and structural parameters for the 33 Wing/Bridge clusters observed with VISCACHA. The values correspond to the median and 1σ level of the posterior distribution. The clusters are ordered by right ascension.

Cluster	RA$_\mathrm{new}$ (h:m:s)	Dec.$_\mathrm{new}$ (°:′:″)	ρ_0 (arcsec^{-2})	r_c (arcsec)	r_t (arcsec)	c	ρ_bg (10^{-3} arcsec^{-2})
HW55	01:07:19.19	−73:22:41.7	0.114 ± 0.007	9.1 ± 0.6	117 ± 32	1.11	44.3 ± 0.3
K55	01:07:32.46	−73:07:16.7	0.221 ± 0.011	16.1 ± 0.9	64 ± 4	0.60	38.4 ± 0.3
K57	01:08:13.84	−73:15:28.7	0.187 ± 0.010	19.4 ± 1.1	70 ± 4	0.56	41.6 ± 0.3
HW59	01:08:54.3	−73:14:38	–	–	–	–	–
HW63	01:10:11.95	−73:12:32.6	0.119 ± 0.007	9.3 ± 0.6	165 ± 34	1.25	27.1 ± 0.3
L92[†]	01:12:34.00	−73:27:24.4	0.194 ± 0.018	10.9 ± 1.0	81 ± 38	0.87	23.6 ± 1.6
L93[†]	01:12:47.27	−73:28:29.0	0.261 ± 0.024	17.4 ± 1.1	86 ± 20	0.69	34.6 ± 2.0
L91	01:12:51.58	−73:07:07.4	0.346 ± 0.011	13.3 ± 0.4	158 ± 24	1.07	27.7 ± 0.6
B147	01:14:48.02	−73:06:36.7	0.037 ± 0.005	16.6 ± 2.7	–	–	30.7 ± 0.3
HW71se	01:15:32.36	−72:22:45.1	0.065 ± 0.006	10.8 ± 1.2	99 ± 32	0.96	21.0 ± 0.2
HW75	01:17:30.34	−73:34:18.3	0.109 ± 0.011	11.5 ± 1.3	57 ± 12	0.69	23.7 ± 0.3
HW77	01:20:10.00	−72:37:27.3	0.099 ± 0.009	22.7 ± 2.3	79 ± 7	0.54	15.2 ± 0.2
HW78	01:21:22.18	−72:05:33.6	0.054 ± 0.007	20.3 ± 2.6	72 ± 10	0.55	8.5 ± 0.2
L101	–	–	–	–	–	–	–

Continued on next page...

Tabela 4.1 - continued

Cluster	RA$_{new}$	Dec.$_{new}$	ρ_0	r_c	r_t	c	ρ_{bg}
HW81[†]	01:24:10.05	−73:09:14.8	0.193 ± 0.018	15.5 ± 1.4	48 ± 3.6	0.49	20.7 ± 0.4
HW82[†]	01:24:27.78	−73:09:17.2	0.061 ± 0.008	9.0 ± 1.4	67 ± 46	0.87	28.8 ± 1.1
L104	01:25:26.40	−73:23:11.7	0.027 ± 0.002	23.4 ± 2.9	157 ± 33	0.83	7.8 ± 0.3
B165[†]	01:30:50.95	−73:26:02.9	0.027 ± 0.005	7.6 ± 1.9	91 ± 44	1.08	7.6 ± 0.3
BS187	01:31:00.87	−72:51:05.8	0.060 ± 0.008	8.3 ± 1.2	148 ± 36	1.25	6.8 ± 0.2
L107	01:31:06.30	−73:24:50.8	0.091 ± 0.008	21.9 ± 2.2	88 ± 9	0.60	10.8 ± 0.3
L109	01:33:13.26	−74:10:02.7	0.285 ± 0.015	11.6 ± 1.0	81 ± 12	0.84	9.4 ± 0.3
L110	01:34:26.12	−72:52:28.8	0.513 ± 0.017	37.9 ± 0.9	109 ± 3	0.46	10.8 ± 0.4
HW86	01:42:26.06	−74:10:28.4	0.035 ± 0.004	34.3 ± 4.8	152 ± 31	0.65	6.5 ± 0.4
WG1	01:42:52.78	−73:20:13.4	0.214 ± 0.013	8.8 ± 0.6	117 ± 24	1.12	6.4 ± 0.3
BS198	01:47:59.90	−73:07:37.5	0.030 ± 0.005	11.1 ± 2.8	57 ± 24	0.71	5.0 ± 0.3
L113	01:49:29.29	−73:43:43.4	0.214 ± 0.011	43.3 ± 1.4	190 ± 16	0.64	0.0 ± 0.0
L114	01:50:19.37	−74:21:20.9	0.521 ± 0.018	10.5 ± 0.6	72 ± 4	0.84	6.8 ± 0.2
NGC796	01:56:44.33	−74:13:10.0	0.475 ± 0.019	9.0 ± 0.4	72 ± 4	0.90	2.9 ± 0.1
WG13	02:02:42.44	−73:56:16.1	0.056 ± 0.007	10.2 ± 1.4	109 ± 39	1.03	3.3 ± 0.17
BS226	02:05:41.47	−74:22:55.3	0.034 ± 0.006	7.0 ± 1.8	66 ± 38	0.97	1.8 ± 0.12
ICA45	02:27:16.73	−73:45:28.8	0.022 ± 0.003	30.9 ± 3.5	133 ± 30	0.63	3.7 ± 0.3
BS245	02:27:29.35	−73:58:36.7	0.094 ± 0.031	13.9 ± 5.6	43 ± 8	0.49	1.6 ± 0.1
OGLB33	02:41:03.43	−73:15:12.2	0.340 ± 0.051	4.1 ± 0.6	55 ± 9	1.13	1.6 ± 0.1

† Clusters with a pair within the same SAMI field. In these cases, a smaller region was considered to compute the local density, possibly leading to underestimated r_t.

The derived concentration parameters vary from ~ 0.5 (L110, HW81 and BS245) to 1.25 (HW63 and BS187), whereas background densities vary from ~ 1.5 to $44 \times 10^{-3}\,\mathrm{arcsec}^{-2}$, showing that some fields closer to the SMC (e.g. HW55, K57) are much more contaminated by field stars than others and that the background density decreases with higher RA (i.e. towards the middle of the Bridge).

Figure 4.1 shows the results for the young, well-studied cluster NGC796 ($36 \pm 3\,\mathrm{Myr}$) and the old cluster L109 ($4.1 \pm 0.5\,\mathrm{Gyr}$). The points are colour-coded by the computed likelihood, where those that better resemble the best-fitting King model have higher values. Good fits were derived in both cases, making it clear that NGC796 has a much larger central density but a much lower background density, compared to L109. A comparison with the literature values from Hill and Zaritsky (2006) and Paper II is given in Section 4.4.
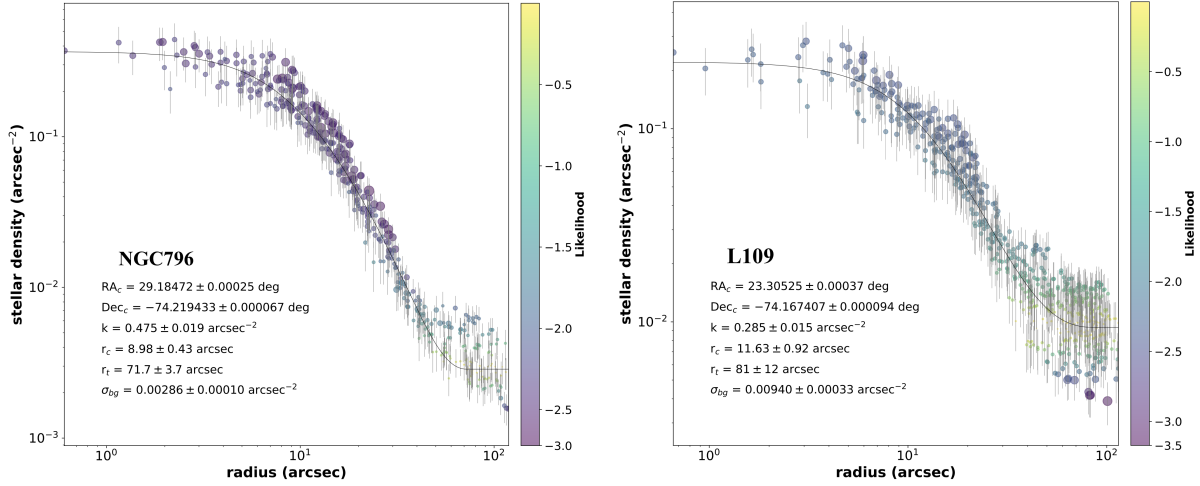
Figure 4.1: Results of the fitting of King models for the young cluster NGC796 $(36 \pm 3\,\mathrm{Myr})$ and the old cluster L109 $(4.1 \pm 0.5\,\mathrm{Gyr})$. The points are colour-coded by likelihood and their sizes are proportional to the V magnitude of the star around which the density is calculated. The result for NGC796 can be compared with Santos et al. (2020): $k = 0.36 \pm 0.05\,\mathrm{arcsec}^{-2}$, $r_c = 8 \pm 1\,\mathrm{arcsec}$, $r_t = 99 \pm 7\,\mathrm{arcsec}$ and $\sigma_{\mathrm{bg}} = 0.002 \pm 0.001\,\mathrm{arcsec}^{-2}$.
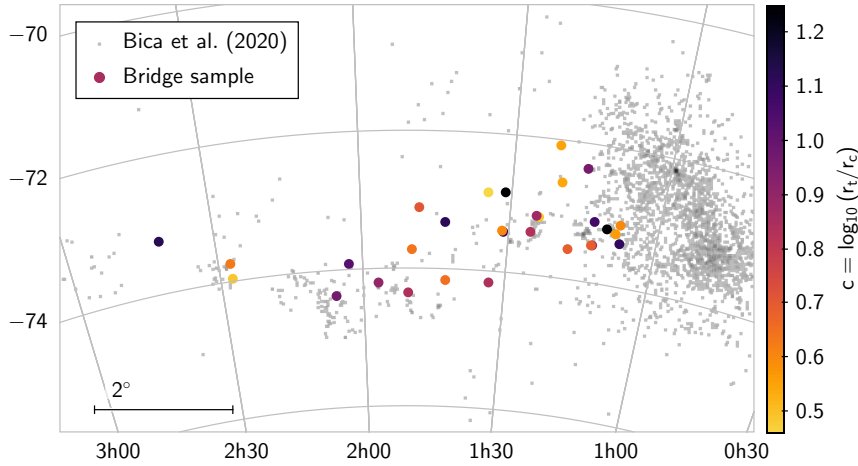
Figure 4.2: Spatial distribution of the derived concentration parameters.

Figure 4.2 presents the spatial distribution of the concentration parameter for the 33 sample clusters, showing that the old clusters closer to the Wing are slightly more concentrated than the younger ones. A larger sample is needed to draw stronger conclusions, and a proper comparison with the rest of SMC objects will verify that the Bridge objects (and in external regions) present in general a smaller concentration.

As discussed in Section 3.3, no correction for completeness is applied so far. However, Paper II shows that the tidal radius derived from RDPs is largely unaffected by incompleteness, in contrast with the core radius, which depends a lot on the stellar counts close to the center. We will defer a more complete structural analysis of these clusters to a future

work (Oliveira et al., in prep.), which will also include the mass determination from the luminosity and mass functions.

4.2　Isochrone fitting: 33 clusters from VISCACHA

The determination of fundamental parameters from decontaminated CMDs of such a large and homogeneous sample of Wing/Bridge clusters can provide important constraints to the dynamical and chemical evolution models. A lot of these clusters are not included in any literature work: we obtained the first age derivation for nine sample clusters (HW78, L101, L104, B165, L107, WG1, BS198, ICA45 and OGLB33) and the first metallicity derivation for eighteen clusters (the nine aforementioned, as well as L92, L93, B147, HW71se, HW75, HW77, HW81, HW82 and BS187). The remaining clusters, with previous studies in the literature, are listed in Section 4.4

Table 4.2 contains the derived ages, metallicities, distances, reddening values, integrated absolute magnitudes and masses for the 33 Wing/Bridge clusters with VISCACHA data. Figure 4.3 presents the isochrone fits for three of the youngest sample clusters (HW81, L107 and L114), illustrating the vertical MS and the lack of giant stars. In such cases, we iterated the method, first trying an unconstrained fit and then adopting a wide [Fe/H] prior around the most prominent peak in the initial posterior distribution. This was needed in order to obtain a better convergence and circumvent degeneracies. Figure 4.4 shows the results for the young cluster L92 (pair of L93; Figure 3.5), with the CMD showing the best-fit isochrone to the member stars, and corner plot showing the posterior distributions and correlations between the parameters. In such cases, where some giant stars are present, the MSTO (visually detected as a sharp reduction in the number of stars in the upper MS) was adopted as a constraint, helping to break the degeneracies.

Table 4.2 - Isochrone fitting results for the 33 Wing/Bridge clusters with VISCACHA data, obtained by fitting PARSEC isochrones with the `SIRIUS` code.

Cluster	Age (Gyr)	[Fe/H] (dex)	$d_\odot$ (kpc)	$E(B-V)$ (mag)	M_V (mag)	$\log(M/M_\odot)$
HW55	2.22 ± 0.29	-0.71 ± 0.26	64.3 ± 5.0	0.09 ± 0.09	-4.59 ± 0.18	3.58 ± 0.13
K55	0.52 ± 0.03	-0.38 ± 0.10	52.0 ± 1.7	0.02 ± 0.02	-5.01 ± 0.07	3.37 ± 0.10

Continued on next page. . .

Tabela 4.2 - continued

Cluster	Age	[Fe/H]	$d_\odot$	$E(B-V)$	M_V	$\log(M/M_\odot)$
K57	0.53 ± 0.15	-0.40 ± 0.30	53.0 ± 3.4	0.03 ± 0.03	-5.33 ± 0.14	3.50 ± 0.14
HW59	6.8 ± 2.4	-0.99 ± 0.35	69.2 ± 8.0	0.09 ± 0.08	-4.01 ± 0.26	3.64 ± 0.18
HW63	2.53 ± 0.24	-0.62 ± 0.23	67.6 ± 6.5	0.05 ± 0.05	-4.66 ± 0.21	3.64 ± 0.14
L92	0.117 ± 0.028	-0.50 ± 0.17	54.7 ± 4.8	0.11 ± 0.03	-5.55 ± 0.19	3.19 ± 0.14
L93	3.0 ± 0.3	-0.70 ± 0.22	57.5 ± 2.4	0.06 ± 0.04	-4.63 ± 0.09	3.68 ± 0.11
L91	3.9 ± 0.5	-0.82 ± 0.08	59.2 ± 2.5	0.15 ± 0.03	-5.39 ± 0.09	4.05 ± 0.12
B147	0.19 ± 0.06	-0.26 ± 0.15	50.0 ± 4.1	0.18 ± 0.05	-5.61 ± 0.19	3.33 ± 0.15
HW71se	0.16 ± 0.05	-0.53 ± 0.21	57.3 ± 7.1	0.03 ± 0.03	-5.07 ± 0.27	3.07 ± 0.17
HW75	0.11 ± 0.03	-0.56 ± 0.13	53.7 ± 4.9	0.13 ± 0.05	-5.08 ± 0.21	2.99 ± 0.15
HW77	1.12 ± 0.10	-1.02 ± 0.11	58.3 ± 3.2	0.04 ± 0.03	-4.44 ± 0.15	3.35 ± 0.12
HW78	0.051 ± 0.007	-0.39 ± 0.09	53.0 ± 3.9	0.15 ± 0.04	-6.31 ± 0.17	3.27 ± 0.12
L101	$0.013^{+0.025}_{-0.003}$	-0.27 ± 0.13	51.1 ± 4.2	0.09 ± 0.04	-5.74 ± 0.18	2.68 ± 0.29
HW81	0.004 ± 0.001	-0.11 ± 0.18	68.2 ± 9.4	0.21 ± 0.04	-7.53 ± 0.30	3.09 ± 0.16
HW82	0.050 ± 0.013	-0.41 ± 0.15	61.4 ± 7.6	0.13 ± 0.05	-6.69 ± 0.28	3.42 ± 0.16
L104	0.030 ± 0.007	-0.25 ± 0.16	65.8 ± 6.1	0.08 ± 0.04	-6.95 ± 0.20	3.39 ± 0.14
B165	0.33 ± 0.08	-0.54 ± 0.18	52.0 ± 7.4	0.01 ± 0.05	-3.86 ± 0.31	2.79 ± 0.17
BS187	1.01 ± 0.22	-0.92 ± 0.15	52.7 ± 3.9	0.15 ± 0.05	-4.36 ± 0.17	3.28 ± 0.13
L107	0.013 ± 0.005	-0.41 ± 0.17	55.7 ± 7.7	0.06 ± 0.04	-7.03 ± 0.31	3.20 ± 0.18
L109	4.1 ± 0.5	-0.79 ± 0.21	58.6 ± 2.7	0.09 ± 0.04	-4.15 ± 0.10	3.56 ± 0.12
L110	5.0 ± 0.7	-0.94 ± 0.11	61.7 ± 4.3	0.07 ± 0.04	-5.59 ± 0.15	4.19 ± 0.13
HW86	1.46 ± 0.10	-0.69 ± 0.12	51.3 ± 2.8	0.08 ± 0.04	-4.13 ± 0.13	3.29 ± 0.12
WG1	0.031 ± 0.005	-0.23 ± 0.14	54.5 ± 4.8	0.20 ± 0.04	-5.94 ± 0.20	2.99 ± 0.13
BS198	0.011 ± 0.005	-0.37 ± 0.22	58.3 ± 7.5	0.15 ± 0.06	-3.97 ± 0.29	1.93 ± 0.19
L113	3.9 ± 0.4	-0.87 ± 0.08	54.7 ± 1.3	0.03 ± 0.03	-5.62 ± 0.05	4.14 ± 0.11
L114	0.033 ± 0.004	-0.47 ± 0.08	54.7 ± 3.5	0.03 ± 0.03	-6.77 ± 0.15	3.34 ± 0.11
NGC 796	0.036 ± 0.003	-0.22 ± 0.06	60.5 ± 3.6	0.03 ± 0.02	-6.58 ± 0.13	3.29 ± 0.11
WG13	0.33 ± 0.11	-0.28 ± 0.15	55.0 ± 7.3	0.07 ± 0.06	-5.78 ± 0.31	3.55 ± 0.18
BS226	1.09 ± 0.21	-1.12 ± 0.17	53.5 ± 4.9	0.07 ± 0.05	-3.50 ± 0.21	2.95 ± 0.14
ICA45	0.021 ± 0.005	-0.38 ± 0.15	58.3 ± 5.6	0.08 ± 0.04	-5.48 ± 0.21	2.70 ± 0.14
BS245	0.10 ± 0.03	-0.55 ± 0.25	50.6 ± 7.9	0.10 ± 0.07	-5.36 ± 0.36	3.08 ± 0.18
OGLB33	4.0 ± 1.1	-0.75 ± 0.17	66.1 ± 6.1	0.12 ± 0.07	-2.24 ± 0.23	2.80 ± 0.16

In Figure 4.5, the isochrone fits of three old clusters are given (L91, L110 and HW59), all of them with a well-defined MS reaching $V \sim 24\,\mathrm{mag}$ and well-populated giant branches
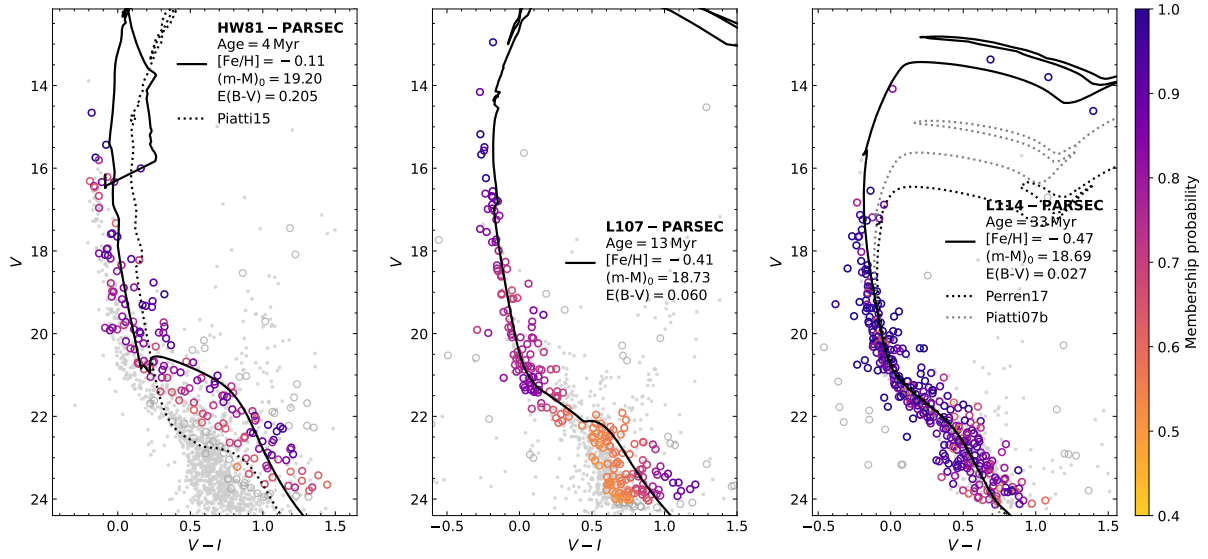
Figure 4.3: V vs. $V - I$ decontaminated CMD of three of the youngest sample clusters, with the best-fit isochrone and a comparison with literature results (Piatti et al., 2015; Perren et al., 2017; Piatti et al., 2007a, see Section 4.4;)
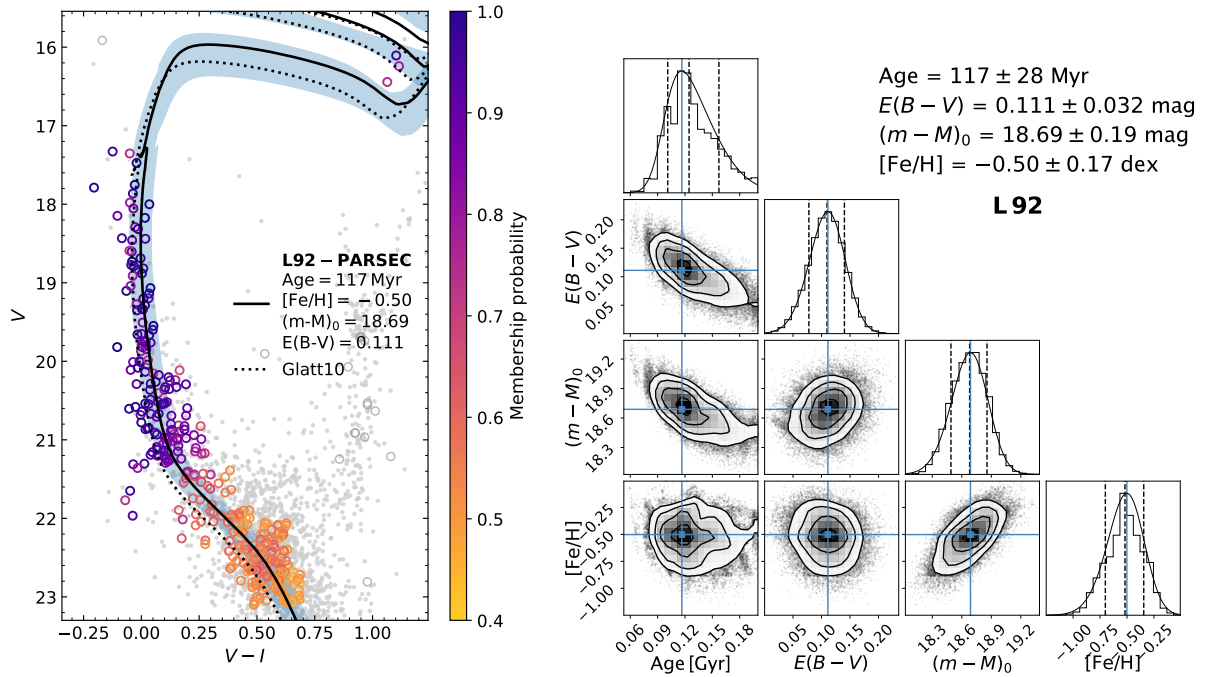
Figure 4.4: *(Left:)* V vs. $V - I$ decontaminated CMD of the young cluster L92 with the best-fit isochrone, as compared to (Glatt et al., 2010), and a shaded region with the solutions within 1σ. *(Right:)* Corner plot of this fit, showing the posterior distribution and correlations between the parameters (dashed lines give the 16th, 50th and 86th percentiles, and the blue line marks the center of the fitted skewed gaussian as the solution).

Figure 4.5: V vs. *V − I* decontaminated CMD of three old sample clusters, with the best-fit isochrone and a comparison with the literature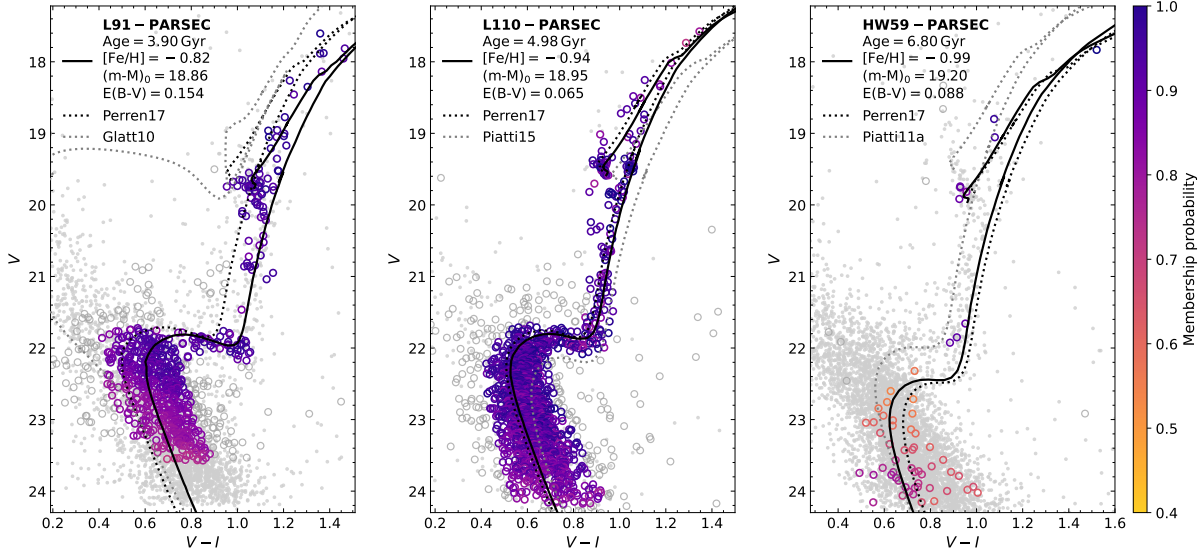 (Perren et al., 2017; Glatt et al., 2010; Piatti et al., 2015; Piatti, 2011a). A metallicity prior was adopted for L91 and L110, centred in the literature values from CaT spectroscopy.

and red clump, which helped to constrain the metallicity and distance. Following what we have done in Dias et al. (2021, 2022, see Section 5.1), we applied a narrower gaussian prior in the [Fe/H] for the old clusters with metallicity derived from the near-infrared CaII triplet lines (CaT) spectroscopy in the literature: -0.90 ± 0.06 for L91 (De Bortoli et al., 2022), -1.03 ± 0.05 for L110 and -0.61 ± 0.06 for HW86 (Parisi et al., 2009), and -1.03 ± 0.04 for L113 (Parisi et al., 2015). The resulting CMDs for all the clusters are given in Appendix A.

With the ages, metallicities and distances in hand, we are able to study several aspects of the Bridge stellar population, to be compared with what is expected from the models. In Figure 4.6, we show how the derived ages and metallicities of the 33 clusters are distributed on the sky along the Wing/Bridge. As an update of Figure 1.5 from Bica et al. (2020), now with a homogeneous data set and method of analysis, our Bridge sample suggests that most of the older clusters are projected close to the SMC, whereas the younger ones are more spread out along the Bridge. The same pattern is observed in the metallicity: the clusters closer to the SMC are slightly more metal-poor than those along the Bridge. These results suggest a stratification of the cluster groups of similar age and metallicity, with more recent cluster formation predominating in Bridge regions farther from the SMC.

In order to obtain a 3D view of these clusters, we converted the equatorial coordinates
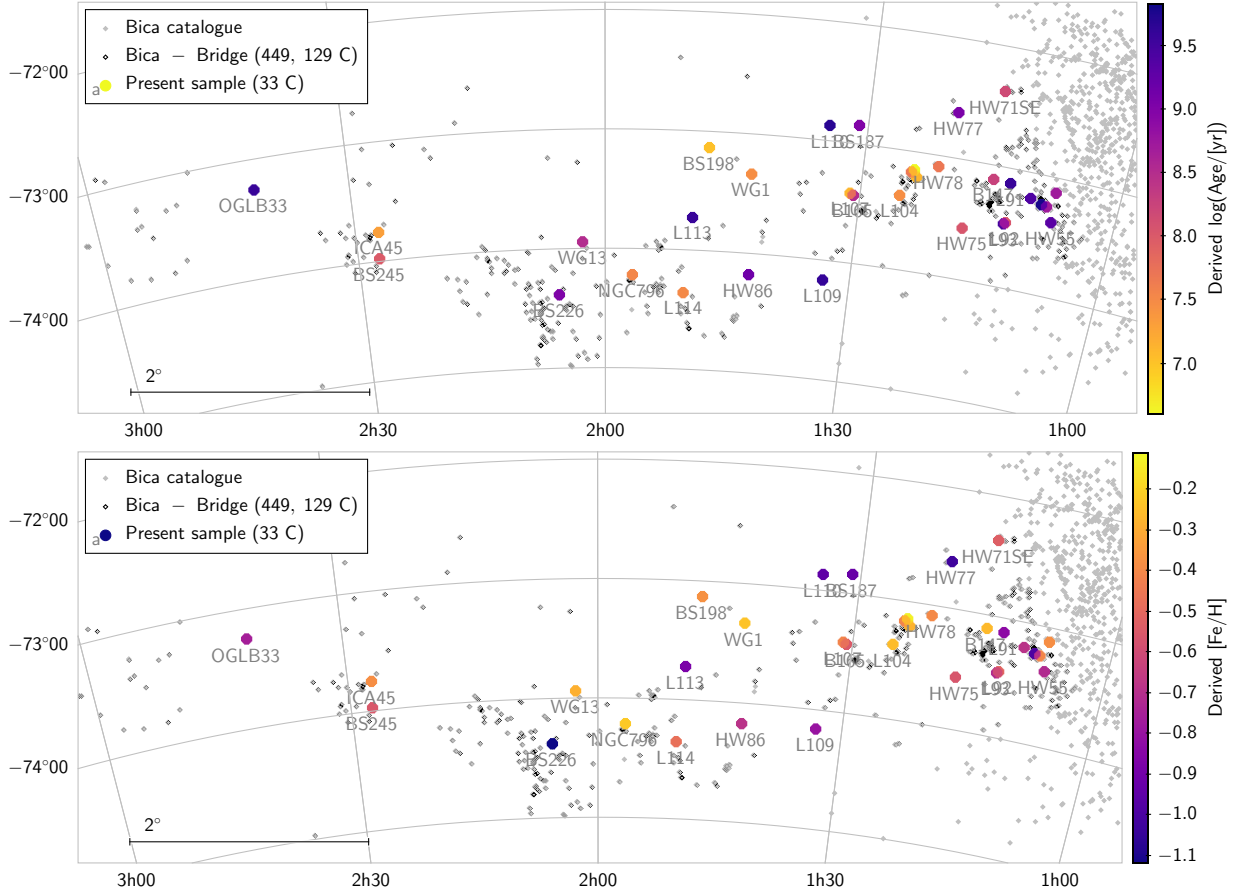
Figure 4.6: Projected distribution of the ages and metallicities derived for the 33 sample clusters. The points are overplotted with the Bica et al. (2020) catalogue (grey dots) and the 449 Bridge objects (black diamonds). The old, metal-poor clusters are located mainly closer to the SMC, and the young, metal-rich ones are present throughout the Bridge.

combined with the derived line-of-sight distances (Table 4.2) into a Cartesian system centred at the SMC centre, according to the equations by van der Marel and Cioni (2001). The plane $z = 0$ is tangent to the sky at the SMC centre, where z increases towards the observer, x increases to the West direction and y increases towards North. This work was carried out in collaboration with Bruno Dias. Figure 4.7 shows three projections of the cluster positions around the SMC, with four of them inside the SMC tidal radius of 4 kpc (Dias et al., 2022). The clusters with ages $\lesssim 300$ Myr follow an homogeneous distribution up to a radius of 13 kpc from the SMC centre, and the older ones are gathered in specific regions. Most of the clusters have $z > 0$ (i.e. distances smaller than the SMC) and point to the LMC, which is consistent with the scenario of a recent collision, with the SMC moving away from the collision region and leaving gas (to form stars) and old stripped clusters in its path.
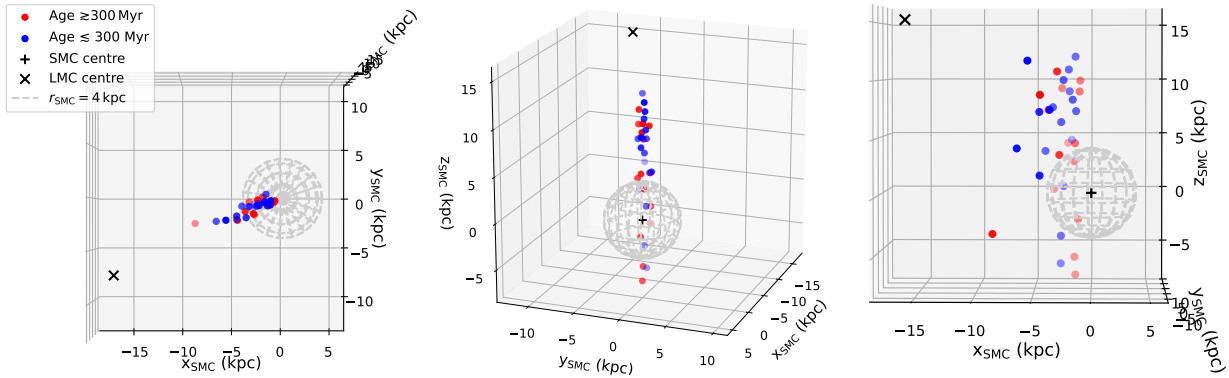
Figure 4.7: Three-dimensional distribution of the 33 sample clusters, identifying the old and the young clusters in red and blue: *(left:)* x vs. y similar to the sky projection; *(middle:)* projection showing the alignment between SMC, LMC and Bridge clusters with different depth; *(right:)* x vs. z projection. The SMC is located at the origin, the LMC is at $(x, y, z) = (-16.0, -7.2, 15.2)$, and the sphere corresponds to the SMC tidal radius of $4\,\mathrm{kpc}$.

Figure 4.8 contains the derived age and metallicity for the 33 sample clusters as a function of the deprojected distance to the SMC, as a complement to Bica et al. (2020, their figure 8, shown in Figure 1.7). The clusters older than $300\,\mathrm{Myr}$ clearly follow the overall age and metallicity gradients of the SMC, with an increasing age and decreasing metallicity until $4-5\,\mathrm{deg}$ and an inversion after that, confirming their probable SMC origin. Five old clusters deviate from the age gradient (HW59, HW77, BS187, HW86 and OGLB33) and only two deviate from the metallicity gradient (BS226 and OGLB33). The young clusters present no clear pattern in the age plot, whereas the metallicity deviate to more metal-rich values than the SMC gradients, with a nearly constant value of $[\mathrm{Fe/H}] \sim -0.4$.

The SMC has an average metallicity of $[\mathrm{Fe/H}] = -0.9 \pm 0.2$ (Parisi et al., 2016), however the younger stellar populations in the SMC main body peaks around -0.4 (Rubele et al., 2018) and there are several young, metal-rich clusters ($[\mathrm{Fe/H}] > -0.5$) in the SMC main body (Bica et al., 2020, see Figure 1.6). Therefore, we interpret our results for the young clusters as evidence that the gas stripped from the SMC to form the Bridge $\sim 200-300\,\mathrm{Myr}$ ago probably came from the innermost regions of the SMC that was enriched by stellar evolution. After the close encounter, this metal-rich gas would have pulled out to form the star clusters along the Wing and beginning of the Bridge ($\mathrm{RA} < 3^{\mathrm{h}}$), forming clusters with similar metallicity around $[\mathrm{Fe/H}] = -0.4$. This result is also in agreement with the analysis of B-type supergiants (Lee et al., 2005). The Bridge region more distant from the SMC ($\mathrm{RA} > 3^{\mathrm{h}}$, mostly gaseous and with very few associations), seems to be more metal-poor (Ramachandran et al., 2021) and could have been formed out of gas from the
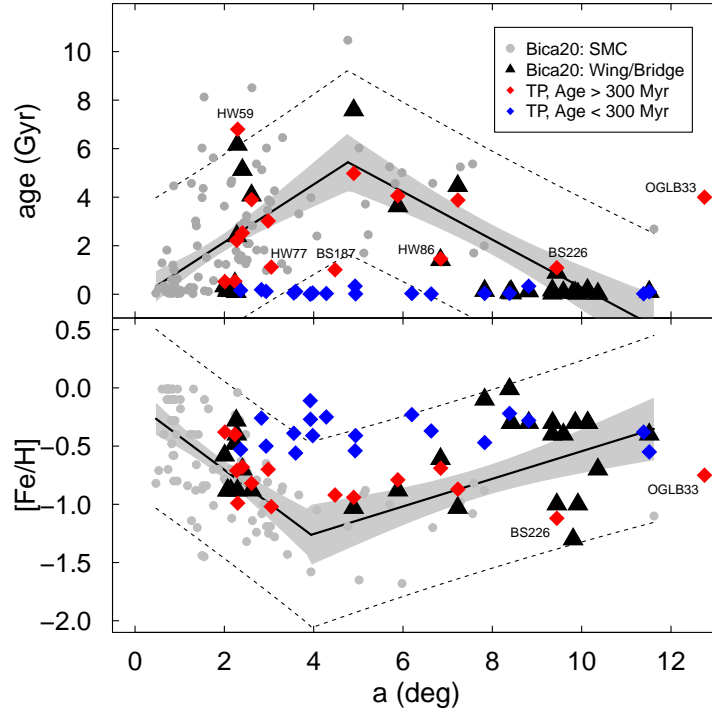
Figure 4.8: Derived age and metallicity as a function of the deprojected distance to the SMC centre. The grey and black symbols are from Bica et al. (2020), and the red and blue diamonds are the present sample of old and young clusters. The solid and dashed lines and the grey shaded areas represent the fit to the Bica et al. (2020) age and metallicity distributions as detailed in that work. It is clear that the old clusters follow the overall SMC gradients (exception are annotated) and the young ones have very similar metallicities.

LMC or from the SMC outskirts. An investigation of this region is to be carried out in a forthcoming publication.

The age-metallicity relation (AMR) is a very useful tool to analyse the chemical history of a galaxy, providing hints about chemical enrichment processes. In Figure 4.9, we show the AMR including literature (from CaT spectroscopy and/or VISCACHA data) and present results, with three chemical evolution models (Pagel and Tautvaisiene, 1998; Demers and Battinelli, 1998; Tsujimoto and Bekki, 2009). Compared to previous AMR plots (e.g. Parisi et al., 2022), our new AMR makes a great contribution with the young objects below 1 Gyr and a peculiar group of 4 clusters with $\sim 1\,\mathrm{Gyr}$ and $[\mathrm{Fe/H}] \sim -1.0$.

The present AMR plot contains some new features: *(i)* the large dip with four metal-poor clusters with ages around $1-1.5\,\mathrm{Gyr}$ (metallicity drop from -0.6 to -1.0), followed by a rapid chemical increase; *(ii)* a smaller dip starting around 200 Myr ago ($[\mathrm{Fe/H}]$ from -0.3 to -0.6); and *(iii)* the sample clusters older than 1.5 Gyr are slightly more metal-rich than the literature points. The larger metallicity dip was not pointed out in the literature, but
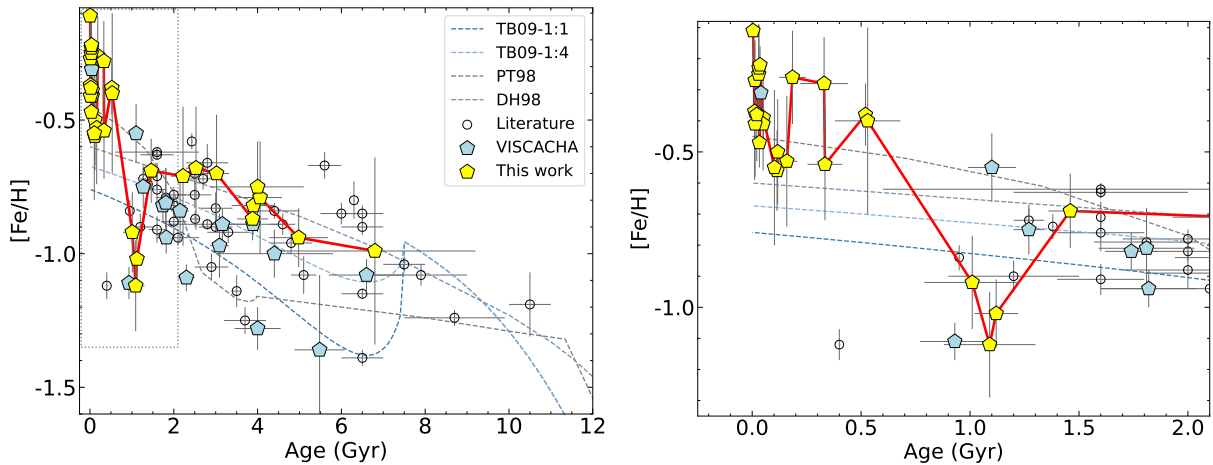
Figure 4.9: Age-metallicity relation of the present results for the Wing/Bridge clusters (yellow pentagons), previous results from VISCACHA (blue pentagons) and literature data with CaT metallicities (open black circles). Chemical evolution models are overplotted: Pagel and Tautvaisiene (1998, PT98), Da Costa and Hatzidimitriou (1998, DH98) and Tsujimoto and Bekki (2009, TB09). A red line connects the results from the older to the younger cluster, suggesting the existence of a large dip around $1 - 1.5\,\text{Gyr}$ and smaller one around $200\,\text{Myr}$. The right panel shows a zoom-in of $< 2\,\text{Gyr}$.

it makes sense in the current context of the Magellanic Clouds history in which their last close encounter has formed the Magellanic Stream (Besla et al., 2010; D'Onghia and Fox, 2016). The smaller metallicity dip could also be related to the Bridge formation episode. In summary, the formation of the Stream and Bridge left marks in the chemical evolution of the Bridge clusters, so that dedicated chemical evolution models shall enlighten the explanation of the metallicity dips.

Finally, the derivation of the integrated mass of the 33 sample clusters (which adds up to $10^5\,M_\odot$, see last column of Table 4.2) allowed us to estimate the Bridge stellar mass. Given that we analysed around one third of the Bridge clusters and extrapolating to the total number of clusters and associations in the Bridge (Bica et al., 2020), a conservative estimate of $3 - 5 \times 10^5\,M_\odot$ appears to be more reasonable than the previous estimate from Harris (2007, $1.5 \times 10^4\,M_\odot$).

A spectroscopic follow-up in the CaT region of Bridge clusters was conducted and is in an advanced stage of analysis (Dias et al., in prep.). This work will complement the analysis of Dias et al. (2021, 2022, Paper III and Paper IV) by adding 6 Bridge and 9 Southern Bridge clusters to a sample of ~ 30 clusters with GMOS spectra. The analysis of the spectra provides radial velocities and metallicity, followed by isochrone fitting with
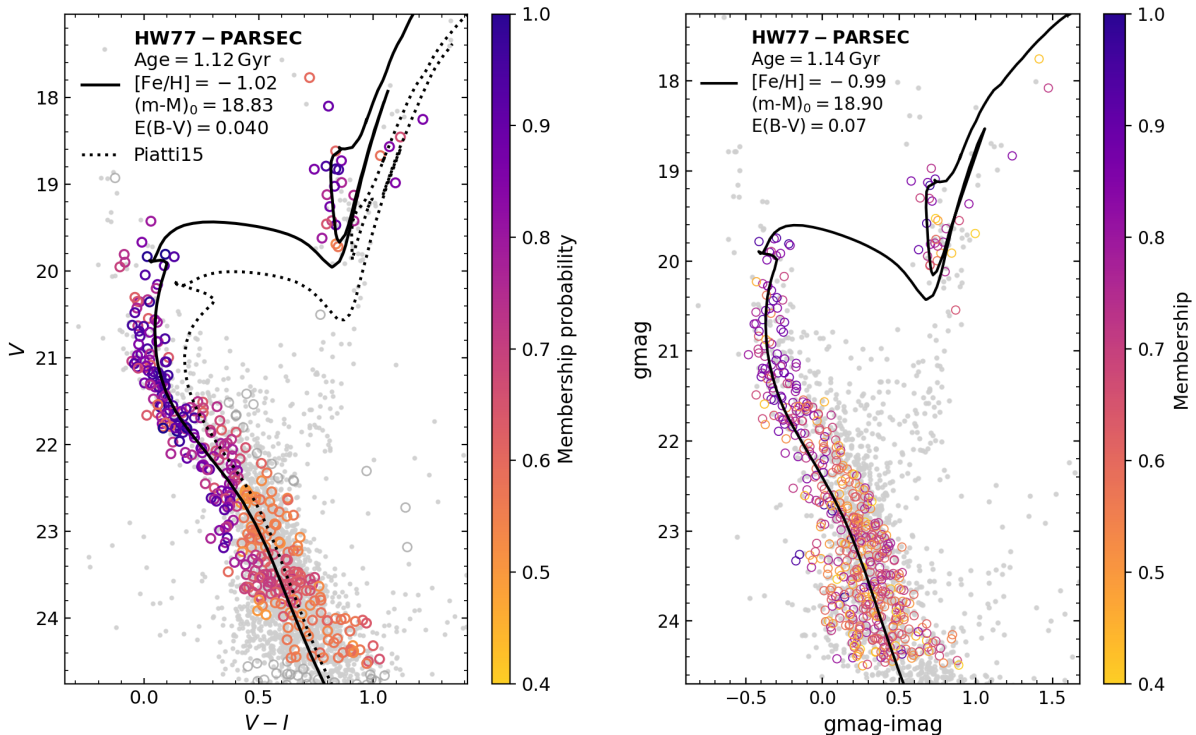
Figure 4.10: Comparison of the isochrone fits obtained from the decontaminated VISCACHA and SMASH CMDs for the Wing cluster HW77. The quantity, membership and distribution of the stars, as well as the position of the isochrone in the different CMD sequences are very similar, except for a small shift close to the MSTO in the VISCACHA CMD.

prior in metallicity to derive the remaining parameters. Section 5.1 presents more details about my contribution to Paper III and Paper IV.

4.3 Isochrone fitting: clusters with SMASH data

As discussed in Section 2.2, the SMASH fields cover ~ 300 clusters and associations in the Bridge, but less than $1/3$ of them have good quality data and are not located inside the detector gaps. Of these ~ 100 objects, fifteen are in common with the VISCACHA sample analysed in Section 4.2. Therefore, we are studying some benchmark clusters (e.g. HW77) to compare the performance of both surveys, and then expanding the analysis of the gradients, AMR and spatial distribution for a larger census of Bridge objects (Oliveira et al., in prep.). The region of $RA > 3^h$ is of particular interest, since it contains very few associations and was not explored by VISCACHA.

Figure 4.10 and 4.11 present the results obtained for HW77 in the isochrone fitting with VISCACHA and SMASH decontaminated CMDs, respectively. The CMD sequences are
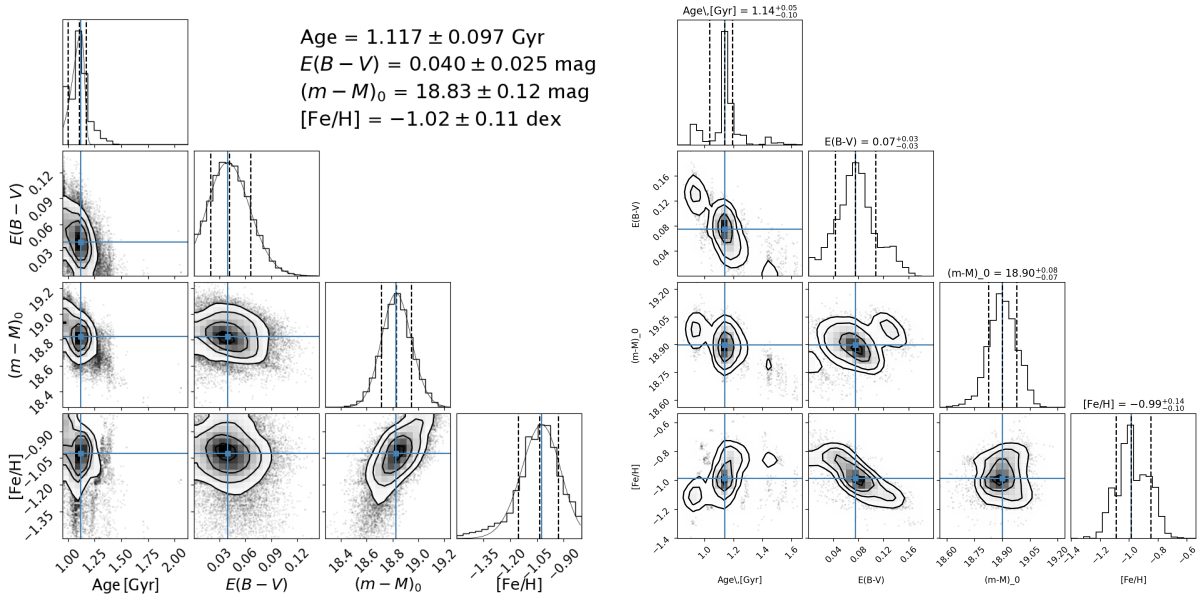
Figure 4.11: Corner plots obtained in the isochrone fitting of VISCACHA and SMASH photometry (left and right panels, respectively) for the Wing cluster HW77. The posteriors have some aspects in common, but the SMASH data provided slightly smaller uncertainties.

very similar including the red clump, leading to very close results between them: 1.12 vs. 1.14 Gyr, [Fe/H] $= -1.02$ vs. -0.99, $(m - M)_0 = 18.83$ vs. 18.90 and $E(B - V) = 0.04$ vs. 0.07. The corner plots also show similar distributions, with the SMASH data leading to slightly smaller uncertainties in age and distance modulus, which is probably a consequence of its smaller photometric errors. In this case, the VISCACHA observations were taken in optimal conditions and the SMASH photometry contains no gaps.

4.4   Comparison with the literature

In Table 4.3, we report the literature results on age and metallicity, based on the compilation by Bica et al. (2020) and subsequent work. Most of the reported works were based on visual isochrone fits, with several of them fixing the metallicity or distance compatible with the SMC: Glatt et al. (2010) and Maia et al. (2014) assumed [Fe/H] $= -0.58$ and 60.3 kpc; Piatti et al. (2007b,a) assumed [Fe/H] $= -0.7$ and 56.8 kpc; and Piatti (2011a,b) and Piatti et al. (2011, 2015) assumed [Fe/H] $= 0.7$ and 60.3 kpc. Table 4.3 also contains the core and tidal radii from Hill and Zaritsky (2006, available for nine sample clusters) and Santos et al. (2020, available for six sample clusters).

Table 4.3 - Ages and metallicities from the literature, obtained either from photometric or spectroscopic data. The core and tidal radii are from Hill and Zaritsky (2006) and Paper II.

Cluster	Age (Gyr)	[Fe/H] (dex)	r_c (arcsec)	r_t (arcsec)	Ref.
HW55	1.00 ± 1.15^1, 2.5 ± 0.7^2, 1.58 ± 2.24^3	-0.40 ± 0.22^3	12.7	70	HZ06
K55	0.25 ± 0.12^1, 0.28 ± 0.03^4, 0.63 ± 0.07^3	-0.58 ± 0.33^3	13.3, 16	136, 82	HZ06, Paper II
K57	0.45 ± 0.31^1, 0.45 ± 0.05^4, 0.56 ± 0.06^3	-0.48 ± 0.26^3	8.3, 23	98, 80	HZ06, Paper II
HW59	6.7 ± 1.1^5, 7.9 ± 5.5^3	-0.88 ± 1.3^3	–	–	–
HW63	0.45 ± 0.31^1, 5.4 ± 1.0^5, 3.55 ± 0.49^3	-0.70 ± 0.43^3	17.7	26	HZ06
L92	0.13 ± 0.09^1	–	10.4	89	HZ06
L93	1.00 ± 0.69^1	–	34.0	46	HZ06
L91	0.79 ± 0.55^1, 4.3 ± 1.0^5, 4.0 ± 0.6^3	-0.90 ± 0.06^6	9.6	107	HZ06
B147	0.13 ± 0.06^1	–	–	–	–
HW71se	$< 0.10^1$, $0.06^{+0.10}_{-0.02}$ (7)	–	7.7	80.6	HZ06
HW75	0.16 ± 0.11^1, 0.20 ± 0.05^8	–	8.2	135	HZ06
HW77	1.41 ± 0.32^8	–	30	85	Paper II
HW81	0.010 ± 0.002^8	–	–	–	–
HW82	0.06 ± 0.01^8	–	–	–	–
BS187	2.00 ± 0.46^8	–	6	43	Paper II
L109	2.5 ± 0.6^9, 4.0 ± 0.9^8, 5.0 ± 2.3^3	-0.88 ± 0.65^3	–	–	–
L110	6.4 ± 1.1^{10}, 6.3 ± 1.5^8, 5.0 ± 0.8^3	-1.03 ± 0.05^{11}	–	–	–
HW86	1.7 ± 0.2^{12}, 1.41 ± 0.32^8	-0.61 ± 0.06^{11}	–	–	–
L113	5.3 ± 1.0^{10}, 3.55 ± 0.41^3, 3.75 ± 0.30^{13}	-1.03 ± 0.04^{15}	–	–	–
L114	0.14 ± 0.03^{16}, 0.16 ± 0.07^3	-0.10 ± 0.11^3	9	87	Paper II
NGC796	0.11 ± 0.03^{16}, 0.04 ± 0.02^{18}	-0.31 ± 0.10^{19}	8	99	Paper II
WG13	0.13 ± 0.07^{17}	-0.20 ± 0.26^{17}	–	–	–
BS226	0.89 ± 0.31^{17}	-0.88 ± 0.43^{17}	–	–	–
BS245	0.10 ± 0.06^{17}	-0.28 ± 0.33^{17}	–	–	–

References. (1) Glatt et al. (2010); (2) Piatti (2011b); (3) Perren et al. (2017); (4) Maia et al. (2014); (5) Piatti (2011a); (6) De Bortoli et al. (2022); (7) Rafelski and Zaritsky (2005); (8) Piatti et al. (2015); (9) Piatti et al. (2011); (10) Piatti et al. (2007b); (11) Parisi et al. (2009); (12) Parisi et al. (2014); (13) Narloch et al. (2021); (14) Da Costa and Hatzidimitriou (1998); (15) Parisi et al. (2015); (16) Piatti et al. (2007a); (17) Bica et al. (2015); (18) Maia et al. (2019, Paper I).

Figure 4.12 compares the physical core and tidal radii derived in this work[1] with the

[1] The physical r_c and r_t were derived using the small-angle approximation, i.e. r_c [pc] $= \theta_c$ [rad] $\cdot d_\odot$ [pc], where $d_\odot$ is distance derived in the isochrone fitting (Table 4.2).
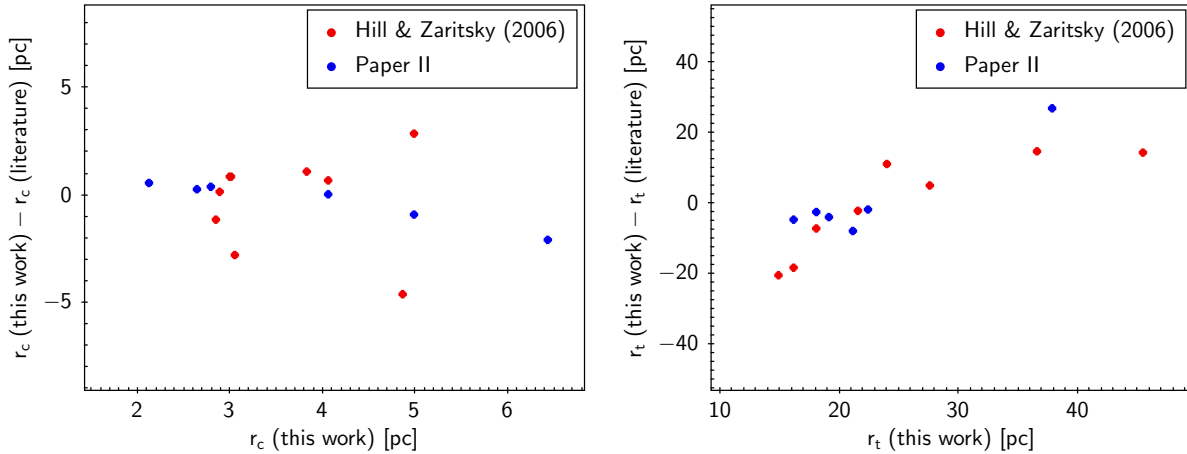
Figure 4.12: Comparison of the core (left) and tidal radii (right panel) with those from Hill and Zaritsky (2006) and Paper II. Our results have a very good agreement with Paper II (which applies the same photometry), but a much larger scatter compared to Hill and Zaritsky (2006, with shallower MCPS photometry).

values found in the literature for common clusters. It can be seen that, except for one deviant cluster, both structural parameters showed a good agreement with those derived in Paper II, using the same dataset but different techniques. When compared with the results by Hill and Zaritsky (2006) the core radii residuals show a somewhat large scatter, but no obvious trends; the tidal radii residuals on the other hand, present a linear trend with respect to cluster size. This behaviour can be understood by noting the shallower depth the MCPS photometry (used in their analysis) which usually misses the extended outer halo of faint stars present in large, populous clusters.

A comparison between the derived ages and metallicities and the values from Bica et al. (2020) is presented in Figure 4.13. Both the ages and metallicities show a good agreement within the uncertainties, with some discrepancies in the young, metal-rich end. More specifically, the largest discrepancy in metallicity is for L114 ([Fe/H] $= -0.47$, compared to -0.10 from Perren et al., 2017), followed by NGC796, K55 and L113. Such disagreement among young clusters in not unexpected, given the intrinsic difficulties associated with age-dating such stellar populations (e.g. differential reddening and pre-main sequence scattering in the lower main sequence, lack of giants due to stochasticity in the upper main sequence). A more thorough comparison with the literature cluster by cluster is given in Oliveira et al. (submitted).
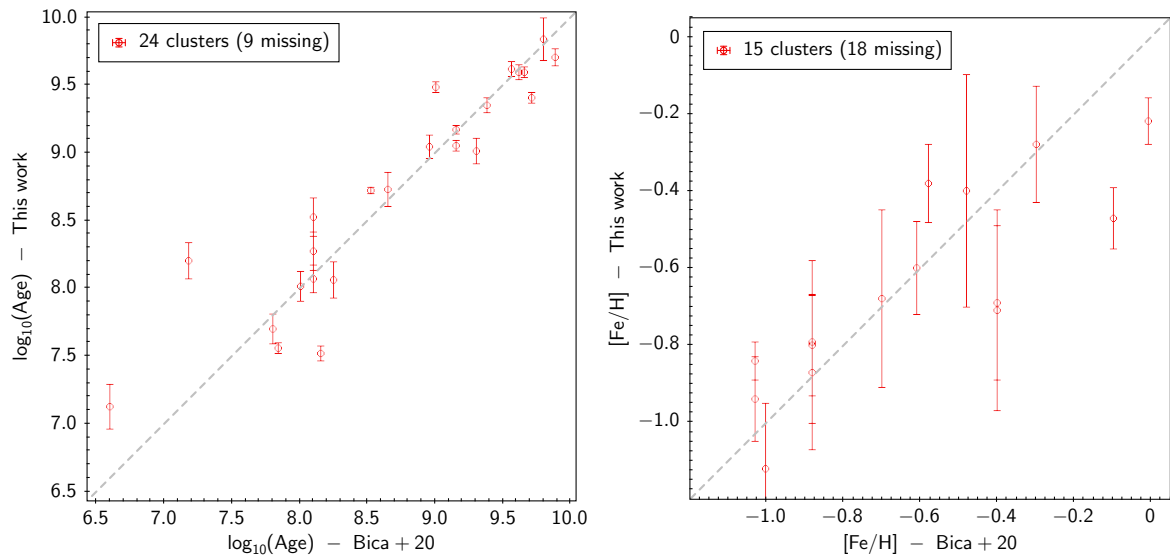
Figure 4.13: Comparison of the derived ages and metallicities to the ones from Bica et al. (2020). The ages and metallicities were derived for the first time for nine and eighteen clusters, respectively.

Chapter 5

Other works: clusters in other SMC regions and distances of bulge globular clusters from RR Lyrae

During the study of Wing/Bridge clusters, some studies were conducted in parallel, as already outlined in the initial FAPESP project. The first of them was the completion of the main paper of my Master research about multiple populations in bulge GCs with *HST* data (GO-13297 program Piotto et al., 2015), conducted in close collaboration with Stefano Souza. Some months were eventually used to make some final adjustments, obtain the final parameters and to submit and publish the paper after several interactions with the international collaboration. As described in Oliveira et al. (2020), we obtained an average of $12.3 \pm 0.4\,\mathrm{Gyr}$ assuming the sample clusters as simple stellar populations (with two of them closer to $\sim 13.5\,\mathrm{Gyr}$), and a mean age difference between the multiple populations of $41 \pm 170\,\mathrm{Myr}$ (canonical He) and $17 \pm 170\,\mathrm{Myr}$ (higher He for the second generation). The other two works in parallel are described in the following sections.

5.1   Ages and metallicities of clusters in other SMC regions

Since 2020, I have been actively participating in other VISCACHA papers with analysis of clusters in other SMC regions. My main contributions were in the data acquisition and statistical decontamination, and leading the isochrone fitting efforts, to get a proper characterisation of these clusters. In Paper III, GMOS spectra were obtained to complement the VISCACHA data for seven clusters in the Northern Bridge and Counter-Bridge. In Paper IV, the same analysis was carried out for five clusters in the West Halo. In Bica et al. (2022, Paper V), three clusters marked as very old ($> 5\,\mathrm{Gyr}$) in the literature were analysed and much younger ages were derived. Table 5.1 contains the derived parameters

for these clusters, and some more details are given in the following paragraphs.

Table 5.1 - Results of the isochrone fitting for SMC clusters in the Northern Bridge, Counter-Bridge, West Halo and Southern Bridge (Paper III, Paper IV and Paper V), obtained with VISCACHA data and PARSEC isochrones.

Cluster	Age	$[Fe/H]_{CMD}$	$[Fe/H]_{CaT}$	$d_\odot$	$E(B-V)$	M_V	$\log(M/M_\odot)$
	(Gyr)	(dex)	(dex)	(kpc)	(mag)		
BS196	$3.89^{+0.68}_{-0.50}$	$-0.75^{+0.22}_{-0.19}$	-0.89 ± 0.04	$50.1^{+1.6}_{-2.2}$	$0.05^{+0.04}_{-0.04}$	–	–
BS188	$1.82^{+0.22}_{-0.20}$	$-0.58^{+0.13}_{-0.13}$	-0.94 ± 0.06	$52.7^{+3.0}_{-3.1}$	$0.00^{+0.03}_{-0.00}$	–	–
HW56	$3.09^{+0.22}_{-0.14}$	$-0.54^{+0.07}_{-0.12}$	-0.97 ± 0.12	$53.5^{+1.2}_{-1.2}$	$0.03^{+0.02}_{-0.02}$	–	–
HW85	$1.74^{+0.08}_{-0.12}$	$-0.83^{+0.07}_{-0.05}$	-0.82 ± 0.06	$54.0^{+1.2}_{-2.0}$	$0.04^{+0.02}_{-0.02}$	–	–
L100	$3.16^{+0.15}_{-0.14}$	$-0.73^{+0.03}_{-0.03}$	-0.89 ± 0.06	$58.6^{+0.8}_{-0.5}$	$0.01^{+0.01}_{-0.01}$	–	–
B168	$6.6^{+0.8}_{-0.9}$	$-1.22^{+0.20}_{-0.15}$	-1.08 ± 0.06	$61.9^{+2.3}_{-2.0}$	$0.00^{+0.02}_{-0.00}$	–	–
IC1708	$0.93^{+0.16}_{-0.04}$	$-1.02^{+0.05}_{-0.10}$	-1.11 ± 0.06	$65.2^{+1.2}_{-1.8}$	$0.06^{+0.02}_{-0.02}$	–	–
NGC152	$1.27^{+0.04}_{-0.26}$	$-0.77^{+0.07}_{-0.21}$	-0.75 ± 0.08	$55.2^{+1.8}_{-1.5}$	$0.11^{+0.07}_{-0.04}$	–	–
Kron 8	$2.15^{+0.21}_{-0.21}$	$-0.75^{+0.07}_{-0.07}$	-0.84 ± 0.12	$65.2^{+3.4}_{-3.2}$	$0.07^{+0.04}_{-0.05}$	–	–
Kron 7	$2.34^{+0.20}_{-0.08}$	$-1.04^{+0.05}_{-0.05}$	-0.76 ± 0.07	$64.3^{+2.4}_{-2.3}$	$0.09^{+0.03}_{-0.04}$	–	–
L2	$3.98^{+0.37}_{-0.55}$	$-1.27^{+0.10}_{-0.08}$	-1.28 ± 0.08	$55.5^{+2.9}_{-2.7}$	$0.10^{+0.05}_{-0.05}$	–	–
AM3	$4.4^{+1.3}_{-1.4}$	$-1.00^{+0.10}_{-0.10}$	-1.00 ± 0.09	$63.7^{+4.2}_{-3.7}$	$0.04^{+0.04}_{-0.07}$	–	–
RZ82	$3.9^{+0.8}_{-0.8}$	$-0.68^{+0.33}_{-0.33}$	–	$51.1^{+4.5}_{-4.5}$	$0.14^{+0.07}_{-0.07}$	-5.39 ± 0.32	4.05 ± 0.17
HW42	$2.6^{+0.3}_{-0.3}$	$-0.57^{+0.37}_{-0.37}$	–	$56.0^{+4.1}_{-4.1}$	$0.08^{+0.08}_{-0.08}$	-5.45 ± 0.32	3.97 ± 0.17
RZ158	$4.8^{+1.6}_{-1.3}$	$-0.90^{+0.43}_{-0.39}$	–	$54.7^{+3.5}_{-3.5}$	$0.06^{+0.05}_{-0.04}$	-4.77 ± 0.30	3.88 ± 0.18

Paper III and Paper IV obtained GMOS spectra in the CaT region (three lines at 8498, 8542 and 8662 Å) to derive a spectroscopic metallicity and radial velocity which, together with the derived distance and proper motions from *Gaia*, provide a complete 6D phase-space vector. Radial velocities between 120 and 200 km s^{-1} were derived, as well as metallicities between -1.3 and -0.8, which were then applied as a prior in the isochrone fitting, in order to reduce the degeneracies and achieve a more precise solution. Figure 5.1 shows two interesting plots from Paper III: one shows the sky projection of the sample clusters and the derived distance, identifying one of them (IC1708, in purple) as projected in the Northern Bridge but belonging to the Counter-Bridge; the other shows the 3D distribution of the clusters, together with the velocity vectors, showing that IC1708 and the other clusters are moving in opposite directions.
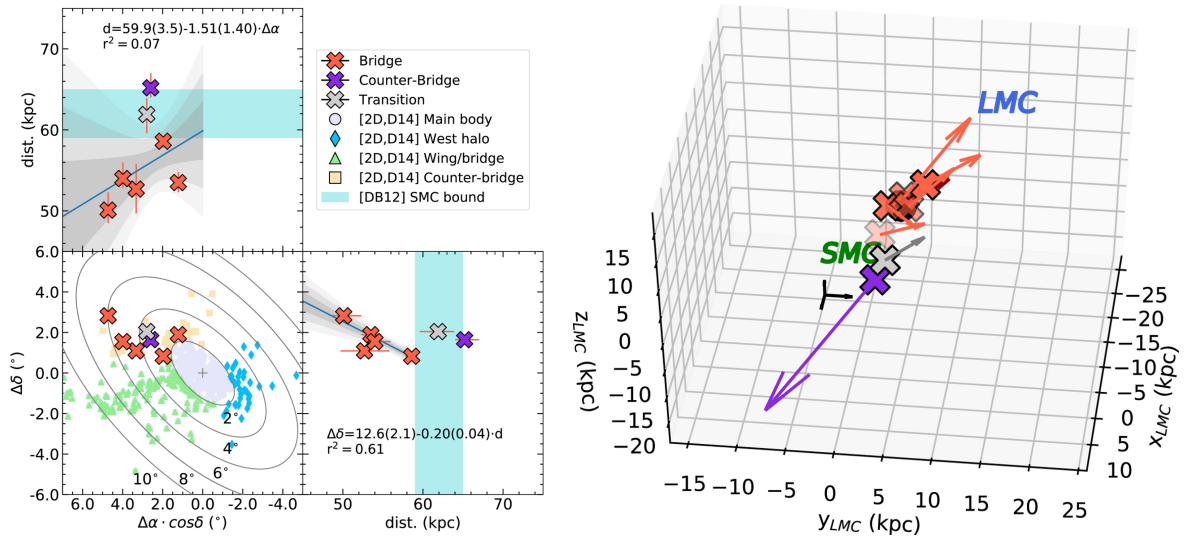
Figure 5.1: (Left:) Panels showing the sky projection of the seven analysed clusters located in the Northern Bridge and Counter-Bridge, and related to the derived distance. *(Right:)* 3D distribution of clusters, with the velocities relative to the SMC mean velocity are shown as arrows. Extracted from Paper III.

In Paper V, the clusters RZ82, HW42 and RZ158 were observed by VISCACHA with an unprecedented depth of $V \sim 23 - 24$ mag. It allowed us to make a reliable statistical decontamination including two magnitudes below the MSTO, and retrieve ages of 3.9, 2.6 and 4.8 Gyr, respectively, compared to 7.1, 5.0 and 8.3 Gyr from the literature. As shown in Figure 5.2, the new values of age and metallicity repositioned the three clusters closer to the overall distribution in the age-metallicity relation (previously considered outliers) and in the age-mass relation. It is interesting to note that our new data reached $1 - 2$ mag deeper than previous data, but we derived younger ages with a younger MSTO, which was probably a consequence of a more complete statistical decontamination.

5.2   *Distances of Bulge GCs from RR Lyrae stars*

In terms of Galaxy structure, stellar population components and calculations of orbits, globular cluster distances are the most uncertain information in their studies (Bica et al., 2006). The RR Lyrae variables (RRLs) are instability strip pulsators with a short period ($0.2 - 1.0$ days), representative of the older and fainter stellar populations (Population II, in contrast to classical Cepheid variables). The RRLs are very common in more metal-poor GCs ([Fe/H] ≤ -0.80), with a bluer HB and more stars on the instability strip. Assuming [Fe/H] and $E(B-V)$ values for a cluster with RRLs, we can precisely determine
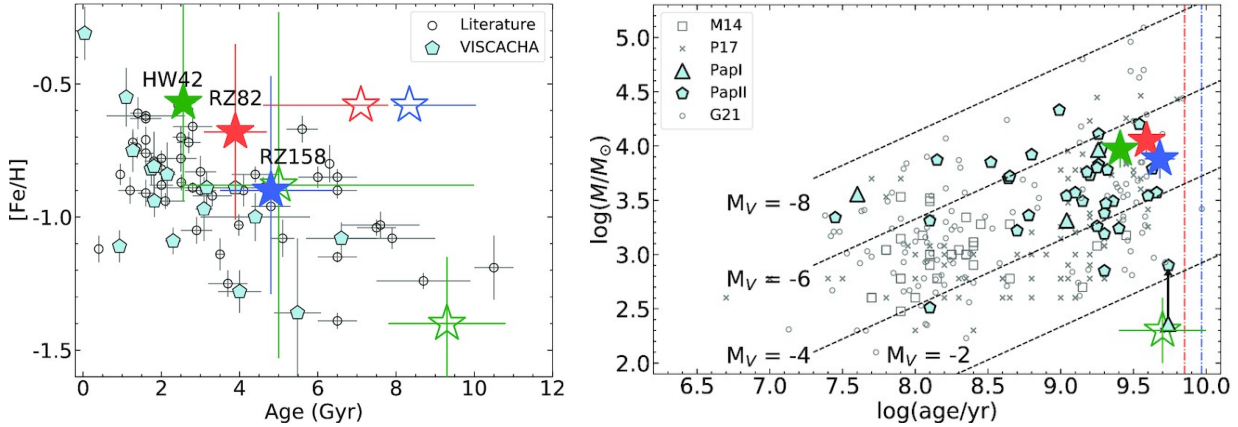
Figure 5.2: (Left:) Age-metallicity relation of SMC star clusters. The black circles are a compilation of clusters with metallicities derived from CaT spectroscopy, whereas the blue pentagons are the results from VISCACHA papers (Maia et al. (2019); Dias et al. (2021); Deason et al. (2020)). The new derivations of age and metallicity are shown as filled stars, compared to the empty stars with the literature values. *(Right:)* Updated age and mass for the three clusters, where HW42 was an outlier (Perren et al., 2017) and is repositioned to closer to the other clusters. Extracted from Paper V.

its distance by using well-calibrated period-luminosity and luminosity-metallicity (M_V − [Fe/H]) relations (Gaia Collaboration et al., 2017).

Soszyński et al. (2019) revealed larger samples of RRLs from OGLE-IV data, covering the bulge GCs NGC 6266, NGC 6441, NGC 6626, NGC 6638, NGC 6642 and NGC 6717, compared to the previous catalogues. We investigated this sample of metal-poor ([Fe/H] ∼ −1.2), central, and relatively reddened GCs, together with the catalogues or RRLs from OGLE-IV, Clement et al. (2001) and Holl et al. (2018, *Gaia* DR2). These catalogues were also cross-identified with the absolute proper motions from *Gaia* EDR3 (Gaia Collaboration et al., 2021), in order to select a reliable sample of cluster RRLs by calculating their astrometric membership probability.

We implemented a two-dimensional Gaussian mixture models (GMM) to identify the two distributions in the proper motions space. The GMM method assumes the data are clustered in the parameter space following a superposition of Gaussian distributions, using the expectation-maximisation algorithm to determine the parameters of each distribution and a correlation matrix (Pedregosa et al., 2011; Press et al., 2007). In this case, two Gaussian distributions are identified, where the cluster distribution has a lower dispersion. The membership probabilities of the RRLs were computed using the equations from Bellini et al. (2009), which consider not only the RRLs proper motions, but also those from the cluster and field (obtained from the GMM), and their respective uncertainties.
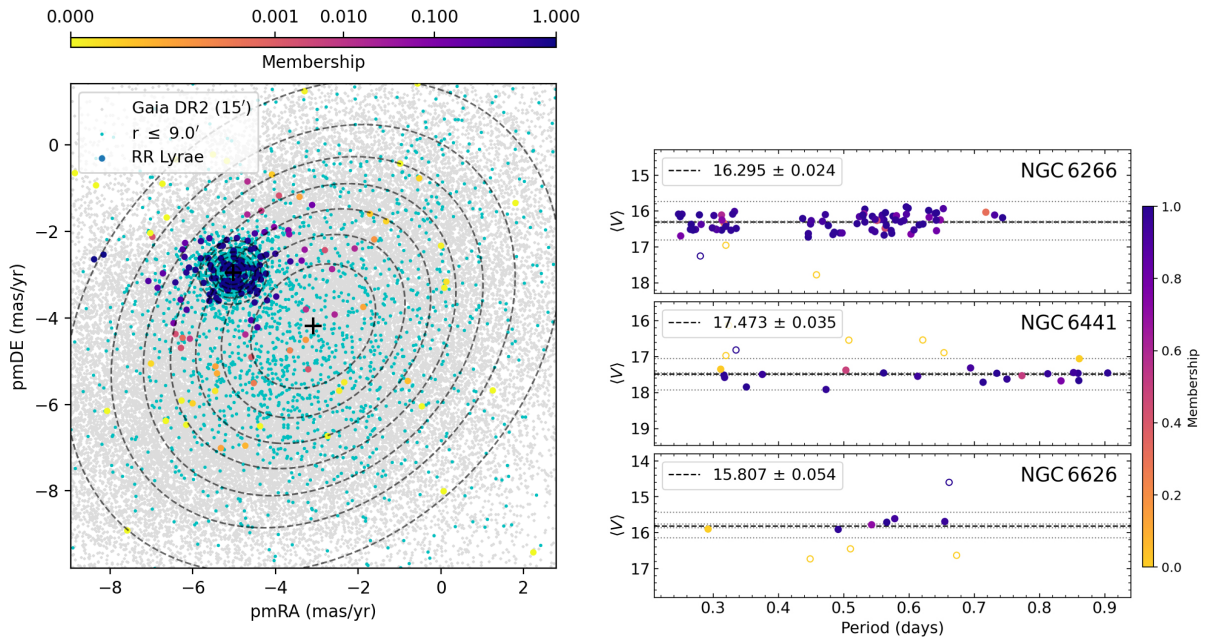
Figure 5.3: *(Left:)* Proper motions diagram of NGC 6266, showing the 242 RRLs colour-coded by the derived memberships, and the two Gaussian distributions (cluster and field), derived from the two-dimensional GMM. *(Right:)* Mean V magnitudes (Clement et al., 2001) of three clusters versus period of pulsation, where the dashed lines represent the average and the 2σ level, used to calculate the distance.

Figure 5.3 shows the proper motion diagram for NGC 6266 (colour-coded by the computed membership) and the mean magnitudes obtained from mean V magnitudes.

We also carried out the average of the RRL mean magnitudes, the determination of new $M_\lambda - [\text{Fe/H}]$ relations using updated BaSTI models for the zero-age horizontal branch, and discussed the more appropriated reddening laws and coefficients for a high-reddening regime. We obtained distances ($5-6\%$ precision) of $6.6\,\text{kpc}$, $13.1\,\text{kpc}$, $5.6\,\text{kpc}$, $9.6\,\text{kpc}$, $8.2\,\text{kpc}$ and $7.3\,\text{kpc}$ for NGC 6266, NGC 6441, NGC 6626, NGC 6638, NGC 6642, and NGC 6717, respectively, compatible with those from Baumgardt and Hilker (2018). The paper was published in 2022 (Oliveira et al., 2022).

An observational project with the SAM instrument at the SOAR $4\,\text{m}$ telescope, for detecting new RRL variables in the central regions of Bulge GCs, was also carried out in the 2018A and 2019A semesters (PI L. Kerber). I participated in the observations and initial data reduction with my co-advisor, Prof. Francisco Maia. This analysis will provide important constraints for the distances and helium abundances, by the statistical isochrone fitting. Preliminary results with light curves were presented in a 2018 ESO conference, in Pucón/Chile, and we will continue the work as new observations become available.

Chapter 6————————————————————————————————

Summary and Perspectives

The Magellanic Bridge is the only of the gaseous structures (formed by tidal forces and ram-pressure stripping) of the Magellanic System that hosts a stellar population. In the present work, the main goal was the study of the star formation history of this stellar component, through an homogeneous determination of the age, structural parameters and metallicity of stellar clusters and associations all along the Bridge. It will allow the detection of possible gradients (in age and/or metallicity) and kinematic signatures predicted by the models (e.g. Besla et al., 2012), contributing then for a deeper understanding of the formation and evolution scenarios of the entire System (D'Onghia and Fox, 2016). Data from VISCACHA and SMASH surveys were employed.

We presented the structural parameters, ages, metallicity, distances and masses obtained for 33 star clusters with VISCACHA photometry, located mostly in the SMC Wing and along halfway the Bridge (RA < 3$^{\mathrm{h}}$). The results include metallicities for 18 clusters and ages for 9 clusters derived for the first time. Based on the cluster masses and extrapolating to the number of objects in the Wing/Bridge ($\sim$ 100 clusters and 300 associations), we estimated a minimum stellar mass of $3 - 5 \times 10^5 M_\odot$ for the Bridge, more than one magnitude higher than the previous estimate from Harris (2007).

The 33 clusters consisted of: *(i)* 13 with ages between 500 Myr and 4.7 Gyr and more metal-poor than [Fe/H] = −0.5, probably formed normally along the SMC and then dragged to the Bridge during its formation; *(ii)* 15 young, metal-rich clusters (−0.5 < [Fe/H] < −0.1), formed in-situ after the recent LMC-SMC encounter 200 − 300 Myr ago, probably from enriched gas found mostly in the SMC centre. (Rubele et al., 2018); *(iii)* 5 clusters with intermediate metallicity and age, possibly formed just before the Bridge and require further analysis. The old clusters follow strictly the SMC age and metallicity gradients,

as well as the age-metallicity relation. The young clusters, on the other hand, presented a nearly constant metallicity value around -0.4 dex along the entire bridge, consistent with the enriched gas found mostly in the SMC centre (Oliveira et al., submitted).

When analysing the age-metallicity relation compared to the chemical evolution models, a particularly interesting group was identified: intermediate-age ($\sim 1\,\mathrm{Gyr}$) and metal-poor ($[\mathrm{Fe/H}] < -0.8$), namely BS187, HW77 and BS226 (also BS233 and BS235 from Bica et al., 2015). These clusters mark a metallicity dip around $1 - 1.5\,\mathrm{Gyr}$, with a metallicity drop of $0.4\,\mathrm{dex}$, followed by a rapid chemical enrichment. In general, such decrease in metallicity is explained by an infall of metal-poor gas, which is consistent with the formation epoch of the Magellanic Stream. A smaller metallicity dip is also clear around $200\,\mathrm{Myr}$, with $[\mathrm{Fe/H}]$ dropping from -0.25 to -0.55, coeval with the Bridge formation epoch (Zivick et al., 2018). Therefore, the formation of the Stream and Bridge seems to have left imprints in the chemical evolution of the Bridge clusters, hence dedicated chemical evolution models shall clarify the existence of these dips.

We also present some initial results obtained with SMASH photometry, which contains good quality data for ~ 100 Bridge objects, with similar depth but less complete in the cluster centre when compared to VISCACHA. An analysis of the cluster HW77 with data from both surveys retrieved very similar decontaminated CMDs and isochrone fits, with $1.1\,\mathrm{Gyr}$ and $[\mathrm{Fe/H}] \sim -1.0$. A more in-depth analysis of these data (including new DELVE data) will be completed in the coming months (Oliveira et al., in prep.), in order to complete the census of the Bridge clusters in terms of age and metallicity.

Other perspectives include a reanalysis of six Wing/Bridge clusters with a $[\mathrm{Fe/H}]$ prior provided from GMOS spectra (Dias et al., in prep., complementing Dias et al., 2021, 2022). Concerning new data acquisition, we plan to submit observing proposals to: Goodman@SOAR to obtain photometry for associations not covered in previous surveys, as well as GMOS@Gemini or Goodman@SOAR to obtain low-resolution spectra for the young Bridge clusters, in order to derive radial velocities and understand their assembly and in-situ formation. Some aspects of the analysis will also be improved, such as: implementing 2D density profiles, other analytical profiles and surface brightness profiles; implement machine learning methods in the decontamination; and improving the MCMC application to young clusters and synthetic CMDs in the isochrone fitting.

Bibliography

Abbott T. M. C., Abdalla F. B., Allam S., Amara A., Annis J., Asorey J., Avila S., Ballester O., et al. The Dark Energy Survey: Data Release 1, ApJS, 2018, vol. 239, p. 18

Bagheri G., Cioni M. R. L., Napiwotzki R., The detection of an older population in the Magellanic Bridge, A&A, 2013, vol. 551, p. A78

Barbuy B., Chiappini C., Gerhard O., Chemodynamical History of the Galactic Bulge, ARA&A, 2018, vol. 56, p. 223

Barger K. A., Haffner L. M., Bland-Hawthorn J., Warm Ionized Gas Revealed in the Magellanic Bridge Tidal Remnant: Constraining the Baryon Content and the Escaping Ionizing Photons around Dwarf Galaxies, ApJ, 2013, vol. 771, p. 132

Baumgardt H., Hilker M., A catalogue of masses, structural parameters, and velocity dispersion profiles of 112 Milky Way globular clusters, MNRAS, 2018, vol. 478, p. 1520

Bechtol K., Drlica-Wagner A., Balbinot E., Pieres A., Simon J. D., Yanny B., Santiago B., Wechsler R. H., Frieman J., Walker A. R., et al. Eight New Milky Way Companions Discovered in First-year Dark Energy Survey Data, ApJ, 2015, vol. 807, p. 50

Bellini A., Piotto G., Bedin L. R., Anderson J., Platais I., Momany Y., Moretti A., Milone A. P., Ortolani S., Ground-based CCD astrometry with wide field imagers. III. WFI@2.2m proper-motion catalog of the globular cluster ω Centauri, A&A, 2009, vol. 493, p. 959

Belokurov V., Erkal D., Deason A. J., Koposov S. E., De Angeli F., Evans D. W., Fraternali F., Mackey D., Clouds, Streams and Bridges. Redrawing the blueprint of the Magellanic System with Gaia DR1, MNRAS, 2017, vol. 466, p. 4711

Besla G., Kallivayalil N., Hernquist L., Robertson B., Cox T. J., van der Marel R. P., Alcock C., Are the Magellanic Clouds on Their First Passage about the Milky Way?, ApJ, 2007, vol. 668, p. 949

Besla G., Kallivayalil N., Hernquist L., van der Marel R. P., Cox T. J., Kereš D., Simulations of the Magellanic Stream in a First Infall Scenario, ApJ, 2010, vol. 721, p. L97

Besla G., Kallivayalil N., Hernquist L., van der Marel R. P., Cox T. J., Kereš D., The role of dwarf galaxy interactions in shaping the Magellanic System and implications for Magellanic Irregulars, MNRAS, 2012, vol. 421, p. 2109

Bessell M. S., UBVRI passbands., PASP, 1990, vol. 102, p. 1181

Bica E., Bonatto C., Barbuy B., Ortolani S., Globular cluster system and Milky Way properties revisited, A&A, 2006, vol. 450, p. 105

Bica E., Bonatto C., Dutra C. M., Santos J. F. C., A general catalogue of extended objects in the Magellanic System, MNRAS, 2008, vol. 389, p. 678

Bica E., Dutra C. M., Updating the Census of Star Clusters in the Small Magellanic Cloud, AJ, 2000, vol. 119, p. 1214

Bica E., Maia F. F. S., Oliveira R. A. P., Dias B., Santos J. F. C., Rocha J. P., Kerber L., Gardin J. F., Armond T., Parisi M. C., Souza S. O., Barbuy B., The VISCACHA survey - V. Rejuvenating three faint SMC clusters, MNRAS, 2022, vol. 517, p. L41

Bica E., Santiago B., Bonatto C., Garcia-Dias R., Kerber L., Dias B., Barbuy B., Balbinot E., Bridge over troubled gas: clusters and associations under the SMC and LMC tidal stresses, MNRAS, 2015, vol. 453, p. 3190

Bica E., Westera P., Kerber L. d. O., Dias B., Maia F., Santos João F. C. J., Barbuy B., Oliveira R. A. P., An Updated Small Magellanic Cloud and Magellanic Bridge Catalog of Star Clusters, Associations, and Related Objects, AJ, 2020, vol. 159, p. 82

Bica E. L. D., Schmitt H. R., A Revised and Extended Catalog of Magellanic System Clusters, Associations, and Emission Nebulae. I. Small Magellanic Cloud and Bridge, ApJS, 1995, vol. 101, p. 41

Bica E. L. D., Schmitt H. R., Dutra C. M., Oliveira H. L., A Revised and Extended Catalog of Magellanic System Clusters, Associations, and Emission Nebulae. II. The Large Magellanic Cloud, AJ, 1999, vol. 117, p. 238

Bland-Hawthorn J., Gerhard O., The Galaxy in Context: Structural, Kinematic, and Integrated Properties, ARA&A, 2016, vol. 54, p. 529

Bonatto C., Bica E., Open clusters in dense fields: the importance of field-star decontamination for NGC 5715, Lyngå 4, Lyngå 9, Trumpler 23, Trumpler 26 and Czernik 37, MNRAS, 2007, vol. 377, p. 1301

Bonatto C., Bica E., Structural parameters of star clusters: relations among light, mass and star-count radial profiles, and dependence on photometric depth, A&A, 2008, vol. 477, p. 829

Bressan A., Marigo P., Girardi L., Salasnich B., Dal Cero C., Rubele S., Nanni A., PARSEC: stellar tracks and isochrones with the PAdova and TRieste Stellar Evolution Code, MNRAS, 2012, vol. 427, p. 127

Brüns C., Kerp J., Staveley-Smith L., Mebold U., Putman M. E., Haynes R. F., Kalberla P. M. W., Muller E., Filipovic M. D., The Parkes H I Survey of the Magellanic System, A&A, 2005, vol. 432, p. 45

Cardelli J. A., Clayton G. C., Mathis J. S., The Relationship between Infrared, Optical, and Ultraviolet Extinction, ApJ, 1989, vol. 345, p. 245

Casetti-Dinescu D. I., Moni Bidin C., Girard T. M., Méndez R. A., Vieira K., Korchagin V. I., van Altena W. F., Recent Star Formation in the Leading Arm of the Magellanic Stream, ApJ, 2014, vol. 784, p. L37

Choi Y., Olsen K. A. G., Besla G., van der Marel R. P., Zivick P., Kallivayalil N., Nidever D. L., The Recent LMC-SMC Collision: Timing and Impact Parameter Constraints

from Comparison of Gaia LMC Disk Kinematics and N-body Simulations, ApJ, 2022, vol. 927, p. 153

Choudhury S., Subramaniam A., Cole A. A., Photometric metallicity map of the Large Magellanic Cloud, MNRAS, 2016, vol. 455, p. 1855

Choudhury S., Subramaniam A., Cole A. A., Sohn Y. J., Photometric metallicity map of the Small Magellanic Cloud, MNRAS, 2018, vol. 475, p. 4279

Cignoni M., Cole A. A., Tosi M., Gallagher J. S., Sabbi E., Anderson J., Grebel E. K., Nota A., Mean Age Gradient and Asymmetry in the Star Formation History of the Small Magellanic Cloud, ApJ, 2013, vol. 775, p. 83

Cioni M. R. L., The metallicity gradient as a tracer of history and structure: the Magellanic Clouds and M33 galaxies, A&A, 2009, vol. 506, p. 1137

Cioni M. R. L., Clementini G., Girardi L., Guand alini R., Gullieuszik M., Miszalski B., Moretti M. I., Ripepi V., et al. The VMC survey. I. Strategy and first data, A&A, 2011, vol. 527, p. A116

Clement C. M., Muzzin A., Dufton Q., Ponnampalam T., Wang J., Burford J., Richardson A., Rosebery T., et al. Variable Stars in Galactic Globular Clusters, AJ, 2001, vol. 122, p. 2587

Cohen R. J., Observations of the Magellanic Stream between declinations -20 and 0 degres., MNRAS, 1982, vol. 199, p. 281

Cole A. A., Tolstoy E., Gallagher John S. I., Smecker-Hane T. A., Spectroscopy of Red Giants in the Large Magellanic Cloud Bar: Abundances, Kinematics, and the Age-Metallicity Relation, AJ, 2005, vol. 129, p. 1465

Crowl H. H., Sarajedini A., Piatti A. E., Geisler D., Bica E., Clariá J. J., Santos João F. C. J., The Line-of-Sight Depth of Populous Clusters in the Small Magellanic Cloud, AJ, 2001, vol. 122, p. 220

Da Costa G. S., Hatzidimitriou D., Ca II Triplet Spectroscopy of Giants in Small Magellanic Cloud Star Clusters: Abundances, Velocities, and the Age-Metallicity Relation, AJ, 1998, vol. 115, p. 1934

De Bortoli B. J., Parisi M. C., Bassino L. P., Geisler D., Dias B., Gimeno G., Angelo M. S., Mauro F., Ca II triplet spectroscopy of Small Magellanic Cloud red giants. VI. Analysis of chemical properties of the main body, A&A, 2022, vol. 664, p. A168

de Vaucouleurs G., Pence W. D., An outsider's view of the Galaxy: photometric parameters, scale lengths, and absolute magnitudes of the spheroidal and disk components of our Galaxy., AJ, 1978, vol. 83, p. 1163

Deason A. J., Fattahi A., Frenk C. S., Grand R. J. J., Oman K. A., Garrison-Kimmel S., Simpson C. M., Navarro J. F., The edge of the Galaxy, MNRAS, 2020, vol. 496, p. 3929

Demers S., Battinelli P., The Young Intercloud Population. I. Distances and Ages, AJ, 1998, vol. 115, p. 154

Demers S., Grondin L., Irwin M. J., Kunkel W. E., Young Stars between the Magellanic Clouds. II. an Association on the Far-West Side of the LMC Halo, AJ, 1991, vol. 101, p. 911

Dennefeld M., A History of the Magellanic Clouds and the European Exploration of the Southern Hemisphere, The Messenger, 2020, vol. 181, p. 37

Dias B., The VISCACHA survey: an overview. In A Synoptic View of the Magellanic Clouds: VMC, Gaia and Beyond , 2019, p. 60

Dias B., Angelo M. S., Oliveira R. A. P., Maia F., Parisi M. C., De Bortoli B., Souza S. O., Katime Santrich O. J., Bassino L. P., Barbuy B., Bica E., Geisler D., Kerber L., Pérez-Villegas A., Quint B., Sanmartim D., Santos J. F. C., Westera P., The VISCACHA survey. III. Star clusters counterpart of the Magellanic Bridge and Counter-Bridge in 8D, A&A, 2021, vol. 647, p. L9

Dias B., Parisi M. C., Angelo M., Maia F., Oliveira R. A. P., Souza S. O., Kerber L. O., Santos J. F. C., Pérez-Villegas A., Sanmartim D., Quint B., Fraga L., Barbuy B., Bica E., Santrich O. J. K., Hernandez-Jimenez J. A., Geisler D., Minniti D., De Bórtoli B. J., Bassino L. P., Rocha J. P., The VISCACHA survey - IV. The SMC West Halo in 8D, MNRAS, 2022, vol. 512, p. 4334

Diaz J., Bekki K., Constraining the orbital history of the Magellanic Clouds: a new bound scenario suggested by the tidal origin of the Magellanic Stream, MNRAS, 2011, vol. 413, p. 2015

Diolaiti E., Bendinelli O., Bonaccini D., Close L., Currie D., Parmeggiani G., Analysis of isoplanatic high resolution stellar fields by the StarFinder code, A&AS, 2000, vol. 147, p. 335

D'Onghia E., Fox A. J., The Magellanic Stream: Circumnavigating the Galaxy, ARA&A, 2016, vol. 54, p. 363

D'Onghia E., Lake G., Small Dwarf Galaxies within Larger Dwarfs: Why Some Are Luminous while Most Go Dark, ApJ, 2008, vol. 686, p. L61

Dotter A., Chaboyer B., Jevremović D., Kostov V., Baron E., Ferguson J. W., The Dartmouth Stellar Evolution Database, ApJS, 2008, vol. 178, p. 89

Drlica-Wagner A., Ferguson P. S., Adamów M., Aguena M., Allam S., Andrade-Oliveira F., Bacon D., Bechtol K., Bell E. F., Bertin E., et al. The DECam Local Volume Exploration Survey Data Release 2, ApJS, 2022, vol. 261, p. 38

Einasto J., Saar E., Kaasik A., Chernin A. D., Missing mass around galaxies - Morphological evidence, Nature, 1974, vol. 252, p. 111

Elson R. A. W., Fall S. M., Freeman K. C., The Structure of Young Star Clusters in the Large Magellanic Cloud, ApJ, 1987, vol. 323, p. 54

Foreman-Mackey D., corner.py: Scatterplot matrices in Python, The Journal of Open Source Software, 2016, vol. 1, p. 24

Foreman-Mackey D., Hogg D. W., Lang D., Goodman J., emcee: The MCMC Hammer, PASP, 2013, vol. 125, p. 306

Fox A. J., Wakker B. P., Barger K. A., Hernandez A. K., Richter P., Lehner N., Bland-Hawthorn J., Charlton e., The COS/UVES Absorption Survey of the Magellanic Stream. III. Ionization, Total Mass, and Inflow Rate onto the Milky Way, ApJ, 2014, vol. 787, p. 147

Fujimoto M., Sofue Y., Dynamical evolution of the triple system of the Galaxy, the Large and Small Magellanic Clouds., A&A, 1976, vol. 47, p. 263

Fukugita M., Ichikawa T., Gunn J. E., Doi M., Shimasaku K., Schneider D. P., The Sloan Digital Sky Survey Photometric System, AJ, 1996, vol. 111, p. 1748

Gaia Collaboration Brown A. G. A., Vallenari A., Prusti T., de Bruijne J. H. J., Babusiaux C., Biermann M., Creevey O. L., Evans D. W., Eyer L., et al. Gaia Early Data Release 3. Summary of the contents and survey properties, A&A, 2021, vol. 649, p. A1

Gaia Collaboration Clementini G., Eyer L., Ripepi V., Marconi M., Muraveva T., Garofalo A., Sarro L. M., et al. Gaia Data Release 1. Testing parallaxes with local Cepheids and RR Lyrae stars, A&A, 2017, vol. 605, p. A79

Gaia Collaboration Prusti T., de Bruijne J. H. J., Brown A. G. A., Vallenari A., Babusiaux C., Bailer-Jones C. A. L., Bastian U., et al. The Gaia mission, A&A, 2016, vol. 595, p. A1

Gao X., A Machine-learning-based Investigation of the Open Cluster M67, ApJ, 2018, vol. 869, p. 9

Gardiner L. T., Noguchi M., N-body simulations of the Small Magellanic Cloud and the Magellanic Stream, MNRAS, 1996, vol. 278, p. 191

Gatto M., Ripepi V., Bellazzini M., Tosi M., Cignoni M., Tortora C., Leccia S., Clementini G., Grebel E. K., Longo G., Marconi M., Musella I., STEP survey - II. Structural analysis of 170 star clusters in the SMC, MNRAS, 2021, vol. 507, p. 3312

Gieles M., Zocchi A., A family of lowered isothermal models, MNRAS, 2015, vol. 454, p. 576

Glatt K., Grebel E. K., Koch A., Ages and luminosities of young SMC/LMC star clusters and the recent star formation history of the Clouds, A&A, 2010, vol. 517, p. A50

Graczyk D., Pietrzyński G., Thompson I. B., Gieren W., Zgirski B., Villanova S., Górski M., Wielgórski P., Karczmarek P., et al. A Distance Determination to the Small Magellanic Cloud with an Accuracy of Better than Two Percent Based on Late-type Eclipsing Binary Stars, ApJ, 2020, vol. 904, p. 13

GRAVITY Collaboration Abuter R., Amorim A., Bauböck M., Berger J. P., Bonnet H., Brandner W., Clénet Y., Coudé Du Foresto V., de Zeeuw P. T., et al. A geometric distance measurement to the Galactic center black hole with 0.3% uncertainty, A&A, 2019, vol. 625, p. L10

Grondin L., Demers S., Kunkel W. E., Young Stars Between the Magellanic Clouds. III. Overall Properties of Associations: A Shallow Mass Function, AJ, 1992, vol. 103, p. 1234

Hammer F., Yang Y. B., Flores H., Puech M., Fouquet S., The Magellanic Stream System. I. Ram-Pressure Tails and the Relics of the Collision Between the Magellanic Clouds, ApJ, 2015, vol. 813, p. 110

Harris J., The Magellanic Bridge: The Nearest Purely Tidal Stellar Population, ApJ, 2007, vol. 658, p. 345

Hill A., Zaritsky D., The Star Clusters of the Small Magellanic Cloud: Structural Parameters, AJ, 2006, vol. 131, p. 414

Hindman J. V., Kerr F. J., McGee R. X., A Low Resolution Hydrogen-line Survey of the Magellanic System. II. Interpretation of Results, Australian Journal of Physics, 1963, vol. 16, p. 570

Hodge P. W., Wright F. W., Catalog of 86 new star clusters in the Small Magellanic Cloud., AJ, 1974, vol. 79, p. 858

Holl B., Audard M., Nienartowicz K., Jevardat de Fombelle G., Marchal O., Mowlavi N., Clementini G., De Ridder J., et al. Gaia Data Release 2. Summary of the variability processing and analysis results, A&A, 2018, vol. 618, p. A30

Irwin M. J., Demers S., Kunkel W. E., A Blue Stellar Link Between the Magellanic Clouds, AJ, 1990, vol. 99, p. 191

Irwin M. J., Kunkel W. E., Demers S., A blue stellar population in the HI bridge between the two Magellanic Clouds, Nature, 1985, vol. 318, p. 160

Ivezić Ž., Kahn S. M., Tyson J. A., Abel B., Acosta E., Allsman R., Alonso D., AlSayyad Y., Anderson S. F., Andrew J., et al. LSST: From Science Drivers to Reference Design and Anticipated Data Products, ApJ, 2019, vol. 873, p. 111

Jacyszyn-Dobrzeniecka A. M., Skowron D. M., Mróz P., Skowron J., Soszyński I., Udalski A., Pietrukowicz P., Kozłowski S., Wyrzykowski Ł., Poleski R., et al. OGLE-ing the Magellanic System: Three-Dimensional Structure of the Clouds and the Bridge Using Classical Cepheids, Acta Astron., 2016, vol. 66, p. 149

Jones D. H., Read M. A., Saunders W., Colless M., Jarrett T., Parker Q. A., Fairall A. P., Mauch T., Sadler E. M., Watson F. G., et al. The 6dF Galaxy Survey: final redshift release (DR3) and southern large-scale structures, MNRAS, 2009, vol. 399, p. 683

Kallivayalil N., van der Marel R. P., Alcock C., Is the SMC Bound to the LMC? The Hubble Space Telescope Proper Motion of the SMC, ApJ, 2006, vol. 652, p. 1213

Kallivayalil N., van der Marel R. P., Besla G., Anderson J., Alcock C., Third-epoch Magellanic Cloud Proper Motions. I. Hubble Space Telescope/WFC3 Data and Orbit Implications, ApJ, 2013, vol. 764, p. 161

Karachentsev I. D., Karachentseva V. E., Huchtmeier W. K., Makarov D. I., A Catalog of Neighboring Galaxies, AJ, 2004, vol. 127, p. 2031

Kerber L. O., Libralato M., Souza S. O., Oliveira R. A. P., Ortolani S., Pérez-Villegas A., Barbuy B., Dias B., Bica E., Nardiello D., A deep view of a fossil relic in the Galactic bulge: the Globular Cluster HP 1, MNRAS, 2019, vol. 484, p. 5530

Kerr F. J., Hindman J. F., Robinson B. J., Observations of the 21 cm Line from the Magellanic Clouds, Australian Journal of Physics, 1954, vol. 7, p. 297

King I., The structure of star clusters. I. an empirical density law, AJ, 1962, vol. 67, p. 471

King I. R., The structure of star clusters. III. Some simple dynamical models, AJ, 1966, vol. 71, p. 64

Klypin A., Kravtsov A. V., Valenzuela O., Prada F., Where Are the Missing Galactic Satellites?, ApJ, 1999, vol. 522, p. 82

Koposov S. E., Belokurov V., Torrealba G., Evans N. W., Beasts of the Southern Wild: Discovery of Nine Ultra Faint Satellites in the Vicinity of the Magellanic Clouds., ApJ, 2015, vol. 805, p. 130

Kron G. E., Star Clusters in the Small Magellanic Cloud: I. Identification of 69 Clusters, PASP, 1956, vol. 68, p. 125

Kroupa P., On the variation of the initial mass function, MNRAS, 2001, vol. 322, p. 231

Laevens B. P. M., Martin N. F., Bernard E. J., Schlafly E. F., Sesar B., Rix H.-W., Bell E. F., Ferguson A. M. N., Slater C. T., et al. Sagittarius II, Draco II and Laevens 3: Three New Milky Way Satellites Discovered in the Pan-STARRS 1 3π Survey, ApJ, 2015, vol. 813, p. 44

Lee J. K., Rolleston W. R. J., Dufton P. L., Ryans R. S. I., Chemical compositions of four B-type supergiants in the SMC wing, A&A, 2005, vol. 429, p. 1025

Lehner N., Howk J. C., Keenan F. P., Smoker J. V., Metallicity and Physical Conditions in the Magellanic Bridge, ApJ, 2008, vol. 678, p. 219

Lindegren L., Hernández J., Bombrun A., Klioner S., Bastian U., Ramos-Lerate M., de Torres A., Steidelmüller H., Stephenson C., Hobbs D., et al. Gaia Data Release 2. The astrometric solution, A&A, 2018, vol. 616, p. A2

Lindsay E. M., The cluster system of the Small Magellanic Cloud, MNRAS, 1958, vol. 118, p. 172

López-Corredoira M., Allende Prieto C., Garzón F., Wang H., Liu C., Deng L., Disk stars in the Milky Way detected beyond 25 kpc from its center, A&A, 2018, vol. 612, p. L8

Lu L., Savage B. D., Sembach K. R., Wakker B. P., Sargent W. L. W., Oosterloo T. A., The Metallicity and Dust Content of HVC 287.5+22.5+240: Evidence for a Magellanic Clouds Origin, AJ, 1998, vol. 115, p. 162

Lynden-Bell D., Dwarf galaxies and globular clusters in high velocity hydrogen streams., MNRAS, 1976, vol. 174, p. 695

Maia F. F. S., Corradi W. J. B., Santos J. F. C. J., Characterization and photometric membership of the open cluster NGC1981, MNRAS, 2010, vol. 407, p. 1875

Maia F. F. S., Dias B., Santos J. F. C., Kerber L. d. O., Bica E., Piatti A. E., Barbuy B., Quint B., Fraga L., Sanmartim D., Angelo M. S., Hernandez-Jimenez J. A., Katime Santrich O. J., Oliveira R. A. P., et al. The VISCACHA survey - I. Overview and first results, MNRAS, 2019, vol. 484, p. 5702

Maia F. F. S., Piatti A. E., Santos J. F. C., Mass distribution and structural parameters of Small Magellanic Cloud star clusters, MNRAS, 2014, vol. 437, p. 2005

Martínez-Delgado D., Karim N., Charles E. J. E., Boschin W., Monelli M., Collins M. L. M., Donatiello G., Alfaro E. J., Pisces VII: discovery of a possible satellite of Messier 33 in the DESI legacy imaging surveys, MNRAS, 2022, vol. 509, p. 16

Martínez-Delgado D., Vivas A. K., Grebel E. K., Gallart C., Pieres A., Bell C. P. M., Zivick P., Lemasle B., et al. Nature of a shell of young stars in the outskirts of the Small Magellanic Cloud, A&A, 2019, vol. 631, p. A98

Mastropietro C., Moore B., Mayer L., Wadsley J., Stadel J., The gravitational and hydrodynamical interaction between the Large Magellanic Cloud and the Galaxy, MNRAS, 2005, vol. 363, p. 509

Mathewson D. S., Cleary M. N., Murray J. D., The Magellanic Stream., ApJ, 1974, vol. 190, p. 291

McClure-Griffiths N. M., Pisano D. J., Calabretta M. R., Ford H. A., Lockman F. J., Staveley-Smith L., Kalberla P. M. W., Bailin J., et al. Gass: The Parkes Galactic All-Sky Survey. I. Survey Description, Goals, and Initial Data Release, ApJS, 2009, vol. 181, p. 398

McGee R. X., Newton L. M., HI profiles in the bridge region of the Magellanic Clouds., Proceedings of the Astronomical Society of Australia, 1986, vol. 6, p. 471

Mellinger A., A Color All-Sky Panorama Image of the Milky Way, PASP, 2009, vol. 121, p. 1180

Milone A. P., Cordoni G., Marino A. F., D'Antona F., Bellini A., Di Criscienzo M., Dondoglio E., Lagioia E. P., Langer N., Legnardi M. V., Libralato M., Baumgardt H., Bettinelli M., Cavecchi Y., de Grijs R., Deng L., Hastings B., Li C., Mohandasan A., Renzini A.,

Vesperini E., Wang C., Ziliotto T., Carlos M., Costa G., Dell'Agli F., Di Stefano S., Jang S., Martorano M., Simioni M., Tailo M., Ventura P., Hubble Space Telescope survey of Magellanic Cloud star clusters. Photometry and astrometry of 113 clusters and early results, A&A, 2023, vol. 672, p. A161

Misawa T., Charlton J. C., Kobulnicky H. A., Wakker B. P., Bland-Hawthorn J., The Magellanic Bridge as a Damped Lyman Alpha System: Physical Properties of Cold Gas Toward PKS 0312-770, ApJ, 2009, vol. 695, p. 1382

Momany Y., Zaggia S. R., Bonifacio P., Piotto G., De Angeli F., Bedin L. R., Carraro G., Probing the Canis Major stellar over-density as due to the Galactic warp, A&A, 2004, vol. 421, p. L29

Moore B., Davis M., The origin of the Magellanic Stream., MNRAS, 1994, vol. 270, p. 209

Moore B., Ghigna S., Governato F., Lake G., Quinn T., Stadel J., Tozzi P., Dark Matter Substructure within Galactic Halos, ApJ, 1999, vol. 524, p. L19

Narloch W., Pietrzyński G., Gieren W., Piatti A. E., Górski M., Karczmarek P., Graczyk D., Suchomska K., Zgirski B., Wielgórski P., et al. Metallicities and ages for 35 star clusters and their surrounding fields in the Small Magellanic Cloud, A&A, 2021, vol. 647, p. A135

Navarrete C., Aguado D. S., Belokurov V., Erkal D., Deason A., Cullinane L., Carballo-Bello J., The 3D kinematics of stellar substructures in the periphery of the Large Magellanic Cloud, arXiv e-prints, 2023, p. arXiv:2302.04579

Nidever D. L., Majewski S. R., Butler Burton W., The Origin of the Magellanic Stream and Its Leading Arm, ApJ, 2008, vol. 679, p. 432

Nidever D. L., Majewski S. R., Butler Burton W., Nigra L., The 200° Long Magellanic Stream System, ApJ, 2010, vol. 723, p. 1618

Nidever D. L., Monachesi A., Bell E. F., Majewski S. R., Muñoz R. R., Beaton R. L., A Tidally Stripped Stellar Component of the Magellanic Bridge, ApJ, 2013, vol. 779, p. 145

Nidever D. L., Olsen K., Choi Y., Ruiz-Lara T., Miller A. E., Johnson L. C., Bell C. P. M., Blum R. D., Cioni M.-R. L., et al. The Second Data Release of the Survey of the MAgellanic Stellar History (SMASH), AJ, 2021, vol. 161, p. 74

Nidever D. L., Olsen K., Walker A. R., Vivas A. K., Blum R. D., Kaleida C., Choi Y., Conn B. C., Gruendl R. A., Bell E. F., Besla G., Muñoz R. R., Gallart C., Martin N. F., Olszewski E. W., et al. SMASH: Survey of the MAgellanic Stellar History, AJ, 2017, vol. 154, p. 199

Noël N. E. D., Conn B. C., Carrera R., Read J. I., Rix H. W., Dolphin A., The MAGellanic Inter-Cloud Project (MAGIC). I. Evidence for Intermediate-age Stellar Populations in between the Magellanic Clouds, ApJ, 2013, vol. 768, p. 109

Oliveira R. A. P., Múltiplas populações com filtros UV do Telescópio Espacial Hubble e ajuste de isócronas em aglomerados globulares do Bojo, São Paulo: Instituto de Astronomia, Geofísica e Ciências Atmosféricas, Universidade de São Paulo, 2019, Master Dissertation, 151 p.

Oliveira R. A. P., Ortolani S., Barbuy B., Kerber L. O., Maia F. F. S., Bica E., Cassisi S., Souza S. O., Pérez-Villegas A., Precise distances from OGLE-IV member RR Lyrae stars in six bulge globular clusters, A&A, 2022, vol. 657, p. A123

Oliveira R. A. P., Souza S. O., Kerber L. O., Barbuy B., Ortolani S., Piotto G., Nardiello D., Pérez-Villegas A., Maia F. F. S., et al. The Hubble Space Telescope UV Legacy Survey of Galactic Globular Clusters. XX. Ages of Single and Multiple Stellar Populations in Seven Bulge Globular Clusters, ApJ, 2020, vol. 891, p. 37

Ortolani S., Held E. V., Nardiello D., Souza S. O., Barbuy B., Pérez-Villegas A., Cassisi S., Bica E., et al. Another relic bulge globular cluster: ESO 456-SC38 (Djorgovski 2), A&A, 2019, vol. 627, p. A145

Pagel B. E. J., Tautvaisiene G., Chemical evolution of the Magellanic Clouds: analytical models, MNRAS, 1998, vol. 299, p. 535

Palma T., Gramajo L. V., Clariá J. J., Lares M., Geisler D., Ahumada A. V., Catalogue of Large Magellanic Cloud star clusters observed in the Washington photometric system, A&A, 2016, vol. 586, p. A41

Parisi M. C., Geisler D., Carraro G., Clariá J. J., Costa E., Grocholski A. J., Sarajedini
A., Leiton R., Piatti A. E., Age Determination of 15 Old to Intermediate-age Small
Magellanic Cloud Star Clusters, AJ, 2014, vol. 147, p. 71

Parisi M. C., Geisler D., Carraro G., Clariá J. J., Villanova S., Gramajo L. V., Sarajedini
A., Grocholski A. J., Ca II Triplet Spectroscopy of Small Magellanic Cloud Red Giants.
IV. Abundances for a Large Sample of Field Stars and Comparison with the Cluster
Sample, AJ, 2016, vol. 152, p. 58

Parisi M. C., Geisler D., Clariá J. J., Villanova S., Marcionni N., Sarajedini A., Grocholski
A. J., Ca II Triplet Spectroscopy of Small Magellanic Cloud Red Giants. III. Abundances
and Velocities for a Sample of 14 Clusters, AJ, 2015, vol. 149, p. 154

Parisi M. C., Gramajo L. V., Geisler D., Dias B., Clariá J. J., Da Costa G., Grebel E. K.,
Ca II triplet spectroscopy of Small Magellanic Cloud red giants. V. Abundances and
velocities for 12 massive clusters, A&A, 2022, vol. 662, p. A75

Parisi M. C., Grocholski A. J., Geisler D., Sarajedini A., Clariá J. J., Ca II Triplet Spec-
troscopy of Small Magellanic Cloud Red Giants. I. Abundances and Velocities for a
Sample of Clusters, AJ, 2009, vol. 138, p. 517

Patel E., Kallivayalil N., Garavito-Camargo N., Besla G., Weisz D. R., van der Marel R. P.,
Boylan-Kolchin M., Pawlowski M. S., Gómez F. A., The Orbital Histories of Magellanic
Satellites Using Gaia DR2 Proper Motions, ApJ, 2020, vol. 893, p. 121

Pedregosa F., Varoquaux G., Gramfort A., Michel V., Thirion B., Grisel O., Blondel M.,
Prettenhofer P., Weiss R., Dubourg V., Vanderplas J., Passos A., Cournapeau D., Bru-
cher M., Perrot M., Duchesnay E., Scikit-learn: Machine Learning in Python, Journal
of Machine Learning Research, 2011, vol. 12, p. 2825

Perren G. I., Piatti A. E., Vázquez R. A., Astrophysical properties of star clusters in the
Magellanic Clouds homogeneously estimated by ASteCA, A&A, 2017, vol. 602, p. A89

Perren G. I., Vázquez R. A., Piatti A. E., ASteCA: Automated Stellar Cluster Analysis,
A&A, 2015, vol. 576, p. A6

Piatti A. E., New candidate intermediate-age star clusters in the Small Magellanic Cloud, MNRAS, 2011a, vol. 416, p. L89

Piatti A. E., Towards a comprehensive picture of the star cluster age-metallicity relationship in the Small Magellanic Cloud, MNRAS, 2011b, vol. 418, p. L69

Piatti A. E., Clariá J. J., Bica E., Geisler D., Ahumada A. V., Girardi L., Washington photometry of 14 intermediate-age to old star clusters in the Small Magellanic Cloud, MNRAS, 2011, vol. 417, p. 1559

Piatti A. E., de Grijs R., Rubele S., Cioni M.-R. L., Ripepi V., Kerber L., The VMC survey - XV. The Small Magellanic Cloud-Bridge connection history as traced by their star cluster populations, MNRAS, 2015, vol. 450, p. 552

Piatti A. E., Guandalini R., Ivanov V. D., Rubele S., Cioni M.-R. L., de Grijs R., For B.-Q., Clementini G., Ripepi V., Anders P., Oliveira J. M., The VMC Survey. XII. Star cluster candidates in the Large Magellanic Cloud, A&A, 2014, vol. 570, p. A74

Piatti A. E., Santos J. F. C. J., Clariá J. J., Bica E., Ahumada A. V., Parisi M. C., Integrated spectral analysis of 18 concentrated star clusters in the Small Magellanic Cloud, A&A, 2005, vol. 440, p. 111

Piatti A. E., Sarajedini A., Geisler D., Gallart C., Wischnjewsky M., Five young star clusters in the outer region of the Small Magellanic Cloud, MNRAS, 2007a, vol. 382, p. 1203

Piatti A. E., Sarajedini A., Geisler D., Gallart C., Wischnjewsky M., Two newly identified, relatively old star clusters in the Small Magellanic Cloud, MNRAS, 2007b, vol. 381, p. L84

Pietrinferni A., Cassisi S., Salaris M., Castelli F., A Large Stellar Evolution Database for Population Synthesis Studies. I. Scaled Solar Models and Isochrones, ApJ, 2004, vol. 612, p. 168

Pietrzyński G., Graczyk D., Gallenne A., Gieren W., Thompson I. B., Pilecki B., Karczmarek P., Górski M., Suchomska K., Taormina M., et al. A distance to the Large Magellanic Cloud that is precise to one per cent, Nature, 2019, vol. 567, p. 200

Pietrzynski G., Udalski A., The Optical Gravitational Lensing Experiment. Ages of about 600 Star Clusters from the LMC, Acta Astron., 2000, vol. 50, p. 337

Piotto G., Milone A. P., Bedin L. R., Anderson J., King I. R., Marino A. F., Nardiello D., Aparicio A., et al. The Hubble Space Telescope UV Legacy Survey of Galactic Globular Clusters. I. Overview of the Project and Detection of Multiple Stellar Populations, AJ, 2015, vol. 149, p. 91

Press W. H., Teukolsky S. A., Vetterling W. T., Flannery B. P., Numerical Recipes 3rd Edition: The Art of Scientific Computing 3 edn. Cambridge University Press USA, 2007

Price-Whelan A. M., Nidever D. L., Choi Y., Schlafly E. F., Morton T., Koposov S. E., Belokurov V., Discovery of a Disrupting Open Cluster Far into the Milky Way Halo: A Recent Star Formation Event in the Leading Arm of the Magellanic Stream?, ApJ, 2019, vol. 887, p. 19

Putman M. E., Gibson B. K., Staveley-Smith L., Banks G., Barnes D. G., Bhatal R., Disney M. J., Ekers R. D., et al. Tidal disruption of the Magellanic Clouds by the Milky Way, Nature, 1998, vol. 394, p. 752

Rafelski M., Zaritsky D., The Star Clusters of the Small Magellanic Cloud: Age Distribution, AJ, 2005, vol. 129, p. 2701

Ramachandran V., Oskinova L. M., Hamann W. R., Discovery of O stars in the tidal Magellanic Bridge. Stellar parameters, abundances, and feedback of the nearest metal-poor massive stars and their implication for the Magellanic System ecology, A&A, 2021, vol. 646, p. A16

Richstein H., Patel E., Kallivayalil N., Simon J. D., Zivick P., Tollerud E., Fritz T., Warfield J. T., Besla G., van der Marel R. P., Wetzel A., Choi Y., Deason A., Geha M., Guhathakurta P., Jeon M., Kirby E. N., Libralato M., Sacchi E., Sohn S. T., Structural Parameters and Possible Association of the Ultra-faint Dwarfs Pegasus III and Pisces II from Deep Hubble Space Telescope Photometry, ApJ, 2022, vol. 933, p. 217

Ripepi V., Cignoni M., Tosi M., Marconi M., Musella I., Grado A., Limatola L., Clementini G., et al. STEP: the VST survey of the SMC and the Magellanic Bridge - I. Overview and first results, MNRAS, 2014, vol. 442, p. 1897

Rodríguez M. J., Feinstein C., Baume G., Dias B., Maia F. S. M., Santos J. F. C., Kerber L., Minniti D., Pérez-Villegas A., De Bórtoli B., Parisi M. C., Oliveira R. A. P., The VISCACHA survey - VI. Dimensional study of the structure of 82 star clusters in the Magellanic Clouds, MNRAS, 2023, vol. 519, p. 3357

Rolleston W. R. J., Trundle C., Dufton P. L., The present-day chemical composition of the LMC, A&A, 2002, vol. 396, p. 53

Rubele S., Pastorelli G., Girardi L., Cioni M.-R. L., Zaggia S., Marigo P., Bekki K., Bressan A., Clementini G., de Grijs R., Emerson J., Groenewegen M. A. T., Ivanov V. D., Muraveva T., Nanni A., Oliveira J. M., Ripepi V., Sun N.-C., van Loon J. T., The VMC survey - XXXI: The spatially resolved star formation history of the main body of the Small Magellanic Cloud, MNRAS, 2018, vol. 478, p. 5017

Salpeter E. E., The Luminosity Function and Stellar Evolution., ApJ, 1955, vol. 121, p. 161

Santos João F. C. J., Maia F. F. S., Dias B., Kerber L. d. O., Piatti A. E., Bica E., Angelo M. S., Minniti D., Pérez-Villegas A., Roman-Lopes A., Westera P., Fraga L., Quint B., Sanmartim D., The VISCACHA survey - II. Structure of star clusters in the Magellanic Clouds periphery, MNRAS, 2020, vol. 498, p. 205

Savage B. D., The Gaseous Galactic Corona. In The Physics of the Interstellar Medium and Intergalactic Medium , vol. 80 of Astronomical Society of the Pacific Conference Series, 1995, p. 233

Schmidt T., Cioni M.-R. L., Niederhofer F., Bekki K., Bell C. P. M., de Grijs R., Diaz J., El Youssoufi D., Emerson J., Groenewegen M. A. T., Ivanov V. D., Matijevic G., Oliveira J. M., Petr-Gotzens M. G., Queiroz A. B. A., Ripepi V., van Loon J. T., The VMC survey. XXXVIII. Proper motion of the Magellanic Bridge, A&A, 2020, vol. 641, p. A134

Schmidt T., Cioni M.-R. L., Niederhofer F., Bekki K., Bell C. P. M., de Grijs R., El Youssoufi D., Ivanov V. D., Oliveira J. M., Ripepi V., van Loon J. T., The VMC survey. XLV. Proper motion of the outer LMC and the impact of the SMC, A&A, 2022, vol. 663, p. A107

Shapley H., An Extension of the Small Magellanic Cloud, Harvard College Observatory Bulletin, 1940, vol. 914, p. 8

Skowron D. M., Jacyszyn A. M., Udalski A., Szymański M. K., Skowron J., Poleski R., Kozłowski S., Kubiak M., et al. OGLE-ING the Magellanic System: Stellar Populations in the Magellanic Bridge, ApJ, 2014, vol. 795, p. 108

Skowron D. M., Skowron J., Udalski A., Szymański M. K., Soszyński I., Wyrzykowski Ł., Ulaczyk K., Poleski R., Kozłowski S., Pietrukowicz P., Mróz P., Rybicki K., Iwanek P., Wrona M., Gromadzki M., OGLE-ing the Magellanic System: Optical Reddening Maps of the Large and Small Magellanic Clouds from Red Clump Stars, ApJS, 2021, vol. 252, p. 23

Soszyński I., Udalski A., Wrona M., Szymański M. K., Pietrukowicz P., Skowron J., Skowron D., Poleski R., et al.. Over 78 000 RR Lyrae Stars in the Galactic Bulge and Disk from the OGLE Survey, Acta Astron., 2019, vol. 69, p. 321

Souza S. O., Kerber L. O., Barbuy B., Pérez-Villegas A., Oliveira R. A. P., Nardiello D., Self-consistent Analysis of Stellar Clusters: An Application to HST Data of the Halo Globular Cluster NGC 6752, ApJ, 2020, vol. 890, p. 38

Stanimirović S., Staveley-Smith L., Jones P. A., A New Look at the Kinematics of Neutral Hydrogen in the Small Magellanic Cloud, ApJ, 2004, vol. 604, p. 176

Stetson P. B., Homogeneous Photometry for Star Clusters and Resolved Galaxies. II. Photometric Standard Stars, PASP, 2000, vol. 112, p. 925

Subramanian S., Rubele S., Sun N.-C., Girardi L., de Grijs R., van Loon J. T., Cioni M.-R. L., Piatti A. E., Bekki K., Emerson J., Ivanov V. D., Kerber L., Marconi M., Ripepi V., Tatton B. L., The VMC Survey - XXIV. Signatures of tidally stripped stellar populations from the inner Small Magellanic Cloud, MNRAS, 2017, vol. 467, p. 2980

Subramanian S., Subramaniam A., The Three-dimensional Structure of the Small Magellanic Cloud, ApJ, 2012, vol. 744, p. 128

Tokovinin A., Cantarutti R., Tighe R., Schurter P., Martinez M., Thomas S., van der Bliek N., SOAR Adaptive Module (SAM): Seeing Improvement with a UV Laser, PASP, 2016, vol. 128, p. 125003

Torrealba G., Belokurov V., Koposov S. E., Li T. S., Walker M. G., Sanders J. L., Geringer-Sameth A., Zucker D. B., Kuehn K., Evans N. W., Dehnen W., The hidden giant: discovery of an enormous Galactic dwarf satellite in Gaia DR2, MNRAS, 2019, vol. 488, p. 2743

Tsujimoto T., Bekki K., Chemical Signature of a Major Merger in the Early Formation of the Small Magellanic Cloud, ApJ, 2009, vol. 700, p. L69

Udalski A., Szymański M. K., Szymański G., OGLE-IV: Fourth Phase of the Optical Gravitational Lensing Experiment, Acta Astron., 2015, vol. 65, p. 1

van den Bergh S., The Galaxies of the Local Group, 2007

van der Marel R. P., Alves D. R., Hardy E., Suntzeff N. B., New Understanding of Large Magellanic Cloud Structure, Dynamics, and Orbit from Carbon Star Kinematics, AJ, 2002, vol. 124, p. 2639

van der Marel R. P., Cioni M.-R. L., Magellanic Cloud Structure from Near-Infrared Surveys. I. The Viewing Angles of the Large Magellanic Cloud, AJ, 2001, vol. 122, p. 1807

von Hippel T., Robinson E., Jeffery E., Wagner-Kaiser R., DeGennaro S., Stein N., Stenning D., Jefferys W. H., van Dyk D., Bayesian Analysis for Stellar Evolution with Nine Parameters (BASE-9): User's Manual, arXiv e-prints, 2014, p. arXiv:1411.3786

Wakker B. P., van Woerden H., High-Velocity Clouds, ARA&A, 1997, vol. 35, p. 217

Westerlund B. E., Glaspey J., On the structure of the wing of the Small Magellanic Cloud., A&A, 1971, vol. 10, p. 1

Willman B., Blanton M. R., West A. A., Dalcanton J. J., Hogg D. W., Schneider D. P., Wherry N., Yanny B., Brinkmann J., A New Milky Way Companion: Unusual Globular Cluster or Extreme Dwarf Satellite?, AJ, 2005, vol. 129, p. 2692

Wolf C., Onken C. A., Luvaul L. C., Schmidt B. P., Bessell M. S., Chang S.-W., Da Costa G. S., Mackey D., Martin-Jones T., Murphy S. J., Preston T., Scalzo R. A., Shao L., Smillie J., Tisserand P., White M. C., Yuan F., SkyMapper Southern Survey: First Data Release (DR1), PASA, 2018, vol. 35, p. e010

Zaritsky D., Harris J., Thompson I. B., Grebel E. K., Massey P., The Magellanic Clouds
    Photometric Survey: The Small Magellanic Cloud Stellar Catalog and Extinction Map,
    AJ, 2002, vol. 123, p. 855

Zivick P., Kallivayalil N., Besla G., Sohn S. T., van der Marel R. P., del Pino A., Linden
    S. T., Fritz T. K., Anderson J., The Proper-motion Field along the Magellanic Bridge:
    A New Probe of the LMC-SMC Interaction, ApJ, 2019, vol. 874, p. 78

Zivick P., Kallivayalil N., van der Marel R. P., Besla G., Linden S. T., Kozłowski S.,
    Fritz T. K., Kochanek C. S., Anderson J., Sohn S. T., Geha M. C., Alcock C. R., The
    Proper Motion Field of the Small Magellanic Cloud: Kinematic Evidence for Its Tidal
    Disruption, ApJ, 2018, vol. 864, p. 55

Appendix

Appendix A

Isochrone fits of the 33 Wing/Bridge clusters

Figures A.1, A.2 and A.3 present the decontaminated V vs. $V - I$ CMDs of the remaining Bridge clusters. The CMDs are colour-coded by membership probability and include the best-fitting isochrone, as well as previous literature results when available.
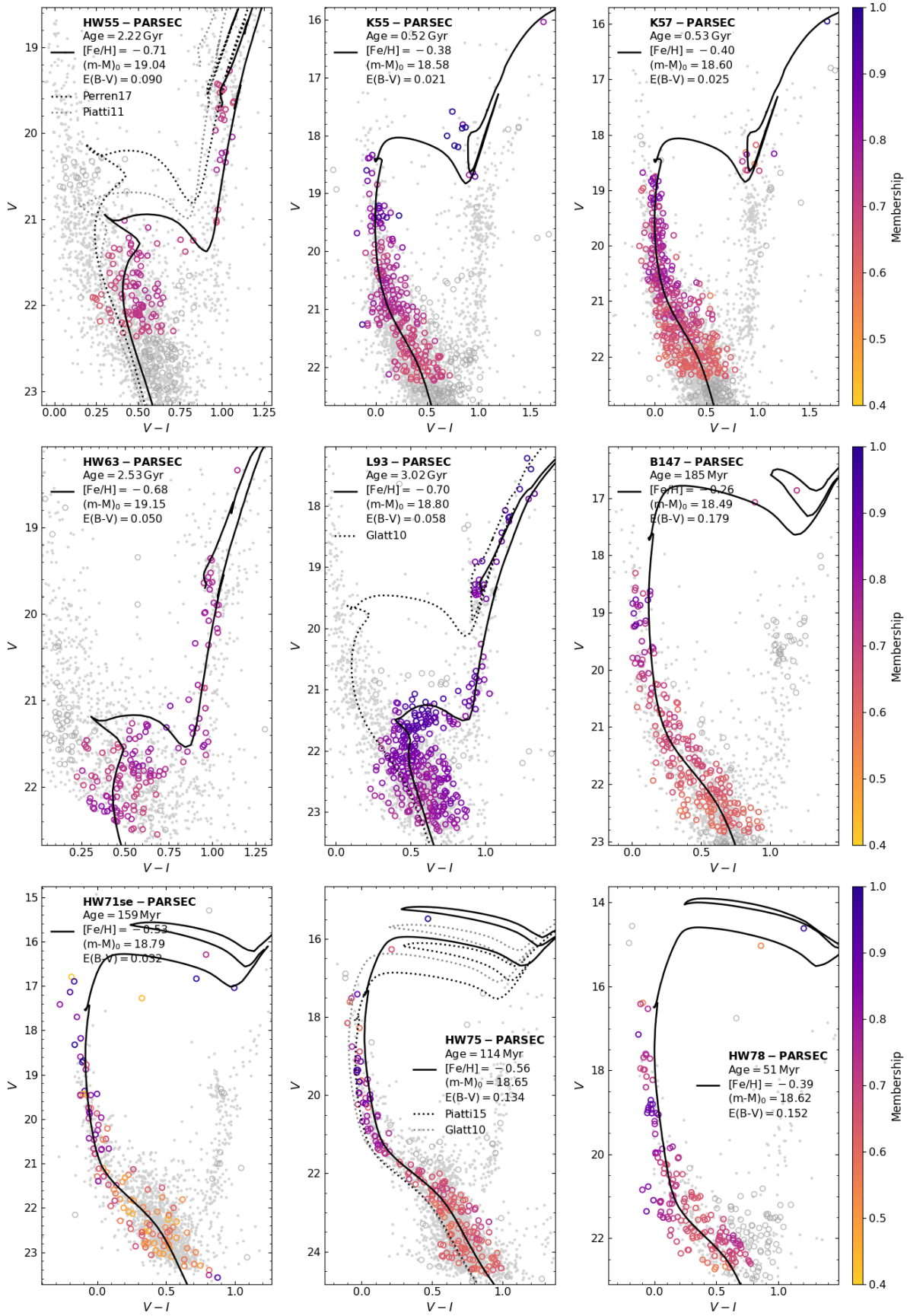
Figure A.1: Decontaminated V vs. $V - I$ CMDs containing the results for HW55, K55, K57, HW63, L93, B147, HW71se, HW75 and HW78.
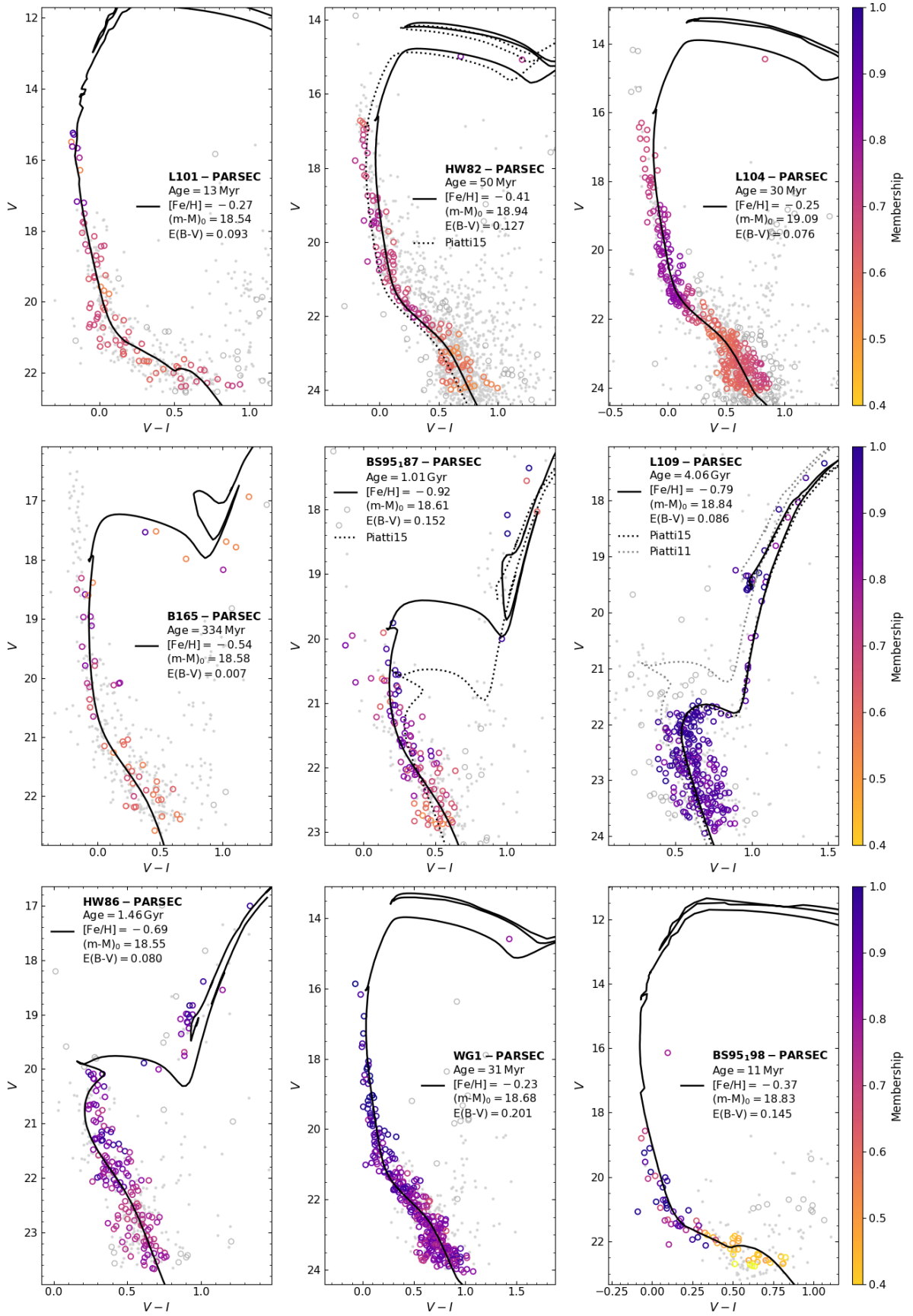
Figure A.2: Same as Figure A.1, with the results for L101, HW82, L104, B165, BS187, L109, HW86, WG1 and BS198.
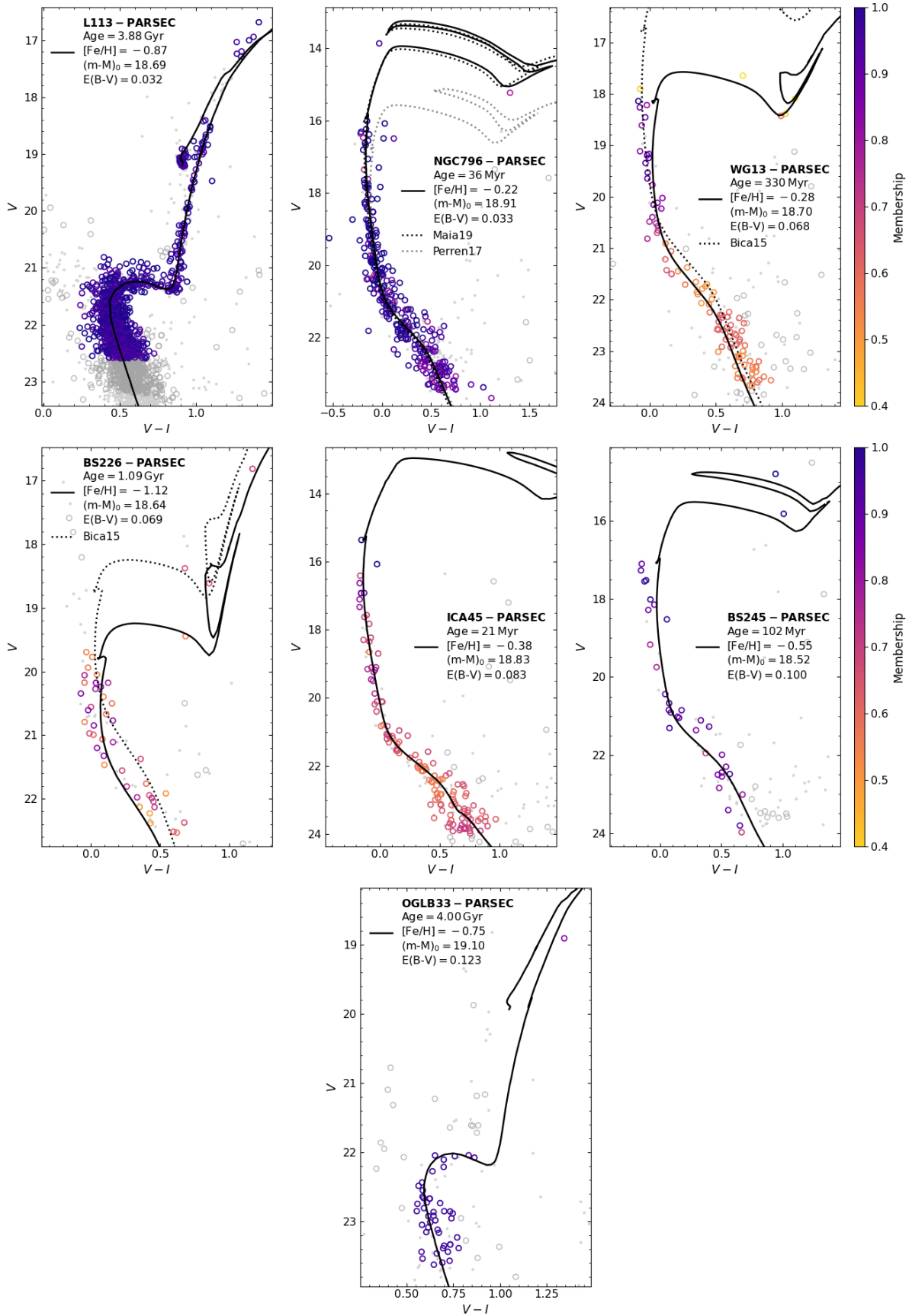
Figure A.3: Same as Figure A.1, with the results for L113, NGC796, WG13, BS226, ICA45, BS245 and OGLB33.

Papers in the period 2019-2023

Figures B.1 to B.8 show the abstracts of all the papers published during the present doctoral project (in chronological order), both as first author or co-author. Figure B.9 presents the main paper of this analysis, containing the results for the 33 Wing/Bridge clusters with VISCACHA data. It was submitted to MNRAS in 7 February 2023 and is still awaiting the reviewer reports.

CrossMark

Self-consistent Analysis of Stellar Clusters: An Application to *HST* Data of the Halo Globular Cluster NGC 6752

S. O. Souza[1] , L. O. Kerber[1,2] , B. Barbuy[1] , A. Pérez-Villegas[1] , R. A. P. Oliveira[1] , and D. Nardiello[3,4,5]

[1] Universidade de São Paulo, IAG, Rua do Matão 1226, Cidade Universitária, São Paulo 05508-900, Brazil; stefano.souza@usp.br
[2] Universidade Estadual de Santa Cruz, Rodovia Jorge Amado km 16, Ilhéus 45662-000, Brazil
[3] Dipartimento di Fisica e Astronomia "Galileo Galilei," Università di Padova, Vicolo dell'Osservatorio 3, Padova, I-35122, Italy
[4] Istituto Nazionale di Astrofisica— Osservatorio Astronomico di Padova, Vicolo dell'Osservatorio 5, Padova, I-35122, Italy
[5] Aix Marseille Université, CNRS, CNES, LAM, Marseille, France

Abstract

The Bayesian isochrone fitting using the Markov chain Monte Carlo algorithm is applied, to derive the probability distribution of the parameters age, metallicity, reddening, and absolute distance modulus. We introduce the SIRIUS code by means of simulated color–magnitude diagrams (CMDs), including the analysis of multiple stellar populations (MPs). The population tagging is applied from the red giant branch to the bottom of the main sequence. Through sanity checks using synthetic *Hubble Space Telescope* CMDs of globular clusters we verify the code reliability in the context of simple and MPs. In such tests, the formal uncertainties in age or age difference, metallicity, reddening, and absolute distance modulus can reach 400 Myr, 0.03 dex, 0.01 mag, and 0.03 mag, respectively. We apply the method to analyze NGC 6752, using Dartmouth stellar evolutionary models. Assuming a single stellar population, we derive an age of 13.7 ± 0.5 Gyr and a distance of $d_\odot = 4.11 \pm 0.08$ kpc, with the latter in agreement within 3σ with the inverse *Gaia* parallax. In the analysis of the MPs, three populations are clearly identified. From the Chromosome Map and UV/Optical two-color diagrams inspection, we found a fraction of stars of 25 ± 5, 46 ± 7, and 29 ± 5 %, for the first, second, and third generations, respectively. These fractions are in good agreement with the literature. An age difference of 500 ± 410 Myr between the first and the third generation is found, with the uncertainty decreasing to 400 Myr when the helium enhancement is taken into account.

Unified Astronomy Thesaurus concepts: Bayesian statistics (1900); Globular star clusters (656); Open star clusters (1160); Hertzsprung Russell diagram (725)
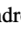
Figure B.1: Abstract of Souza et al. (2020).

CrossMark

An Updated Small Magellanic Cloud and Magellanic Bridge Catalog of Star Clusters, Associations, and Related Objects

Eduardo Bica[1], Pieter Westera[2] , Leandro de O. Kerber[3] , Bruno Dias[4,5] , Francisco Maia[6,7] , João F. C. Santos Jr.[8] , Beatriz Barbuy[7], and Raphael A. P. Oliveira[7]

[1] Universidade Federal do Rio Grande do Sul, Instituto de Física, Av. Bento Gonçalves 9500, 91501-970, Porto Alegre, Brazil
[2] Universidade Federal do ABC, Centro de Ciências Naturais e Humanas, Avenida dos Estados, 5001, 09210-580, Santo André, Brazil; pieter.westera@ufabc.edu.br
[3] Universidade Estadual de Santa Cruz, Depto. de Ciências Exatas e Tecnológicas, Rodovia Jorge Amado km 16, 45662-900, Ilhéus, Brazil
[4] Universidad Andrés Bello, Facultad de Ciencias Exactas, Departamento de Física, Av. Fernandez Concha 700, Las Condes, Santiago, Chile
[5] Instituto Milenio de Astrofísica, Av. Vicuña Makenna 4860, Macul, 7820436 Santiago, Chile
[6] Universidade Federal do Rio de Janeiro, Instituto de Física, Av. Athos da Silveira Ramos, 149, 21941-972, Rio de Janeiro, Brazil
[7] Universidade de São Paulo, Instituto de Astronomia, Geofísica e Ciências Atmosféricas, Rua do Matão 1226, 05508-090, São Paulo, Brazil
[8] Universidade Federal de Minas Gerais, Departamento de Física, ICEx, Av. Antonio Carlos 6627, 31270-901 Belo Horizonte, MG, Brazil

Abstract

We present a catalog of star clusters, associations, and related extended objects in the Small Magellanic Cloud (SMC) and the Magellanic Bridge with 2741 entries, a factor 2 more than a previous version from a decade ago. Literature data up until 2018 December are included. The identification of star clusters was carried out with digital atlases in various bands currently available in the Digitized Sky Survey and the Machine Automatique à Mésurer pour l'Astronomie. imaging surveys. In particular, we cross-identified recent cluster samples from the Visible and Infrared Survey Telescope for Astronomy near-infrared YJK_s survey of the Magellanic System, Optical Gravitational Lensing Experiment IV, and Survey of the MAgellanic Stellar History surveys, confirming new clusters and pointing out equivalencies. A major contribution of the present catalog consists of the accurate central positions for clusters and small associations, including a new sample of 45 clusters or candidates in the SMC and 19 in the Magellanic Bridge, as well as a compilation of the most reliable age and metallicity values from the literature. A general catalog must also deal with the recent discoveries of 27 faint and ultra-faint star clusters and galaxies projected on the far surroundings of the Clouds, most of them from the Dark Energy Survey. The information on these objects has been complemented with photometric, spectroscopic, and kinematical follow-up data from the literature. The underluminous galaxies around the Magellanic System, still very few as compared to the predictions from Λ Cold Dark Matter simulations, can bring constraints to galaxy formation and hierarchical evolution. Furthermore, we provide diagnostics, when possible, of the nature of the ultra-faint clusters, searching for borders of the Magellanic System extensions into the Milky Way gravitational potential.

Unified Astronomy Thesaurus concepts: Celestial objects catalogs (212); Small Magellanic Cloud (1468); Star clusters (1567); Galaxy interactions (600)

Figure B.2: Abstract of Bica et al. (2020).

The *Hubble Space Telescope* UV Legacy Survey of Galactic Globular Clusters. XX. Ages of Single and Multiple Stellar Populations in Seven Bulge Globular Clusters

R. A. P. Oliveira[1], S. O. Souza[1], L. O. Kerber[1,2], B. Barbuy[1], S. Ortolani[3,4], G. Piotto[3,4], D. Nardiello[3,4,5], A. Pérez-Villegas[1], F. F. S. Maia[6], E. Bica[7], S. Cassisi[8,9], F. D'Antona[10], E. P. Lagioia[3,4], M. Libralato[11], A. P. Milone[3,4], J. Anderson[11], A. Aparicio[12,13], L. R. Bedin[4], T. M. Brown[11], I. R. King[14], A. F. Marino[3], A. Pietrinferni[8], A. Renzini[4], A. Sarajedini[15], R. van der Marel[11,16], and E. Vesperini[17]

[1] Universidade de São Paulo, IAG, Rua do Matão 1226, Cidade Universitária, São Paulo 05508-900, Brazil; rap.oliveira@usp.br, stefano.souza@usp.br
[2] Universidade Estadual de Santa Cruz, Rodovia Jorge Amado km 16, Ilhéus 45662-000, Brazil
[3] Dipartimento di Fisica e Astronomia "Galileo Galilei," Università di Padova, Vicolo dell'Osservatorio 3, Padova I-35122, Italy
[4] Istituto Nazionale di Astrofisica—Osservatorio Astronomico di Padova, Vicolo dell'Osservatorio 5, Padova I-35122, Italy
[5] Aix Marseille Univ, CNRS, CNES, LAM, Marseille, France
[6] Universidade Federal do Rio de Janeiro, Av. Athos da Silveira Ramos, 149—Cidade Universitária, Rio de Janeiro 21941-909, Brazil
[7] Universidade Federal do Rio Grande do Sul, Departamento de Astronomia, CP 15051, Porto Alegre 91501-970, Brazil
[8] INAF—Astronomical Observatory of Abruzzo, Via M. Maggini, sn, I-64100 Teramo, Italy
[9] INFN—Sezione di Pisa, Largo Pontecorvo 3, I-56127 Pisa, Italy
[10] INAF—Osservatorio Astronomico di Roma, Via Frascati 33, I-00040, Monte Porzio Catone, Roma, Italy
[11] Space Telescope Science Institute, 3700 San Martin Dr., Baltimore, MD 21218, USA
[12] Instituto de Astrofisica de Canarias, E-38200 La Laguna, Canary Islands, Spain
[13] Department of Astrophysics, University of La Laguna, E-38200 La Laguna, Tenerife, Canary Islands, Spain
[14] Department of Astronomy, University of Washington, Box 351580, Seattle, USA
[15] Charles E. Schmidt College of Science, Florida Atlantic University, 777 Glades Rd, Boca Raton, FL 33431, USA
[16] Center for Astrophysical Sciences, Department of Physics & Astronomy, Johns Hopkins University, Baltimore, MD 21218, USA
[17] Department of Astronomy, Indiana University, Bloomington, IN 47401, USA

Abstract

In the present work we analyzed seven globular clusters (GCs) selected from their location in the Galactic bulge and with metallicity values in the range $-1.30 \lesssim [\mathrm{Fe/H}] \lesssim -0.50$. The aim of this work is first to derive cluster ages assuming single stellar populations and second to identify the stars from first (1G) and second generations (2G) from the main sequence, subgiant, and red giant branches, and to derive their age differences. Based on a combination of UV and optical filters used in this project, we apply the Gaussian mixture models to distinguish the multiple stellar populations. Applying statistical isochrone fitting, we derive self-consistent ages, distances, metallicities, and reddening values for the sample clusters. An average age of 12.3 ± 0.4 Gyr was obtained both using DSED and BaSTI (accounting atomic diffusion effects) isochrones, without a clear distinction between the moderately metal-poor and the more metal-rich bulge clusters, except for NGC 6717 and the inner halo NGC 6362 with ~ 13.5 Gyr. We derived a weighted mean age difference between the multiple populations hosted by each GC of 41 ± 170 Myr adopting canonical He abundances; whereas for higher He in 2G stars, this difference reduces to 17 ± 170 Myr, but with individual uncertainties of 500 Myr.

Unified Astronomy Thesaurus concepts: Globular star clusters (656); Galactic bulge (2041)

Figure B.3: Abstract of Oliveira et al. (2020).

Astronomy & Astrophysics

LETTER TO THE EDITOR

The VISCACHA survey

III. Star clusters counterpart of the Magellanic Bridge and Counter-Bridge in 8D[⋆]

B. Dias[1], M. S. Angelo[2], R. A. P. Oliveira[3], F. Maia[4], M. C. Parisi[5,6], B. De Bortoli[7,8], S. O. Souza[3],
O. J. Katime Santrich[9], L. P. Bassino[7,8], B. Barbuy[3], E. Bica[10], D. Geisler[11,12,13], L. Kerber[9], A. Pérez-Villegas[3,14],
B. Quint[15], D. Sanmartim[16], J. F. C. Santos Jr.[17], and P. Westera[18]

[1] Instituto de Alta Investigación, Sede Esmeralda, Universidad de Tarapacá, Av. Luis Emilio Recabarren 2477, Iquique, Chile
e-mail: `bdiasm@academicos.uta.cl`
[2] Centro Federal de Educação Tecnológica de Minas Gerais Av. Monsenhor Luiz de Gonzaga, 103, 37250-000 Nepomuceno, MG,
Brazil
[3] Universidade de São Paulo, IAG, Rua do Matão 1226, Cidade Universitária, São Paulo 05508-900, Brazil
[4] Instituto de Física, Universidade Federal do Rio de Janeiro, 21941-972 Rio de Janeiro, RJ, Brazil

ABSTRACT

Context. The interactions between the Small and Large Magellanic Clouds (SMC and LMC) created the Magellanic Bridge; a stream of gas and stars pulled out of the SMC towards the LMC about 150 Myr ago. The tidal counterpart of this structure, which should include a trailing arm, has been predicted by models but no compelling observational evidence has confirmed the Counter-Bridge so far.
Aims. The main goal of this work is to find the stellar counterpart of the Magellanic Bridge and Counter-Bridge. We use star clusters in the SMC outskirts as they provide a 6D phase-space vector, age, and metallicity which help characterise the outskirts of the SMC.
Methods. Distances, ages, and photometric metallicities were derived from fitting isochrones to the colour-magnitude diagrams from the VISCACHA survey. Radial velocities and spectroscopic metallicities were derived from the spectroscopic follow-up using GMOS in the CaII triplet region.
Results. Among the seven clusters analysed in this work, five belong to the Magellanic Bridge, one belongs to the Counter-Bridge, and the other belongs to the transition region.
Conclusions. The existence of the tidal counterpart of the Magellanic Bridge is evidenced by star clusters. The stellar component of the Magellanic Bridge and Counter-Bridge are confirmed in the SMC outskirts. These results are an important constraint for models that seek to reconstruct the history of the orbit and interactions between the LMC and SMC as well as constrain their future interaction including with the Milky Way.

Key words. Magellanic Clouds – galaxies: star clusters: general – galaxies: evolution

Figure B.4: Abstract of Dias et al. (2021, Paper III).

Astronomy & Astrophysics

Precise distances from OGLE-IV member RR Lyrae stars in six bulge globular clusters[⋆]

R. A. P. Oliveira[1], S. Ortolani[2,3,4], B. Barbuy[1], L. O. Kerber[5], F. F. S. Maia[6], E. Bica[7], S. Cassisi[8,9], S. O. Souza[1], and A. Pérez-Villegas[10]

[1] Universidade de São Paulo, IAG, Rua do Matão 1226, Cidade Universitária, São Paulo 05508-900, Brazil
  e-mail: `rap.oliveira@usp.br`
[2] Università di Padova, Dipartimento di Fisica e Astronomia, Vicolo dell'Osservatorio 2, 35122 Padova, Italy
[3] INAF-Osservatorio Astronomico di Padova, Vicolo dell'Osservatorio 5, 35122 Padova, Italy
[4] Centro di Ateneo di Studi e Attività Spaziali "Giuseppe Colombo" – CISAS, Via Venezia 15, 35131 Padova, Italy
[5] Universidade Estadual de Santa Cruz, Rodovia Jorge Amado km 16, Ilhéus 45662-000, Brazil
[6] Universidade Federal do Rio de Janeiro, Av. Athos da Silveira, 149, Cidade Universitária, Rio de Janeiro 21941-909, Brazil
[7] Universidade Federal do Rio Grande do Sul, Departamento de Astronomia, CP 15051, Porto Alegre 91501-970, Brazil
[8] INAF – Astronomical Observatory of Abruzzo, Via M. Maggini, sn, 64100 Teramo, Italy
[9] INFN – Sezione di Pisa, Largo Pontecorvo 3, 56127 Pisa, Italy
[10] Instituto de Astronomía, Universidad Nacional Autónoma de México, A.P. 106, 22800 Ensenada, B.C., México

Received 19 June 2021 / Accepted 6 October 2021

ABSTRACT

Context. RR Lyrae stars are useful standard candles allowing one to derive accurate distances for old star clusters. Based on the recent catalogues from OGLE-IV and *Gaia* Early Data Release 3 (EDR3), the distances can be improved for a few bulge globular clusters.
Aims. The aim of this work is to derive an accurate distance for the following six moderately metal-poor, relatively high-reddening bulge globular clusters: NGC 6266, NGC 6441, NGC 6626, NGC 6638, NGC 6642, and NGC 6717.
Methods. We combined newly available OGLE-IV catalogues of variable stars containing mean I magnitudes, with Clement's previous catalogues containing mean V magnitudes, and with precise proper motions from *Gaia* EDR3. Astrometric membership probabilities were computed for each RR Lyrae, in order to select those compatible with the cluster proper motions. Applying luminosity–metallicity relations derived from BaSTI α-enhanced models (He-enhanced for NGC 6441 and canonical He for the other clusters), we updated the distances with relatively low uncertainties.
Results. Distances were derived with the I and V bands, with a 5–8% precision. We obtained 6.6 kpc, 13.1 kpc, 5.6 kpc, 9.6 kpc, 8.2 kpc, and 7.3 kpc for NGC 6266, NGC 6441, NGC 6626, NGC 6638, NGC 6642, and NGC 6717, respectively. The results are in excellent agreement with the literature for all sample clusters, considering the uncertainties.
Conclusions. The present method of distance derivation, based on recent data of member RR Lyrae stars, updated BaSTI models, and robust statistical methods, proved to be consistent. A larger sample of clusters will be investigated in a future work.

Key words. stars: variables: RR Lyrae – globular clusters: general – Galaxy: bulge

Figure B.5: Abstract of Oliveira et al. (2022).

The VISCACHA survey – IV. The SMC West Halo in 8D

B. Dias [1], M. C. Parisi,[2,3] M. Angelo,[4] F. Maia,[5] R. A. P. Oliveira,[6] S. O. Souza,[6] L. O. Kerber,[7] J. F. C. Santos, Jr.,[8] A. Pérez-Villegas,[9] D. Sanmartim,[10] B. Quint,[11] L. Fraga,[12] B. Barbuy,[6] E. Bica,[13] O. J. Katime Santrich,[7] J. A. Hernandez-Jimenez,[14] D. Geisler,[15,16,17] D. Minniti,[18] B. J. De Bórtoli,[19,20] L. P. Bassino[19,20] and J. P. Rocha[7]

[1]*Instituto de Alta Investigación, Sede Esmeralda, Universidad de Tarapacá, Av. Luis Emilio Recabarren 2477, Iquique, Chile*
[2]*Observatorio Astronómico, Universidad Nacional de Córdoba, Laprida 854, X5000BGR, Córdoba, Argentina*
[3]*Instituto de Astronomía Teórica y Experimental (CONICET-UNC), Laprida 854, X5000BGR, Córdoba, Argentina*
[4]*Centro Federal de Educação Tecnológica de Minas Gerais, Av. Monsenhor Luiz de Gonzaga, 103, 37250-000 Nepomuceno, MG, Brazil*
[5]*Instituto de Física, Universidade Federal do Rio de Janeiro, 21941-972, Rio de Janeiro, RJ, Brazil*
[6]*Universidade de São Paulo, IAG, Rua do Matão 1226, Cidade Universitária, São Paulo 05508-900, Brazil*
[7]*Departamento de Ciências Exatas e Tecnológicas, UESC, Rodovia Jorge Amado km 16, 45662-900, Brazil*
[8]*Departamento de Física, ICEx - UFMG, Av. Antônio Carlos 6627, Belo Horizonte 31270-901, Brazil*
[9]*Instituto de Astronomía, Universidad Nacional Autonóma de México, Apartado Postal 106, C.P. 22800, Ensenada, Baja California, Mexico*
[10]*Carnegie Observatories, Las Campanas Observatory, Casilla 601, La Serena, Chile*
[11]*Rubin Observatory Project Office, 950 N. Cherry Ave., Tucson, AZ 85719, USA*
[12]*Laboratório Nacional de Astrofísica, Rua Estados Unidos 154, Itajubá 37504-364, Brazil*
[13]*Departamento de Astronomia, IF - UFRGS, Av. Bento Gonçalves 9500, Porto Alegre, RS, 91501-970, Brazil*
[14]*IP&D-Universidade do Vale do Paraíba-Av. Shishima Hifumi, 2911-12244-000 - São José dos Campos - SP, Brazil*
[15]*Departamento de Física y Astronomía, Universidad de La Serena, Avenida Juan Cisternas 1200, La Serena, Chile*
[16]*Instituto de Investigación Multidisciplinario en Ciencia y Tecnología, Universidad de La Serena Benavente 980, La Serena, Chile*
[17]*Departmento de Astronomía, Universidad de Concepción, Casilla 160-C, Concepción, Chile*
[18]*Departamento de Ciencias Físicas, Universidad Andres Bello, Fernandez Concha 700, Las Condes, Santiago, Chile*
[19]*Facultad de Ciencias Astronómicas y Geofísicas de la Universidad Nacional de La Plata, and Instituto de Astrofísica de La Plata (CCT La Plata - CONICET, UNLP), Paseo del Bosque S/N, B1900FWA La Plata, Argentina*
[20]*Consejo Nacional de Investigaciones Científicas y Técnicas, Godoy Cruz 2290, C1425FQB, Ciudad Autónoma de Buenos Aires, Argentina*

ABSTRACT
The structure of the Small Magellanic Cloud (SMC) is very complex, in particular in the periphery that suffers more from the interactions with the Large Magellanic Cloud (LMC). A wealth of observational evidence has been accumulated revealing tidal tails and bridges made up of gas, stars, and star clusters. Nevertheless, a full picture of the SMC outskirts is only recently starting to emerge with a 6D phase-space map plus age and metallicity using star clusters as tracers. In this work, we continue our analysis of another outer region of the SMC, the so-called West Halo, and combined it with the previously analysed Northern Bridge. We use both structures to define the Bridge and Counter-bridge trailing and leading tidal tails. These two structures are moving away from each other, roughly in the SMC–LMC direction. The West Halo form a ring around the SMC inner regions that goes up to the background of the Northern Bridge shaping an extended layer of the Counter-bridge. Four old Bridge clusters were identified at distances larger than 8 kpc from the SMC centre moving towards the LMC, which is consistent with the SMC–LMC closest distance of 7.5 kpc when the Magellanic Bridge was formed about 150Myr ago; this shows that the Magellanic Bridge was not formed only by pulled gas, but it also removed older stars from the SMC during its formation. We also found age and metallicity radial gradients using projected distances on sky, which are vanished when we use the real 3D distances.

Key words: galaxies: evolution – Magellanic Clouds – galaxies: star clusters: general.

Figure B.6: Abstract of Dias et al. (2022, Paper IV).

The VISCACHA survey – V. Rejuvenating three faint SMC clusters

E. Bica,[1]★ F. F. S. Maia [⬤],[2] R. A. P. Oliveira [⬤],[3] B. Dias [⬤],[4]★ J. F. C. Santos, Jr [⬤],[5] J. P. Rocha,[6]
L. Kerber,[6] J. F. Gardin,[5] T. Armond,[7] M. C. Parisi,[8,9] S. O. Souza [⬤][10,3] and B. Barbuy[3]

[1]*Departamento de Astronomia, IF - UFRGS, Av. Bento Gonçalves 9500, 91501-970, Brazil*

[2]*Instituto de Física - Universidade Federal do Rio de Janeiro, Av. Athos da Silveira Ramos, 149, Rio de Janeiro 21941-909, Brazil*

[3]*Universidade de São Paulo, IAG, Rua do Matão 1226, Cidade Universitária, São Paulo 05508-900, Brazil*

[4]*Instituto de Alta Investigación, Sede Esmeralda, Universidad de Tarapacá, Av. Luis Emilio Recabarren 2477, Iquique, Chile*

[5]*Departamento de Física, ICEx - UFMG, Av. Antônio Carlos 6627, Belo Horizonte 31270-901, Brazil*

[6]*Departamento de Ciências Exatas e Tecnológicas, UESC, Rodovia Jorge Amado km 16, 45662-900, Brazil*

[7]*Universidade Federal de São João del-Rei, Departamento de Estatística, Física e Matemática, Campus Alto Paraopeba, Rod.: MG 443, Km 7, Ouro Branco - MG 36420-000, Brazil*

[8]*Observatorio Astronómico, Universidad Nacional de Córdoba, Laprida 854, X5000BGR Córdoba, Argentina*

[9]*Instituto de Astronomía Teórica y Experimental (CONICET-UNC), Laprida 854, X5000BGR Córdoba, Argentina*

[10]*Leibniz-Institut für Astrophysik Potsdam (AIP), An der Sternwarte 16, Potsdam 14482, Germany*

ABSTRACT

We present the analysis of three faint clusters of the Small Magellanic Cloud RZ 82, HW 42, and RZ 158. We employed the SOAR telescope instrument SAM with adaptive optics, allowing us to reach to $V \sim 23$–24 mag, unprecedentedly, a depth sufficient to measure ages of up to about 10–12 Gyr. All three clusters are resolved to their centres, and the resulting colour–magnitude diagrams (CMDs) allow us to derive ages of 3.9, 2.6, and 4.8 Gyr, respectively. These results are significantly younger than previous determinations (7.1, 5.0, and 8.3 Gyr, respectively), based on integrated photometry or shallower CMDs. We rule out older ages for these clusters based on deep photometry and statistical isochrone fitting. We also estimate metallicities for the three clusters of [Fe/H] $= -0.68$, -0.57, and -0.90, respectively. These updated ages and metallicities are in good agreement with the age-metallicity relation for the bulk of SMC clusters. Total cluster masses ranging from ~ 7–$11 \cdot 10^3 \, M_\odot$ were estimated from integrated flux, consistent with masses estimated for other SMC clusters of similar ages. These results reduce the number of SMC clusters known to be older than about 5 Gyr and highlight the need of deep and spatially resolved photometry to determine accurate ages for older low-luminosity SMC star clusters.

Key words: Magellanic Clouds – galaxies: star clusters: general.

Figure B.7: Abstract of Bica et al. (2022, Paper V).

The VISCACHA survey – VI. Dimensional study of the structure of 82 star clusters in the Magellanic Clouds

M. Jimena Rodríguez [1,2,3]★ C. Feinstein,[2,3,4]★ G. Baume,[2,3,4]★ B. Dias [5] F. S. M. Maia [6]
J. F. C. Santos, Jr.,[7] L. Kerber [8] D. Minniti,[9,10] A. Pérez-Villegas,[11] B. De Bórtoli,[2,3,4] M. C. Parisi[3,12,13]
and R. A. P. Oliveira [14]

[1] *Steward Observatory, University of Arizona, 933 N Cherry Ave,Tucson, AZ 85721, USA*
[2] *Instituto de Astrofísica de La Plata, CONICET–UNLP, Paseo del Bosque S/N, B1900FWA La Plata, Argentina*
[3] *Consejo Nacional de Investigaciones Científicas y Técnicas, Godoy Cruz 2290, C1425FQB, Ciudad Autónoma de Buenos Aires, Argentina*
[4] *Facultad de Ciencias Astronómicas y Geofísicas, UNLP, Paseo del Bosque S/N, B1900FWA La Plata, Argentina*
[5] *Instituto de Alta Investigación, Universidad de Tarapacá, Av. Luis Emilio Recabarren 2477, Iquique, Chile*
[6] *Instituto de Física - Universidade Federal do Rio de Janeiro, Av. Athos da Silveira Ramos, 149, Rio de Janeiro, 21941-909, Brazil*
[7] *Departamento de Física, ICEx - UFMG, Av. Antônio Carlos 6627, Belo Horizonte 31270-901, Brazil*
[8] *Departamento de Ciências Exatas e Tecnológicas, UESC, Rodovia Jorge Amado km 16, 45662-900, Brazil*
[9] *Instituto de Astrofísica, Facultad de Ciencias Exactas, Universidad Andres Bello, Av. Fernandez Concha 700, Santiago, Chile*
[10] *Vatican Observatory, I-V00120 Vatican City State, Italy*
[11] *Instituto de Astronomía, Universidad Nacional Autónoma de México, Apartado Postal 106, C. P. 22800, Ensenada, B. C., Mexico*
[12] *Observatorio Astronómico, Universidad Nacional de Córdoba, Laprida 854, X5000BGR, Córdoba, Argentina*
[13] *Instituto de Astronomía Teórica y Experimental (CONICET-UNC), Laprida 854, X5000BGR, Córdoba, Argentina*
[14] *Universidade de São Paulo, IAG, Rua do Matão 1226, Cidade Universitária, São Paulo 05508-900, Brazil*

ABSTRACT

We present a study of the internal structure of 82 star clusters located at the outer regions of the Large Magellanic Cloud and the Small Magellanic Cloud using data of the VISCACHA Survey. Through the construction of the *minimum spanning tree*, which analyses the relative position of stars within a given cluster, it was possible to characterize the internal structure and explore the fractal or subclustered distribution for each cluster. We computed the parameters $\overline{m}$ (which is the average length of the connected segments normalized by the area), $\overline{s}$ (which is the mean points separation in units of cluster radius), and Q (the ratio of these components). These parameters are useful to distinguish between radial, homogeneous, and substructured distributions of stars. The dependence of these parameters with the different characteristics of the clusters, such as their ages and spatial distribution, was also studied. We found that most of the studied clusters present a homogeneous stellar distribution or a distribution with a radial concentration. Our results are consistent with the models, suggesting that more dynamically evolved clusters seem to have larger Q values, confirming previous results from numerical simulations. There also seems to be a correlation between the internal structure of the clusters and their galactocentric distances, in the sense that for both galaxies, the more distant clusters have larger Q values. We also paid particular attention to the effects of contamination by non-member field stars and its consequences finding that field star decontamination is crucial for these kinds of studies.

Key words: (galaxies:) Magellanic Clouds – galaxies: star clusters: general.

Figure B.8: Abstract of Rodríguez et al. (2023, Paper VI).

The VISCACHA survey – VII. Assembly history of the Magellanic Bridge and SMC Wing from star clusters

R. A. P. Oliveira ©,[1]* F. F. S. Maia ©,[2] B. Barbuy ©,[1] B. Dias ©,[3] J. F. C. Santos Jr. ©,[4]
S. O. Souza ©,[5,1] L. O. Kerber ©,[6] E. Bica,[7] D. Sanmartim ©,[8,9] B. Quint,[9] L. Fraga,[10]
T. Armond,[11] D. Minniti,[12,13] M. C. Parisi,[14,15,16] O. J. Katime Santrich ©,[6] M. S. Angelo,[17]
A. Pérez-Villegas ©[18] and B. J. De Bórtoli[19,14,20]

[1] *Universidade de São Paulo, IAG, Rua do Matão 1226, Cidade Universitária, São Paulo 05508-090, Brazil*
[2] *Universidade Federal do Rio de Janeiro, Av. Athos da Silveira, 149, Cidade Universitária, Rio de Janeiro 21941-909, Brazil*
[3] *Instituto de Alta Investigación, Sede Esmeralda, Universidad de Tarapacá, Av. Luis Emilio Recabarren 2477, Iquique, Chile*
[4] *Departamento de Física, ICEx – UFMG, Av. Antônio Carlos 6627, Belo Horizonte 31270-901, Brazil*
[5] *Leibniz-Institut für Astrophysik Potsdam (AIP), An der Sternwarte 16, Potsdam D-14482, Germany*

ABSTRACT

The formation scenario of the Magellanic Bridge during an encounter between the LMC and SMC ~ 200 Myr ago, as proposed by models, would be imprinted in the chemical enrichment and kinematics of its star clusters, and sites of ongoing star formation along its extension. We present an analysis of 33 Bridge clusters using photometry observed with SOAR 4-m telescope assisted by adaptive optics for the VISCACHA survey. We performed a membership selection and derived self-consistent ages, metallicities, distances and reddenings via statistical isochrone fitting, as well as tidal radii and integrated masses from a structure analysis. Two groups are clearly detected: 13 well-studied clusters older than the Bridge, with ages of $0.5 - 4.7$ Gyr and [Fe/H] < -0.5; and 15 clusters younger than 200 Myr and with [Fe/H] > -0.5, probably formed in-situ. The older clusters follow the overall age and metallicity gradients of the SMC, whereas the younger ones are uniformly distributed along the Bridge. The main results from this work include: (*i*) we present ages and metallicities for 9 and 18 clusters for the first time, respectively; (*ii*) we detected two metallicity dips in the age-metallicity relation of the Bridge at about 200 Myr and 1.5 Gyr ago, which are possible chemical signatures of the formation of the Bridge and Magellanic Stream; (*iii*) we estimate a minimum stellar mass for the Bridge of $3 - 5 \times 10^5 M_\odot$; (*iv*) we confirm that the SMC Wing and Bridge for RA $< 3^h$ are metal-rich with all young star clusters with [Fe/H] ~ -0.4.

Key words: Magellanic Clouds – galaxies: evolution – galaxies: star clusters: general

Figure B.9: Abstract of Oliveira et al. (submitted to MNRAS).